Faculty of Physics and Astronomy
University of Heidelberg

Diploma thesis
in Physics

submitted by
Anna Kuhlmann
born in Freiburg

April 2006

Atmospheric Gaseous Sulfuric Acid Measurements: Implications for Aerosol Formation by Homogeneous Nucleation

This diploma thesis was carried out by Anna Kuhlmann at the
Max-Planck-Institute for Nuclear Physics, Heidelberg
(Atmospheric physics division)
under supervision of
Prof. Dr. Frank Arnold

Atmospheric Gaseous Sulfuric Acid Measurements: Implications for Aerosol Formation by Homogeneous Nucleation

This work is focused on the presentation and interpretation of measurements of gaseous sulfuric acid, which we have made at Hyytiälä (Finland) in the framework of the European projects BACCI (Research Unit on Biosphere-Aerosol-Cloud-Climate-Interactions) and QUEST (Quantification of Aerosol Nucleation in the European Boundary Layer). These measurements were conducted using Chemical Ionization Mass Spectrometry (CIMS) and represent one of the few long-term gaseous sulfuric acid measurements. Sulfuric Acid is probably the key trigger of new particle formation by nucleation. On the basis of our sulfuric acid measurements the nucleation process was examined considering the aerosol size distributions which were simultaneously measured. The H_2SO_4 data were compared with particle and meteorological parameters in order to characterize conditions for nucleation. In the next step it was examined to what extent the number concentration of small particles depends on the sulfuric acid concentration. Previous theoretical and experimental investigations showed that new particle concentrations obey a linear or a quadratic dependence on the gaseous sulfuric acid concentration. Both dependencies were observed in this work which indicates that activation (linear) as well as kinetic nucleation theory (quadratic) can explain the formation of new particles in this region.

Messungen atmosphärischer gasförmiger Schwefelsäure: Einfluss auf die Aerosolentstehung durch homogene Nukleation

Diese Arbeit konzentriert sich auf die Darstellung und Interpretation von Messungen gasförmiger Schwefelsäure, die im Rahmen der Europäischen Projekte BACCI (Research Unit on Biosphere-Aerosol-Cloud-Climate-Interactions) und QUEST (Quantification of Aerosol Nucleation in the European Boundary Layer) in Hyytiälä (Finnland) statt fanden. Diese Messungen wurden mittels chemischer Ionisations-Massenspektrometrie (CIMS) durchgeführt und stellen eine der wenigen Langzeit-Beobachtungen von gasförmiger Schwefelsäure dar. Diese spielt bei der Entstehung von Aerosolen wahrscheinlich eine Schlüsselfunktion. Unter Betrachtung gleichzeitig gemessener Aerosol Größenverteilungen wurde anhand unserer H_2SO_4 Messungen der Nukleationsvorgang untersucht. Ein Vergleich der H_2SO_4 Daten mit Partikeldaten und meteorologischen Parametern diente dazu, Bedingungen für die Entstehung dieser Partikel zu charakterisieren. Anschließend wurde versucht die Gesetzmäßigkeit zwischen der Konzentration kleiner Partikel und der H_2SO_4 Konzentration genauer zu bestimmen. Theoretische und experimentelle Untersuchungen zeigen, dass die Konzentration kleiner Partikel einer linearen oder quadratischen Abhängigkeit von der Konzentration gasförmiger Schwefelsäure folgt. Beide Abhängigkeiten konnten innerhalb dieser Studie beobachtet werden, was darauf hinweist, dass sich die Partikelbildung in dieser Region sowohl durch den Mechanismus der Aktivierung (linear) als auch der Kinetischen Nukleation (quadratisch) erklären lässt.

Contents

Chapter 1

Introduction

Aerosols, suspended particles in the atmosphere, are known to significantly impact the earth's climate and human well-being. Particulate matter affects the climate in a direct and in an indirect way by changing the global radiation balance. The direct impact stems from interaction with solar radiation, scattering and absorbing the incoming sunlight. As aerosols reflect sunlight back into outer space, the amount of solar radiation that reaches the Earth's surface is reduced. This leads to a cooling effect whose extent depends on the size and composition of the aerosol particles.
Indirectly they affect the climate by changing the properties of clouds. Aerosols act as cloud condensation nuclei (CCN). They provide the kernel needed to initiate the formation of cloud droplets. When the aerosol concentration is higher within a cloud, more cloud drops of smaller sizes are formed, which reflect more sunlight, due to a higher total cross section. In addition, small droplets possess lower coalescence rates and lower sedimentation velocities, thus extending average retention periods in the atmosphere. This further changes the lifetime of the cloud droplets causing an increased cloud cover and a decreased amount of rainfall, [Hardin and Kahn, 2005], [Roedel, 2000]. Thus, whether direct or indirect, both effects contribute to planetary cooling which partially counteracts the anthropogenic greenhouse effect.

Moreover, several studies report of additional, more immediate impacts that aerosols can have on human well-being. Inhaling particular matter can cause several irreversible damages to the human health. The effects have been widely studied and high particle concentrations seem to have an influence on asthma, lung cancer, cardiovascular diseases and premature death, [Zylka-Menhorn, 2005]. The size of the particle determines how far it penetrates the lungs when inhaled. The smaller the particles the more hazardous they are, since they are less efficiently filtered by the nasal hair and ciliated cells in the trachea. Aerosols which are smaller

than about 10 μm in size cannot be intercepted by these mechanisms and are therefore able to settle in the bronchia and lungs. Corresponding to a higher fine particle load an increasing number of respiratory diseases has occurred in the recent past, [Zylka-Menhorn, 2005]. Particles smaller than 2.5 μm possess the ability to penetrate directly into the lungs, where they may enter the bloodstream, [Bransford, 2002]. There is evidence that these particles can cause vascular inflammation and atherosclerosis which may lead to heart attacks and other cardiovascular problems, [Pope et al., 2002], [Kreyling et al., 2006]. Particles of diameters smaller than 100 nm might even be able to pass through cell membranes. It it discussed that aerosols of these sizes might also reach the brain, [Kreyling et al., 2006].

Since aerosols affect our life in different ways the investigation of particle nucleation is of great importance. In this context the precursor gases, key compounds and conditions which favor the formation of new particles need to be determined. Aerosols can form and grow e.g. by condensation of trace gases. Previous observations indicate that sulfuric acid is supposed to be strongly involved in particle nucleation and their subsequent growth [Reiner and Arnold, 1993, Reiner and Arnold, 1994, Boy et al., 2004, Kulmala, 2003]. Particularly interesting is the mechanism which leads to the formation of new particles. There are different possibilities as to how new particles emerge. Sulfuric acid is mainly involved in heterogeneous, ion induced, [Arnold, 1982, Korhonen et al., 1999, Yue and Chan, 1979], and homogeneous processes. Competing approaches exist describing homogeneous nucleation, e.g. a thermodynamic like binary or ternary, kinetic or the recently proposed activation theory. However, there are still uncertainties in explaining the detailed processes. In recent years measurements of sulfuric acid in combination with aerosols were obtained by our group (MPIK Heidelberg) in Hyytiälä (Finland) and Heidelberg (Germany). The long-term data to be acquired upon continuation of these investigations promises to provide more fundamental insight into particle nucleation.

The present work deals with the recent H_2SO_4 measurements obtained during a campaign which was performed in the boreal forest region of Finland as part of the European projects BACCI and QUEST. Several research groups participated in this campaign in order to measure as many as possible parameters relevant for particle nucleation. Especially the role of organic compounds seems to be very important but is still not completely understood. In the atmosphere mole fractions of H_2SO_4 are below 1 pptv (parts per trillion by volume) and, thus, relatively low. To be able to detect such low atmospheric concentrations, a very sensitive measurement device is required. For the H_2SO_4 measurements discussed in this work, the CIMS (Chemical Ionization Mass Spectrometry) method with an ion trap mass

spectrometer was used. A detailed description of the measurement device and principle can be found in Chapter 3, immediately following the theoretical account in Chapter 2. The specific experimental setup during the BACCI4-QUEST campaign as well as the calibration procedure is elucidated in Chapter 5. The measured H_2SO_4 concentrations will be presented in comparison to relevant aerosol parameters in order to illustrate the favorable conditions for nucleation (Chapter 6). In particular, the dependency of the concentration of the smallest detectable particles (between 3nm and 6nm) on the H_2SO_4 concentration will be examined. According to this criterion, the mechanism which leads to particle formation is to be deduced. When a similar analysis of H_2SO_4 data obtained previously during the QUEST2-campaign at the same site in 2003 was performed by the University of Helsinki, a linear relationship was found in some cases indicating that the activation mechanism led to particle nucleation. In Chapter 7 it will be examined whether similar conclusions can be drawn in our case.

Chapter 2

Theory

In this chapter a theoretical introduction concerning nucleation theories will be given. First, the major sources and sinks of two sulphurous trace gases, sulfuric acid and its precursor gas sulfur dioxide will be mentioned.

2.1 Atmospheric sulphurous trace gases

In the atmosphere the mole fraction of sulfur is relatively low, however these compounds play an important role in the chemistry of the atmosphere. Reduced sulfur compounds can be oxidized with the help of OH-radicals which leads to a production of sulfate and sulfurous acids like H_2SO_4 and Methane Sulfonic Acid (MSA). The water solubility depends on the oxidation number, thus reduced compounds exist mostly in gas-phase, oxidized compounds (with an oxidation number of 6 or more), are mostly available in the aerosol-phase. About 98 - 120 Tg(S) per year are emitted. Anthropogenic sources make up 75% of the total amount, [Roedel, 2000]. Due to localized sources and sinks there is a large variety in concentration of the different sulfur compounds which also reflects the high reactivity of these molecules.

2.1.1 Sulphur Dioxide

Typical concentrations in the atmosphere of SO_2 are in the range of 5 $\mu g/m^3$ - 100 $\mu g/m^3$. In polluted areas amounts up to 400 $\mu g/m^3$ can be found, especially in winter. The typical life time of SO_2 is about 1 - 4 days. [Roedel, 2000]

SO_2 - Sources

The anthropogenic emissions mainly result from combustion of fossil fuels, 28% of cole and 53% of oil. Biomass burning, industry and traffic also contribute substantially to the release.

The global fossil fuel consumption and thus the production of SO_2 is still increasing, but a detailed analysis shows that with new filter technologies and reduction of the industry working on brown cole a drop of sulfur dioxide emissions was achieved in eastern Europe while in Asia SO_2 emission rates are still increasing through a rising demand, [Roedel, 2000]. The most important natural source in the maritime boundary layer is DMS (Dimethylsulfid) which is released by the ocean plankton. Through oxidation with OH-radicals SO_2 and MSA are created. The marine atmosphere is additionally polluted by the increasing ship traffic [Speidel, 2005]. In the stratosphere SO_2 is either created by COS (Carbonylsulfid) which originates from natural or anthropogenic sources on the ground or is directly injected through volcanism, which is the strongest source for stratospheric SO_2 but varies strongly throughout the year. These emissions are highly localized but SO_2 can be transported in the stratosphere over large distances, [Speidel, 2005]. An anthropogenic source in the upper troposphere and lower stratosphere is the increasing air traffic, which is the only significant source of pollutants in these altitudes. Due to the low natural background concentrations small variations might influence the chemical balance of trace gases [Speidel, 2005].

SO_2 - Sinks

The sinks which remove SO_2 directly are dry and wet deposition and oxidation in the gas - or fluid phase [Aufmhoff, 2004]. Wet deposition comprises all processes by which sulfate is transferred to the Earth‘s surface in aqueous form, [Seinfeld and Pandis, 1998]. SO_2 is poorly water soluble, but together with oxidants like H_2O_2 and O_3, oxidation of SO_2 in water droplets is possible in low altitudes. Oxidation with the help of O_3 plays predominantly a role in the stratosphere, while in clouds mainly H_2O_2 is responsible for the oxidation. This leads to a wash-out effect of SO_2 by clouds. These processes which produce liquid H_2SO_4 solved in water droplets, are known as acid deposition or more common, as acid rain. This acid rain causes several environmental problems like deforestation, acidification of water and soil and accelerated deterioration of buildings [Speidel, 2005].
Dry deposition means the direct transfer of SO_2 to the Earths surface, which proceeds without the aid of precipitation, [Seinfeld and Pandis, 1998]. In the boundary layer dry deposition and cloud processes are the predominant sinks while in the stratosphere and upper troposphere SO_2 reacts mostly with OH-radicals. Half of the SO_2 amount in the atmosphere is oxidized to sulphuric acid or sulfate, the other half is removed by rain or absorbed by the ground, [Roedel, 2000]. Since photolytic oxidation is the most important reaction regarding production of H_2SO_4 in summer a higher amount of SO_2 is converted. The detailed mechanism,

which leads to a production of H_2SO_4 will be described in the next section.

2.1.2 Sulphuric Acid

The concentration of Sulfuric Acid in the atmosphere is relatively low, but due to its extremely low saturation vapor pressure, especially in the presence of water vapor, its impact on the atmospheric chemistry is remarkable. The saturation vapor pressure constitutes $3.3 \cdot 10^{-5}$ hPa at a temperature of 23°C, an addition of 20 % water causes a reduction by a factor of hundred. [Roedel, 2000]. That means, it condenses easily on preexisting particles, but also influences new particle formation and growth, which has further effects on the climate.

H_2SO_4 - Sources

Sulfuric acid originates via oxidation of sulfur dioxide. Thereby the most important reaction in the troposphere which leads to the production of gaseous sulphuric acid is the so-called Stockwell-Calvert-Mechanism:

$$SO_2 + OH + M \longrightarrow HSO_3 + M, \tag{2.1}$$

$$HSO_3 + O_2 \longrightarrow SO_3 + HO_2, \tag{2.2}$$

$$SO_3 + H_2O + M \longrightarrow H_2SO_4 + M. \tag{2.3}$$

The first step (2.1) in this process is temperature and pressure dependent and limiting for the reaction velocity. Values for the rate coefficient k, (at a temperature of 295 K and a pressure of 1000 mbar) are

$$k_1 = 9 \cdot 10^{-13} \mathrm{cm}^3 \mathrm{s}^{-1} \tag{2.4}$$

$$k_2 = 4.3 \cdot 10^{-13} \mathrm{cm}^3 \mathrm{s}^{-1} \tag{2.5}$$

The last step (2.3) is not yet completely understood. Its rate constant k_3 is definitely smaller than k_1, but not exactly known [Finlayson-Pitts and Pitts, 2000]. There are two possible pathways, how H_2SO_4 could be formed from SO_3 and water [Reiner and Arnold, 1993, Reiner and Arnold, 1994, Kolb et al., 1994, Lovejoy et al., 1996]:

$$SO_3 + 2H_2O \longrightarrow H_2SO_4 + H_2O \tag{2.6}$$

$$SO_3(H_2O) + H_2O \longrightarrow H_2SO_4 + H_2O. \tag{2.7}$$

An alternative to equation (2.1) might be a reaction of SO_2 and OH via the formation of the peroxy radical HSO_5, which is described in [Wayne, 2000] and summarized in [Scholz, 2004].

But this mechanism can be neglected due to a very small rate constant.
In polluted air masses the following equation could contribute remarkably to the H_2SO_4 production [Wayne, 2000]:

$$CH_3O_2 \cdot + SO_2 \longrightarrow CH_3O \cdot + SO_3 \tag{2.8}$$

Then SO_3 forms sulphuric acid according to reaction (2.3).
Since large amounts of water vapor are always present in the atmosphere and the reaction of SO_3 and water to H_2SO_4 is very fast, it can be assumed that H_2SO_4 is created, whenever SO_3 is produced.

For the production of H_2SO_4, OH-radicals are required. These OH-radicals are in general very important in the chemistry of the atmosphere, since they react with almost all gases due to their high reactivity. OH belongs to the ROx - group (together with HO_2) of radicals which are in steady state with each other. If OH is consumed, equilibrium can be achieved within a few minutes, [Scholz, 2004].
In the troposphere OH is mainly produced by the photolysis of ozone:

$$O_3 + h\nu \longrightarrow O(^1D) + O_2, \ (\lambda \ \leq \ 320 \text{ nm}) \tag{2.9}$$

$$O(^1D) + H_2O \longrightarrow 2 \cdot OH, \ k = 2.2 \cdot 10^{-10} \text{cm}^3\text{s}^{-1} \tag{2.10}$$

$$O(^1D) + M \longrightarrow O(^3P) + M. \tag{2.11}$$

Ozone is dissociated into oxygen and an excited O-atom in singlet D state (metastable state). The excited oxygen atoms loose their energy through collisions with other molecules. 90 % recombine to oxygen [Finlayson-Pitts and Pitts, 2000] or with oxygen to ozone. About 10 % collide with water molecules which leads to OH formation as in reaction (2.10). The typical lifetime of OH in the troposphere is about 1 second.
Other sources of OH are the photolysis of nitrous acid HONO and the photolysis of hydrogen peroxide H_2O_2, which is less reactive and has a lifetime of about 100s in clean air masses. Since UV-radiation is always required for the OH-production, OH-formation stops almost completely during nighttime. Then reaction (2.8) could become the dominant source for H_2SO_4 since CH_3O_2 has a lifetime of several hours.

Another possibility could be that O_3 reacts with sulphur dioxide as the ozone concentrations are in the ppb-range. But due to a very small reaction rate coefficient it does not

Prozess	$k_{Reaktion}$ [cm^3/s]	typische Konzentration [cm^{-3}]	Prod. rate [cm^{-3} /s]
$OH + SO_2$	$9{\cdot}10^{-13}$	$[SO_2]=2{\cdot}10^8$ (10ppt) $[OH]=3{\cdot}10^6$	540
$CH_3O_2 + SO_2$	$<5{\cdot}10^{-17}$	$[SO_2]=2{\cdot}10^8$ (10ppt) $[CH_3O_2]=4{\cdot}10^8$ (20ppt)	< 4
$HO_2 + SO_2$	$<1{\cdot}10^{-18}$	$[SO_2]=2{\cdot}10^8$ (10ppt) $[HO_2]=4{\cdot}10^8$ (20ppt)	~ 0
$SO_2 + h\nu$	($\lambda < 210\,nm$)	$[SO_2]=2{\cdot}10^8$ (10ppt)	~ 0
$O_3 + SO_2$	$<2{\cdot}10^{-22}$	$[SO_2]=2{\cdot}10^8$ (10ppt) $[O_3]=$ 60ppb	~ 0
Criegee Biradikale $+ SO_2$	$\sim 1.7{\cdot}10^{-11}$ ... ...$3{\cdot}10^{-15}$	$[SO_2]=2{\cdot}10^8$ (10ppt) [Criegee Bir.] $\sim 1{\cdot}10^5$	?

Figure 2.1: Comparison of H_2SO_4 production rates, taken from [Uecker, 2002]

contribute remarkably to the H_2SO_4 production. However during night these processes might become more important as well, when OH chemistry is ceasing.
As mentioned above liquid sulphuric acid can also be produced in acid deposition. That means SO_2, dissolved in water droplets, can be oxidized in the liquid phase in the presence of H_2O_2 and thus react to H_2SO_4. More details can be found in [Finlayson-Pitts and Pitts, 2000] and [Wayne, 2000].

Comparing all different mechanisms, illustrated in **Figure 2.1**, (taken from [Uecker, 2002]) it can be concluded that the oxidation of SO_2 by OH is definitely the most important source during daylight, therefore a derivation of the H_2SO_4 production rate includes only equation (2.1).

Sinks

Particle nucleation is one of the sinks for atmospheric gaseous H_2SO_4, but as high concentrations of H_2SO_4 as well as low preexistent particle concentrations are required for nucleation, condensation on the surface of solid aerosol particle and absorption in water droplets (wet deposition) of H_2SO_4 are more effective and are the main removal mechanisms. These processes exhibit a mass transfer to a surface. Therefore the interactions of carrier gas and particle are observed. The forces acting on aerosols depend on the mean free path λ of a molecule in a fluid and the particle radius R_p. This is taken into account by defining the so-called Knudsen-number as an indicator in order to correctly describe aerosol dynamic theory.

The Knudsen-number is

$$Kn = \lambda / R_p \tag{2.12}$$

Very small particles (Kn >> 1) behave like free gas molecules. In this range which is called the free-molecular regime, kinetic gas theory is a good approximation. Are particles large compared to the mean free path, corresponding to Kn << 1 the surrounding gas can be treated like an ideal fluid. Thus fluid dynamic theories come to application in this continuum regime. In the transition range, for Kn $\approx$ 1, dynamics are difficult to describe theoretically. Usually semi-empirical correlations are used in this case, since there is no general theoretical approach to the problem over the whole range of Knudsen - numbers. However, the mostly used approximation by Fuchs and Sutugin describes observations sufficiently in many cases. Using this approach it is possible to derive from an experimentally obtained aerosol size distribution the loss of gas molecules on the surface of these particles. More details about the Fuchs-Sutugin Algorithm and aerosol dynamics can be found in [Seinfeld and Pandis, 1998].

2.2 Aerosols in the Atmosphere

Considerable attention has been given in recent years to epidemiological studies and research into the health effects of ambient air pollution. Thereby aerosol particles play an important role since due to their size distribution over several orders in magnitude especially small, newly formed particles may be easily inhaled by humans. Still there are significant problems in understanding the processes which underlie new particle formation.
The following paragraph will briefly introduce the basic concept of particle nucleation. Some of the theory will later be needed for analysis of shown experimental data.

2.3 Nucleation

Nucleation theory is a very complex matter and thus can be presented here only in a simplified short picture. **Figure 2.2** illustrates the formation of new particles via nucleation. These new particles may scatter sunlight and eventually act as cloud condensation nuclei (CCN) and are thus of relevance for the climate.

Important mechanisms which may play a key role in the process of new particle formation in the atmosphere are:

- Homogeneous nucleation
- Heterogenous nucleation
- Ion induced nucleation

Homogenous nucleation from the gas phase can be homomolecular, when only one gaseous species is involved, or heteromolecular, in case of two or more types of molecules which then form clusters through coagulation from the gas phase. The most important formation pathways found so far are binary nucleation of gaseous sulfuric acid and water and ternary nucleation of H_2SO_4, NH_3 and water. In contrast heterogenous nucleation takes a preexisting aerosol surface into account onto which a gas then condenses. Ion induced nucleation considers the accumulation of ambient molecules onto preexisting natural gaseous ions. This mechanism matters the most in the stratosphere and upper troposphere where galactic cosmic rays lead to an enhanced ion production rate. But also because of low ambient temperatures which slow down the thermal destruction of newly formed small molecular clusters.

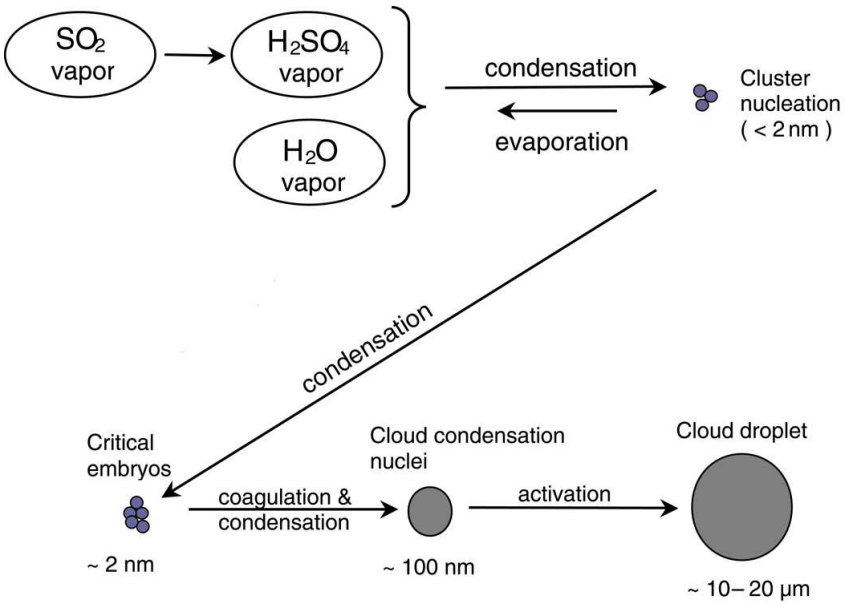

Figure 2.2: Schematic of formation of new particles via nucleation. Clusters are formed from water and sulfuric acid vapor. They grow by condensation and coagulation and can finally affect the climate in acting as cloud condensation nuclei.

2.3.1 Homogeneous Nucleation

The process of nucleation is the condensation of low-vapor-pressure gas species to form new aerosol particles. These newly formed particles are supposed to be spherical and of a radius in the order of nanometers. For spherical particles, the ratio of surface to volume is proportional to the inverse radius. Therefore the impact of a positive surface energy which decreases the negative binding energy is greater for smaller sizes. That means for decreasing particle diameters the vapor pressure, which is required for a equilibrium between fluid and gaseous phase, increases. Thus, the smaller the radius of a particle, the higher the vapor pressure over its surface, i.e. the most likely it is to re-evaporate. Nucleation can therefore only occur through the concepts of supersaturation and molecular clusters, [Mirabel et al., 2001]. The saturation ratio S of a homomolecular system at a temperature T is defined by: S = P/P0, where P is the actual partial pressure of the vapor and P0 its equilibrium vapor pressure. A vapor is supersaturated if S>1, saturated if S=1 and subsaturated if S < 1. A saturated homomelecular gas phase always contains a small number of molecular clusters of two to four molecules among a large majority of monomers. These clusters grow and evaporate very quickly so that their number is approximately constant and there is no stable nucleus at S < 1, [Seinfeld and Pandis, 1998]. In order to nucleate, the gas vapor must be supersaturated such that it is energetically more favorable to accumulate. When S becomes larger than one, the concentration of condensable monomers increases as well as the number and size of the clusters. At a sufficiently large supersaturation, the clusters reach a critical size. This critical size corresponds to a metastable equilibrium at which the clusters can either grow irreversibly by addition of another monomer, leading to formation of a new particle, or evaporate by loss of a monomer, [Mirabel et al., 2001]. These small new particles grow further by condensation of a gas onto their surface but are also scavenged by larger already existing aerosols.

Homomolecular homogeneous nucleation of water vapor does not occur in the atmosphere, since the supersaturation ratios of several hundred percent, necessary to form a cluster out of the vapor phase, are never reached. Therefore nucleation on pre-existing embryos like ion clusters or fine particles, described in the beginning by heterogeneous nucleation is more likely. If particles already exist due to relatively high background pollution e.g. in urban areas, condensation onto these pre-existent particles is more favorable since a smaller saturation ratio is required. Nevertheless, the limiting factor for heterogeneous nucleation is the dynamic of evaporation and condensation onto a surface i.e. the diffusion velocity of

condensable molecules, [Roedel, 2000].
That means homogeneous nucleation is a possible but less likely mechanism in the atmosphere. However, mechanisms more relevant than homomolecular homogeneous nucleation are presented in the next paragraph.

Heteromolecular homogeneous nucleation

Heteromolecular homogeneous nucleation considers a mixture of several species in the gas phase, like the binary system H_2SO_4/H_2O or the ternary system $H_2SO_4/H_2O/HNO_3$. The introduction of a further component in the nucleation process lowers the equilibrium vapor pressure. Therefore less molecules are required in the vapor phase to reach the supersaturation ratio needed for nucleation, [Mirabel et al., 2001]. In other words, the saturation vapor pressure above one component is higher than above a mixture. As a mixture of compounds considerably decreases the energy barrier to form clusters of critical size and the atmosphere always contains a mixture of different gaseous compounds, heteromolecular homogeneous nucleation is most likely to happen in the atmosphere. Typically involved is water, sulphuric acid, but also ammonia (Kulmala et al. 1995), ammonium sulphate, ammonium chloride (Korhonen et al., 1997), and some organic compounds (Hoffmann et al.,1997), which are not yet clearly identified.

At constant pressure the Gibbs free energy is given by

$$\Delta \mathrm{G} = U + p \cdot V - T \cdot S \tag{2.13}$$

From the 2 fundamental theorems of thermodynamics follows that a thermodynamic process develops spontaneously if the Gibbs free energy ΔG diminishes, that means d(ΔG) < 0. A stable state is represented by an extremum of ΔG (ΔG $= 0$), [Roedel, 2000]. That means the evolution of a growing cluster is determined by the Gibbs Free energy.

As an example the formation of a spherical liquid cluster from 2 types of molecules is examined. This process is described by classical binary nucleation theory which was first developed by Flood, Volmer, Neumann, Döring and Reiss [Flood, 1934, Volmer, 1939, Neumann and Döring, 1940, Reiss, 1950]. The change of the Gibbs free energy during formation of such a cluster from the vapor phase depends on the number of molecules of both compounds, it is [Mirabel et al., 2001]:

$$\Delta G = n_a \Delta \mu_a + n_b \Delta \mu_b + 4\pi r^2 \sigma \tag{2.14}$$

with n_i $(i = a, b)$ being the number of the i'th species in the cluster, r being the radius of the cluster and σ the surface tension.
$\Delta\mu_i$ is the change of the chemical potential of species i between the vapor phase and the liquid phase. In thermodynamic equilibrium it can be expressed by

$$\Delta\mu_i = \mu_{il} - \mu_{ig} = -kTln[\frac{p_i}{p_{isol}}] \tag{2.15}$$

in which p_i is the partial pressure of component i in the gas phase and p_{isol} is the vapor pressure of component i over the flat surface of a droplet of the solution. [Mirabel et al., 2001].

ΔG is composed of a volume and a surface term. Nucleation will occur only if $\Delta\mu_i$ is negative, which means that the vapors A and B should be supersaturated with respect to their vapor pressures over the solution. Then in Equation 2.14 the first two terms are negative, while the third term is always positive. For small values of n_a and n_b the surface tension dominates and nucleation will not occur due to a positive ΔG. When the number of molecules of species A and B rises, ΔG increases but the two terms are competing, such that ΔG reaches a maximum. Beyond the maximum the volume term is dominant and ΔG decreases further on, eventually the positive term is compensated. When the free energy surface is studied in the (na, nb)-plane a saddle point is found, where the energy barrier is lowest, [Reiss, 1950]. This point corresponds to the critical cluster of size r*. For r>r* the cluster undergoes irreversible growth since the slope of ΔG becomes negative, [Seinfeld and Pandis, 1998], [Mirabel et al., 2001].

The saddle point on the free energy surface can be calculated by setting

$$\left(\frac{\partial\Delta G}{\partial n_i}\right)_{n_j} = 0 \tag{2.16}$$

by using the Gibbs-Duhem equation this leads to the **binary Kelvin Equation**:

$$\Delta\mu_i + \frac{2\sigma\nu_i}{r^*} = 0 \tag{2.17}$$

(ν_i are the partial molecular volumes: $n_1\nu_1 + n_2\nu_2 = \frac{4}{3}\pi r^3$). The Kelvin equation reveals that the larger the radius r* of the cluster, the smaller the corresponding vapor pressure P. That means, for the same saturation ratio, a small droplet will tend to evaporate more easily than a bigger droplet. Accordingly an increasing saturation ratio decreases the critical radius and also lowers the energy barrier ΔG*.
From the Kelvin equation the radius and the free energy of formation of the critical cluster

can be calculated:

$$r^* = -\frac{2\sigma\nu_i}{\Delta\mu_i} \tag{2.18}$$

$$\Delta G^* = \frac{4}{3}\pi r^{*2}\sigma \tag{2.19}$$

A derivation for the nucleation rate J yields:

$$J = R_{ave} F Z \exp\left(-\Delta G^*/kT\right) \tag{2.20}$$

with R_{ave} being the average condensation rate, F is the number of molecular species in the vapor, Z is the Zeldovich non equilibrium factor (a numerical correction [Stauffer, 1976]), k is the Boltzmann constant and T the temperature. A more detailed derivation is given in [Seinfeld and Pandis, 1998].

A pure H_2SO_4/H_2O - system is adequately described by the binary theory. However a pure H_2SO_4/H_2O system does not correspond to the real conditions. Under real atmospheric conditions the binary system has to be modified. For example due to an ammonia concentration of about 1ppb in the boundary layer, it is assumed that ammonia is also involved in the nucleation process. It is not yet clear whether ammonia is absorbed by the binary system of H_2SO_4 and H_2O, then a binary approximation would be an adequate description or if the condensation process involves the three components directly ([Roedel, 2000]. Then for ternary nucleation the Gibbs free energy of the system has to be changed, but the method to calculate the nucleation rate stays the same like for other thermodynamic theories with more components.

Since the saturation vapor pressure of sulfuric acid is very low it is supposed to participate in particle nucleation. Observations of the composition of nanometer sized particles showed that among water and some still to be specified organic compounds, a certain amount of sulfuric acid molecules is always present. Thus, the question arises to what extend the nucleation rate depends on the concentration of sulfuric acid in the atmosphere.
Since the detection limit of current instrumentation is at about 3 nm, neither critical clusters nor freshly formed particles can be measured. In general the formation rate of a certain particle size is calculated from its measured[1] absolute number concentration.

In order to deduce the formation rate of 3 nm particles, one has to take into account, that after these particles are formed, their fate is determined by growth and cluster scavenging.

[1]The particle number concentration is generally measured with a DMPS (Differential Mobility Particle Sizer

Therefore the actual nucleation rate has to be multiplied with a correction term which includes the competing mechanisms and the size at which particles are observed. The growth rate (GR) can be obtained from experimental observations, the rate of cluster scavenging is proportional to the condensation sink (CS), [Kulmala et al., 2005]. The formation rate of particles of diameter d_m and larger which can be measured is correspondingly determined by the following equation, [Kulmala et al., 2005]:

$$J_m = J^* \exp[0.23(1/d_m - 1/d^*)\frac{CS}{GR}], \tag{2.21}$$

with J^* being the actual nucleation rate and d^* the diameter at which particles form.
J_m is smaller than the actual nucleation rate J^* because not all particles are included in J_m and some are already scavenged. Using this equation, an estimate[2] for the formation rate J_3 of particles of 3 nm in diameter can be obtained. Setting nucleation at 1 nm, J_3 is:

$$J_3 = J_1 \exp[0.23(1/3 - 1/1)\frac{CS}{GR}] = J_1 \exp[-0.153\frac{CS}{GR}], \tag{2.22}$$

This equation exhibits a interrelation of the nucleation rate, which is in this case the formation rate of 1 nm particles and the formation rate of 3nm particles. In experimental observations [Weber et al., 1996, Weber et al., 1997] an implication of sulfuric acid concentrations for particle formation was found. Field measurements during Quest 2 indicated that the formation rate of 3 nm particles can be empirically expressed in terms of a power-law dependency.

$$J_3 \propto [H_2SO_4]^{n3}, \tag{2.23}$$

In analogy it is assumed that the formation rate of 1nm particles shows a similar behavior

$$J_1 \propto [H_2SO_4]^{n1}, \tag{2.24}$$

The formation rate dependency on $[H_2SO_4]$ is illustrated in **Figure 2.3**. By taking the logarithm on both sides, **Equation 2.24** can be transformed into a linear equation.

$$\ln[J_1] \propto n1 * \ln[H_2SO_4], \tag{2.25}$$

This means, that the curve representing J1 is a straight line with the slope n1. Taking the logarithm on both sides of **Equation 2.33**, using the expression in **Equation 2.25** for $\ln[J_1]$ results in

$$\ln[J_3] = n1 * \ln[H_2SO_4] - 0.153\frac{CS}{GR}, \tag{2.26}$$

[2] constant growth rate was assumed, but the growth rate between 1-3nm is actually size dependent

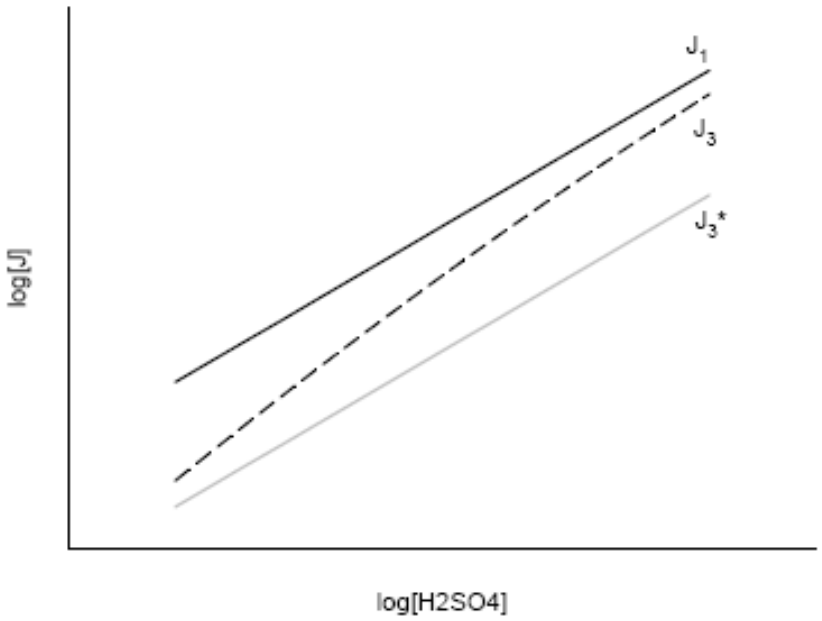

Figure 2.3: Schematic of the dependency of the nucleation rate on the sulfuric acid concentration. J1 is the particle formation rate at 1nm, J3 the particle formation rate at 3nm and J3* the particle formation rate at 3nm if sulphuric acid does not contribute to growth. (taken from [Kulmala et al., 2005])

for the formation rate J_3 of 3nm particles.

It is not clear whether the growth rate GR depends on the presence of H_2SO_4 in the atmosphere. If this is the case, the slope of J3 is necessarily steeper than the slope of J1 because increasing H_2SO_4 causes increasing GR and therefore a decreasing magnitude of CS/GR in (**Equation 2.21**). This case is represented by J_3 in **Figure 2.3**. If H_2SO_4 does not effect the growth rates, the lines in **Figure 2.3** run parallel, (represented by J_3*). That means

$$n1 \leq n3, \tag{2.27}$$

According to the nucleation theorem, the slope determines the number of molecules in a critical cluster [Kashchiev, 1982]. The theorem is a general relation that extends down to the smallest cluster sizes, independent of a specific nucleation theory, [Kulmala et al., 2005]. That means the power-law dependency is determined by the theoretical approach which is chosen to describe the problem.

Thermodynamic theories like binary nucleation predict a very high exponent of more than 10 [Kulmala et al., 2005]. If three components are considered (ternary nucleation) values between 5 and 10 are expected, [Bernd et al., 2005].
However, a very small power-law exponent between one and two was observed on all days during the Quest 2 campaign. [Kulmala et al., 2005]. To investigate the dependency, their time series of the measured sulfuric acid and particle concentrations were compared. In some cases a linear relationship holds between both time series, but that was not seen on all days. Thus a purely thermodynamic approach does not describe the observed phenomenon which means that the model needs to be improved. Further theories exist which could explain a power-law relationship, but lead to a smaller exponent. In this context, we will now present 2 additional mechanisms and derive the dependency of the formation rate on H_2SO_4.
Besides the thermodynamic approach, homogenous nucleation can also be explained by a kinetic process which will be presented now. Hereafter we will elucidate a recently developed approach, the so-called activation theory, which assumes that a combination of homogenous and heterogeneous processes leads to particle formation. This interaction has been neglected so far.

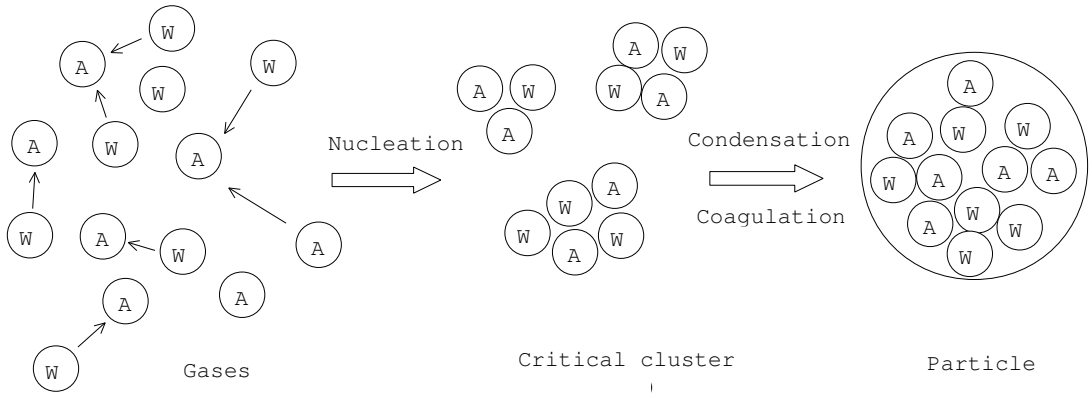

Figure 2.4: Schematic of particle nucleation according to the kinetic mechanism. Clusters containing 2 sulfuric acid molecules are formed by collision of gas molecules, these grow further by coagulation and by condensation of sulfuric acid and water)

Kinetic nucleation

The kinetic approach assumes that a critical cluster consists of 2 sulfuric acid molecules. Since these clusters grow by collision with each other, nucleation is limited only by gas-phase kinetics. Earlier analysis of Quest2 data indicated that this process is more likely than a purely thermodynamical approach [Kulmala et al., 2000, Kulmala et al., 2004b]. Since the gas-phase concentration of ammonia which is supposed to stabilize the clusters [Korhonen et al., 1999, Lee et al., 2003] is clearly higher than the H_2SO_4 concentration [Finlayson-Pitts and Pitts, 2000], it is expected that the formation rate of e.g. ammonium bisulphate clusters is limited by the concentration of sulphuric acid, [Laakso et al., 2004]. According to the nucleation theorem an involvement of 2 H_2SO_4 molecules in the critical cluster causes a quadratic dependency in the nucleation rate J. This becomes understandable from the following equations.

$$A + W \longrightarrow AW + A \longrightarrow A_2W$$

with A being an acid and W a water molecule. k1 represents the reaction coefficient for the first step, k2 the reaction coefficient for the second step.
From the binary reaction kinetics follows a quadratic dependency of the nucleation rate J:

$$J = \frac{dA_2W}{dt} = k_2 \cdot AW \cdot A = k2k1 \cdot A \cdot A \propto A^2, \tag{2.28}$$

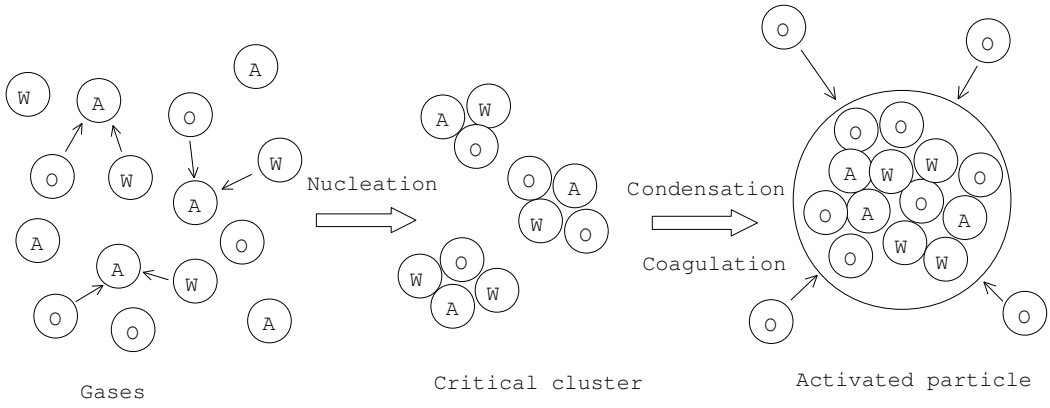

Figure 2.5: Schematic of particle nucleation according to the activation mechanism. Critical clusters containing 1 sulfuric acid molecule are formed, these are activated by condensation of organics to subsequent growth)

Accordingly, J is calculated using the following equation:

$$J = k[H_2SO_4]^2, \tag{2.29}$$

with k being the coagulation kernel between ammonium bisulphate clusters
This means in kinetic nucleation theory the value of the power-law exponent should be 2.
In Figure **Figure 2.4** a schematic of the kinetic nucleation process is illustrated.

Activation of Clusters

Analysis of previous data led to the conclusion that the observed gaseous concentrations of sulphuric acid cannot solely explain the particle formation, [Fiedler et al., 2005], [Laakso et al., 2004]. VOCs are supposed to play an important role, but hints for the existence of a certain threshold size below which low-volatile organic vapors do not contribute to the cluster growth were found, [Laakso et al., 2004].

The activation theory, presented in [Kulmala et al., 2004a], [Kulmala et al., 2005], assumes that ion or neutral clusters containing one sulfuric acid molecule are activated by condensation of organic vapors. Large amounts of so-called thermodynamically stable clusters (TSCs), e.g. ammonia-water-sulphuric acid clusters, are supposed to exist below the detection limit of current instrumentation [Kulmala et al., 2000] which is typically about

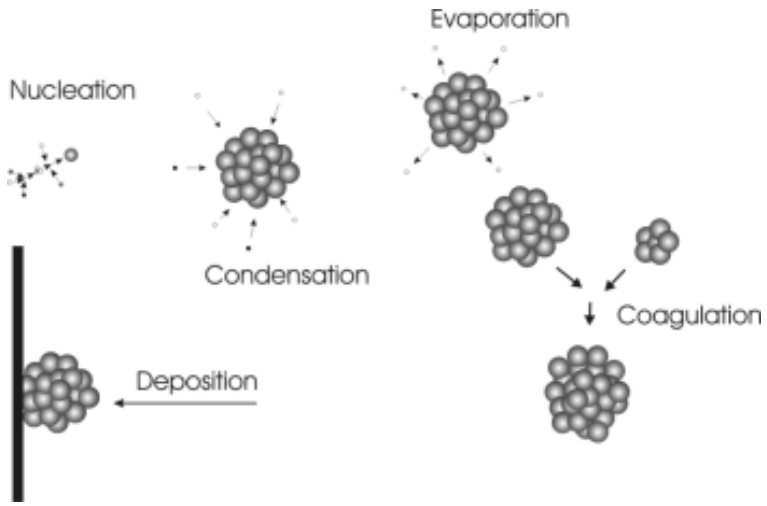

Figure 2.6: Schematic of relevant processes after a particle is formed. The processes of condensation, evaporation, coagulation and deposition determine wether a particle reaches distinct sizes [graphic from Ari Asmi].

3 nm. Presumably, these TSCs grow by self coagulation and condensation of sulphuric acid into a threshold size. That means in the first step growth of the nuclei to the critical cluster involving sulfuric acid and organic vapors takes place, in the second activation via condensation of organic vapors. This mechanism enables new particle formation if these elementary clusters, which consist mainly of water-sulphuric-acid molecules, ammonia and organics, grow beyond the critical size. Thermodynamic interactions between organic and inorganic compounds, which have been neglected so far, are included in this dual-step-process, [Kulmala et al., 2004a]. The processing from gas molecules to a particle according to activation mechanism is depicted in **Figure 2.5**.

After a particle is formed, it grows with the help of low-volatile gases rapidly into detectable sizes via condensation. A distinguishable particle formation occurs only under favorable conditions since TSCs are scavenged rapidly by pre-existing particles. Therefore these particles plays a major role in suppressing the atmospheric new particle formation [Laakso et al., 2004]. Processes which determine the particles fate after it is formed are shown in **Figure 2.6**.

Since in the mechanism a critical cluster containing only one sulfuric acid molecule is involved, the nucleation rate is expected to be linear to the concentration of H_2SO_4. The formation rate will be derived in more detail now on the basis of the activation probability concept, [Kulmala et al., 2005].
The activation probability is derived from the time evolution of an activating cluster concentration which is assumed to be

$$\frac{\mathrm{dN_{clusters}}}{\mathrm{dt}} = \mathrm{kN_{clusters}}, \tag{2.30}$$

With $N_{cluster}$ being the number concentration of clusters and k a proportionality coefficient which is related to the specific nucleation theory.
That means the activation rate is

$$\mathrm{J_{act}} = \mathrm{kN_{clusters}}. \tag{2.31}$$

Since the formation of particles with 3nm in diameter results from the activation mechanism, J_{act} can be treated like the actual nucleation rate J^* in **Equation 2.21**. Combining **Equation 2.21** for the formation of particles of 3nm in diameter or larger and **Equation 2.31**, the observed slope of unity for J_3 can be explained if an ion or neutral cluster activation containing one sulphuric acid molecule is supposed. Correspondingly, the formation rate of 3nm particles is described by

$$\mathrm{J_3} = \mathrm{kN_{cluster}}\exp[0.23(1/3 - 1/\mathrm{d_{act}})\frac{\mathrm{CS}}{\mathrm{GR}}], \tag{2.32}$$

$$\mathrm{J_3} = \mathrm{C_1[H_2SO_4]}\exp[0.23(1/3 - 1/\mathrm{d_{act}})\frac{\mathrm{CS}}{\mathrm{GR}}]. \tag{2.33}$$

in which d_{act} is the size at which activation occurs.

Other vapors than H_2SO_4 are present in the activation process and contribute to J3, but the exact contribution is more complicated to determine [Kulmala et al., 2005].

Summary

According to [Kulmala et al., 2005], atmospheric measurements show that the formation rate of 3nm particles depends on the sulfuric acid concentration with a power-law exponent of smaller than 2. Common theories predict an exponent of more than or equal to 2. A linear relation between the nucleation rate J3 of particles of 3nm in diameter and the H_2SO_4 concentration i.e. an exponent n3 of unity in **Equation 2.23** can be explained with the activation mechanism. A quadratic relationship means that nucleation process occurs according

to a kinetic mechanism.
A comparison by Kulmala [Kulmala et al., 2005] between theoretical formation rates drawn for different models (cluster activation (n3=1), kinetic nucleation (n3=2) and a conservative slope estimate for thermodynamic nucleation(n3=3)) and an experimentally derived formation rate which was calculated from an observed number concentration of 3-6nm particles during the previous campaign in Hyytiälä (Quest2), showed that the activation theory fits best the observed nucleation rate. But the values before noon were in all models underestimated.
In chapter 7 we will analyze the data which was obtained during the recent Bacci4-Quest campaign and will try to specify the mechanism which led to the occurrence of nucleation.

Chapter 3

Measurement Principle

3.1 Chemical Ionization Mass Spectrometry (CIMS)

Ultra-trace gases are due to their low concentrations in the atmosphere very difficult to measure quantitatively. For instance H_2SO_4 occurs in concentrations below 1 pptv. However, on the basis of Ion-Molecule Reactions (IMR) a detection is possible. The following section will present a method called Chemical Ionization Mass Spectrometry (CIMS) - Method which exhibits a very sensitive and selective measurement principle. This method was first applied to detect trace gases by [Arnold, 1978, Arnold and Fabian, 1980, Arnold and Viggiano, 1980, Knop and Arnold, 1985] and further developed by [Eisele and Tanner, 1993].

The measurement principle is based on the systematic transformation of neutral molecules into ions by Ion-Molecule reactions which makes the detection of trace gases with mass spectrometers possible. In a flow reactor neutral molecules of the analyte specifically react with ions which were produced by an ion source. A reaction will only occur if the neutral molecules have a greater gas-phase acidity corresponding to a higher electron affinity than the ions. If the educt ions in turn also have a high electron affinity they are stable with respect to proton transfer and only a few compounds will react with them.
A reaction of trace gas molecules to product ions can be initiated by educt ions which were artificially produced, this method is called Active Chemical Ionization Spectrometry (ACIMS) and applied by our group. Another possibility is the so-called Passive Chemical Ionization Spectrometry (PACIMS) which uses naturally occurring ions in the atmosphere.
Due to permanent or induced dipole moments, ion-molecule reactions have a high cross-section leading to a very high efficiency, such that each collision is assumed to lead to a reaction.

To be able to reason the trace gas concentration from the detected product ions the

reaction kinetics have to be observed.
If only one type of product ions is produced, the ion molecule reaction is generally described by:

$$\mathrm{E}^{\pm} + \mathrm{A} \longrightarrow \mathrm{P}^{\pm} + \mathrm{B} \tag{3.1}$$

where A are the neutral gas molecules to be measured, E are the educt ions, P are the product ions and B a neutral reaction product.

The reaction rate is proportional to the concentration of the neutral reactant A and of the educt ions, $[E^{\pm}]$:

$$R(t) = \frac{d}{dt}[\mathrm{E}^{\pm}] = -\frac{d}{dt}[\mathrm{P}^{\pm}] = -k[\mathrm{E}^{\pm}][\mathrm{A}] \tag{3.2}$$

in which k is the rate coefficient, which is generally temperature and pressure dependent. Backward reaction is neglected.

Assumed that there is a high surplus of A, meaning $[A] >> [E^{\pm}]$, A can be presumed to be constant $[\mathrm{A}](t) = [\mathrm{A}]$. Thus integration of equation (3.2) yields:

$$[\mathrm{E}^{\pm}] = [\mathrm{E}^{\pm}]_0 \cdot e^{-k[\mathrm{A}]\mathrm{t}} \tag{3.3}$$

with $[\mathrm{E}](0) = [\mathrm{E}]_0$.
Under the assumption that there are no further loss processes (i.e. conservation of all charges), the concentration of product ions can be calculated by integration from 0 to t:

$$[\mathrm{P}^{\pm}] = [\mathrm{E}^{\pm}]_0 \cdot (1 - e^{-k[\mathrm{A}]t}) \tag{3.4}$$

Equation (3.4) divided by equation (3.3) leads to an expression for the concentration of the neutral analyte A, the so-called **ACIMS-Formula**:

$$[\mathrm{A}] = \frac{1}{k \cdot t_r} \ln\left(1 + \frac{[\mathrm{P}^{\pm}]}{[\mathrm{E}^{\pm}]}\right) \tag{3.5}$$

in which t_r is the reaction time.
Since the educt ions usually react with several types of molecules,

$$\mathrm{E}^{\pm} + \mathrm{A}_i \longrightarrow \mathrm{P}_i^{\pm} + \mathrm{B_i} \tag{3.6}$$

the above derived ACIMS-Formula, which presumes the bimolecular case needs to be modified. Thus, if reactions with other ions cannot be neglected, the concentration of A is determined by the **Parallel-ACIMS-Formula**

$$[\mathrm{A}_i] = \frac{1}{k \cdot t_r} \cdot \frac{[\mathrm{P}_i^{\pm}]}{\sum_{j=1}^{n}[\mathrm{P}_j^{\pm}]} \cdot \ln\left(1 + \frac{\sum_{j=1}^{n}[\mathrm{P}_j^{\pm}]}{[\mathrm{E}^{\pm}]}\right) \tag{3.7}$$

A detailed derivation is given in [Wollny, 1998].

3.1.1 Measurements of sulfuric acid

If H_2SO_4 is measured with the CIMS-method, $NO_3^-(HNO_3)_n$ is used as educt ions. Due to the high gas phase acidity of HNO_3, reactions with HNO_3-compounds are very selective [Arnold and Fabian, 1980, Viggiano et al., 1997]. H_2SO_4 possesses an even higher electron affinity, (about $0.5eV$). Correspondingly, sulfuric acid reacts according to:

$$NO_3^-(HNO_3)_n + H_2SO_4 \xrightarrow{k_n} HSO_4^-(HNO_3)_n + HNO_3 \tag{3.8}$$

The principle was devised by [Arnold and Fabian, 1980] and advanced by [Arnold and Viggiano, 1980]. Since the upper Ion-Molecule Reaction (3.8) is a bimolecular reaction, the ACIMS-formula (3.5) can be applied:

$$[H_2SO_4] = \frac{1}{k \cdot t} \cdot \ln(1 + R) \tag{3.9}$$

with

$$R = \frac{\sum_n [HSO_4^-(HNO_3)_n]}{\sum_n [NO_3^-(HNO_3)_n]} \tag{3.10}$$

where k is the weighted average of the k_n[1].
According to equation 3.9 the absolute concentrations of gaseous H_2SO_4 can be attained from the measured ratio R, if the rate coefficient k and the reaction time t are known.
The proportionality factor $CF := \frac{1}{kt}$ can be experimentally derived by use of an artificial H_2SO_4 source which delivers a known concentration of H_2SO_4. This calibration procedure will be described in Chapter 5.

Measurements of very low concentrations exhibit a difficulty. Either high reaction time or a high amount of educt ions is required. However, the time is limited by losses to the walls of the flow reactor and ion-ion-recombination, [Fiedler, 2004].

[1] k_n is the rate constant for the reaction in which n HNO_3 molecules are involved

3.2 Quadrupole Storage Mass Spectrometry

As shown above the ratio of product to educt ions needs to be determined for the calculation of a trace gas concentration. Thus individual mass fractions of ions are measured using a mass spectrometer. In particular, a quadrupole storage system is integrated in our CIMS - instrument. In this section the underlying theory and the actual measurement device used by our group in recent campaigns for ground measurements of atmospheric gaseous sulfuric acid will be explained.

Quadrupole mass spectrometer are mass filters working only on the basis of electric fields. These are dynamic devices which means the ion trajectories are determined by changing time-dependent forces, [March and Hughes, 1989].
According to [March and Hughes, 1989], the potential ϕ of a single ion moving in an quadrupole field is described by

$$\phi = \frac{\phi_0}{r_0^2}(\lambda x^2 + \sigma y^2 + \gamma z^2) \tag{3.11}$$

where ϕ_0 is an externally applied electric potential, λ, σ and γ are constants, r_0 is a constant describing the device.
The applied ϕ_0 potential is chosen as a superposition of a radio frequency potential $V \cos \omega t$ and a constant potential U:

$$\phi_0 = U - V \cos \omega t \tag{3.12}$$

In general the equations of motion are given by the force which an ion of mass m and charge e experiences in each direction:

$$F_u = ma = m\frac{d^2u}{dt^2} = -e\frac{\partial \phi}{\partial u} \tag{3.13}$$

in which F_u is the force in u-direction (with $u = x, y, z$) and a is the acceleration of the ion. The motion of a single charged positive ion in an electric quadrupole field is determined by the potential ϕ in equation (3.11). Differentiation of ϕ with respect to x, y and z leads to

$$\frac{d^2x}{dt^2} + \frac{2\lambda e}{mr_0^2}(U - V \cos \omega t)x = 0 \tag{3.14}$$

$$\frac{d^2y}{dt^2} + \frac{2\sigma e}{mr_0^2}(U - V \cos \omega t)y = 0 \tag{3.15}$$

$$\frac{d^2z}{dt^2} + \frac{2\gamma e}{mr_0^2}(U - V \cos \omega t)z = 0. \tag{3.16}$$

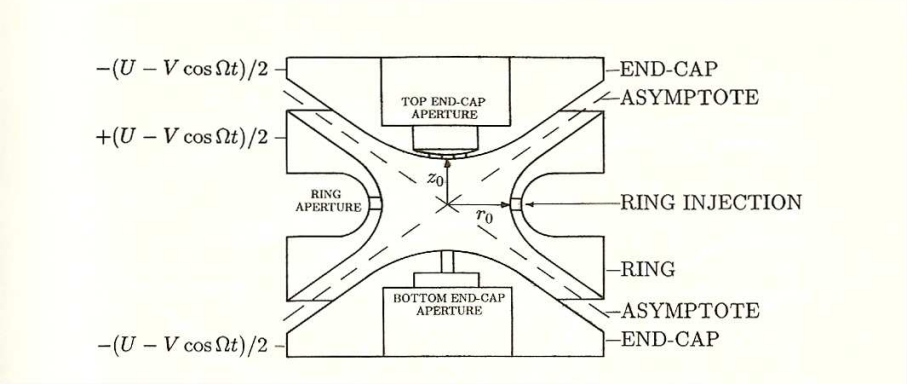

Figure 3.1: Schematic of a Paul Ion Trap. It consists of a hyperboloid ring electrode and two hyperboloid end-cap electrodes, [Gosh, 1995]

By introducing the following parameters

$$\xi = \omega t/2, \qquad a_u = \frac{8eU}{mr_0^2\omega^2}, \qquad q_u = \frac{4eV}{mr_0^2\omega^2} \tag{3.17}$$

we attain the so-called **Mathieu-equation**:

$$\frac{d^2u}{d\xi^2} + (a_u - 2q_u\cos 2\xi)\mu \cdot u = 0 \tag{3.18}$$

with u being x, y or z and μ being λ, σ or γ.

According to the Mathieu-equation the stable conditions for each ion identified by $\frac{e}{m}$ can be calculated yielding values for U and V at which the device is to be operated. For more information, see [Mathieu, 1868, McLachlan, 1947, March and Hughes, 1989].

3.2.1 Ion Trap Mass Spectrometry (ITMS)

The later in the work presented H_2SO_4 data was obtained using an Ion Trap Mass Spectrometer. The electric quadrupole field of this spectrometer is generated by an ion trap. The trap stores the by chemical ionization charged molecules and is able to selectively measure their abundance and mass.

Such an ion trap is realized by a hyperboloid ring electrode and two hyperboloid end-cap electrodes as shown in **Figure 3.1**. The potential ϕ_0 (3.12) is applied at the electrodes. Thus the Mathieu-equation (3.18) provides stable and unstable solutions in dependency of a and q for each type of ion (specified by $\frac{e}{m}$). Values of a and q correspond to values of U

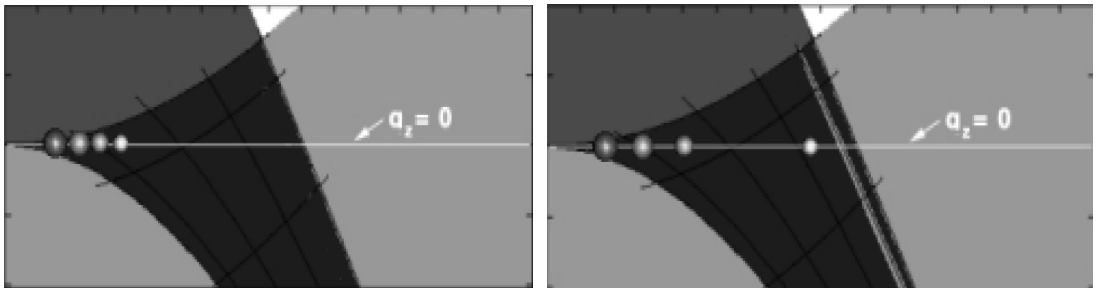

Figure 3.2: Illustration of the Mathieu stability diagram. Shown are mass storage (left) and selection (right) by changing the electrical potential in the trap. [graphic by Finnigan].

and V which lead to stable trajectories in the trap. In **Figure 3.2** the solutions are shown in the (a,q) - plane. The stable solutions are represented by the dark area. The potential can be adjusted in such a way, that a range of masses is kept inside the trap, (left graph of the figure). A mass scan is conducted by gradually changing the voltages applied in the ring electrode of the ion trap. Then masses that were stored are selectively ejected (right graph of the figure).

Figure 3.3 shows the main components of the IT-CIMS instrument which is used by our group in a three dimensional view. This PITMAS (Paul Ion Trap Mass Spectrometer) named after W. Paul who first developed a quadrupole mass filter in 1953, [Paul and Steinwedel, 1953, Paul and Raether, 1955, Paul et al., 1958] is made by Thermo Finnigan and was originally built for the analysis of liquids (electro-spray). The injection system was removed and adapted to measurements of gaseous compounds by our group.

In **Figure 3.4** the interior of the whole setup is shown in more detail. It contains the ion optics, the ion trap and the detection devices. As shown in the Figure it is separated into a prechamber, where the pressure is about $4 \cdot 10^3$ Pa and two pumping stages. In the first pumping stage the pressure constitutes 10^{-1} Pa, in the second it is smaller than 10^{-3} Pa. Ambient atmospheric air streams through the critical front orifice (sampling electrode) into the spectrometer. The ions reach the ion trap by passing the ion optics, composed of two octapoles and an inter-octapole lens, which are oppositely charged to focus the ions. They are then injected into the trap and stored by applying the appropriate potential, such that all masses reach stable trajectories. Helium is passed into the trap as damping gas in order to decelerate the ions and to sustain the trajectories closer to the trap center. When a sufficient

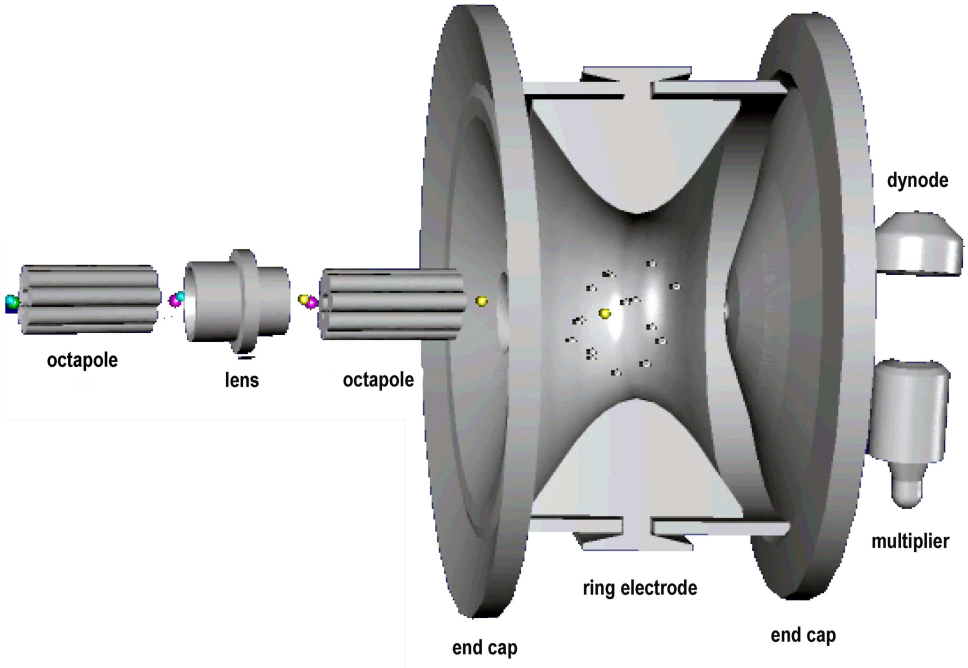

Figure 3.3: Three dimensional view of the ion optic and ion trap of the IT-CIMS instrument [graphic by Finnigan].

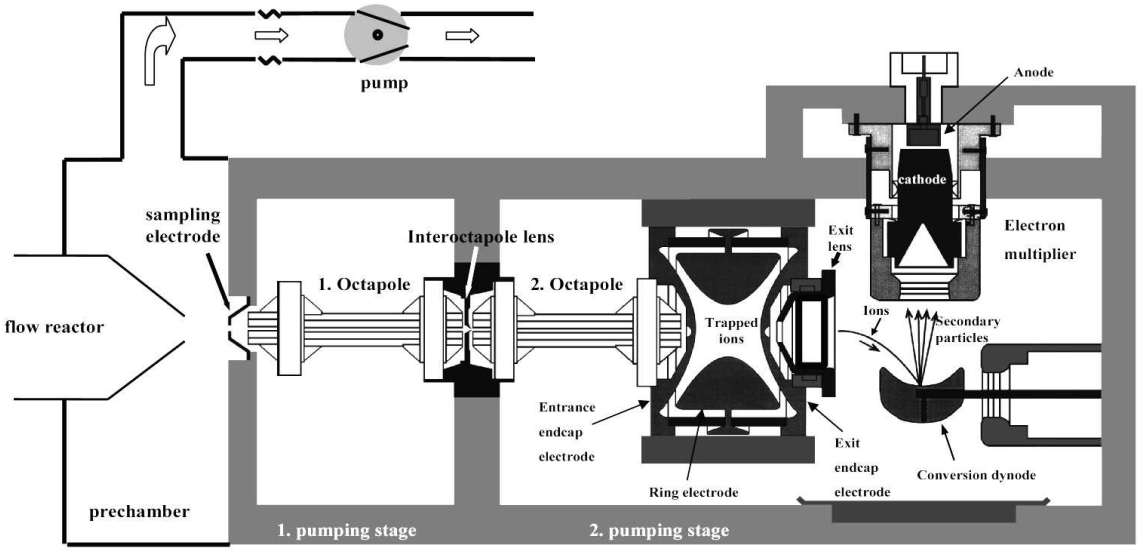

Figure 3.4: Scheme of the IT-CIMS apparatus (PITMAS). It comprises the ion optics, a paul ion trap and the detection device consisting of a Conversion dynode and a electron multiplier. The interior is divided into two pumping stages.

amount of ions is collected within the trap, a mass scan commences. During the scan ions are ejected onto a conversion dynode where they spark electrons, which are detected by an electron multiplier and converted into an ion current. The signal is digitalized and software processed.

Chapter 4

Projects BACCI and QUEST

As the existence of aerosols in the atmosphere is of particular importance for the climate and human health, a lot of research is done on this topic. There are several projects which deal with the sources for increased nucleation and growth of aerosols and interactions between aerosols and the atmosphere. BACCI (Research Unit on Biosphere - Aerosol - Cloud - Climate Interactions) and QUEST (Quantification of Aerosol Nucleation in the European Boundary Layer) are 2 projects out of these with similar objectives concentrating their research work partially on measurements in boreal forest. The focus of the BACCI project lies on effects of secondary biogenic aerosols, global aerosol load, the aerosol-cloud-climate interaction and the relationship between the atmosphere and different ecosystems, particularly Boreal Forest, [Kulmala, 2004]. The objective of the QUEST project is to determine the source and strength of new aerosol particle formation (nucleation) in the European boundary layer.

One of the most important factors to determine with respect to these issues are volatile organic compounds (VOCs) whose impact has remained quite speculative. Especially the growth rates are still not fully explained, VOCs may play a fundamental role and may contribute significantly in initiating nucleation and early growth. Therefore, a description of the gas-phase chemistry and aerosol dynamics including both VOCs released by the biosphere and H_2SO_4 is needed. Thus, a further objective is to extend the recently developed model (University of Helsinki Multicomponent Aerosol model UHMA, [Korhonen et al., 2004]), as detailed as possible, i.e. taking multi-component condensation of organic and inorganic vapors into consideration [Bonn et al., 2005]. To be able to predict regional and global distribution of aerosols and their contribution to radiative forcing and regional pollution, an implementation of aerosol formation for large scale models is desirable. More information about the BACCI-project, research aims and work packages can be found on the BACCI - webpage,

http://www.atm.helsinki.fi/BACCI/.

To approach these research aims the most important method besides laboratory work are continuous field campaigns. Within QUEST three intensive field campaigns were carried out where all types of formation and growth of aerosols have been observed at atmospheric conditions in different European regions to get a qualitative and quantitative analysis of aerosol production. Boreal, Coastal Atlantic and Southern European regional settings were chosen in order to cover nucleation events basing on sea salt aerosols in a coastal, maritime region to be compared with new particle formation in continental regions, both in relatively clean air (Finland) and in polluted air (Italy and Germany).

4.1 The BACCI4-QUEST campaign

These measurements were continued in spring 2005 in the boreal forest region of Finland during the BACCI4 - QUEST campaign. It was part of the QUEST- and the BACCI-project, funded by the EU (European Union) as part of the EU 5th Framework Programme and the EU Network of Excellence (ACCENT).

The campaign focused on aerosol formation and subsequent particle growth. Concerning this matter several questions like nucleation precursors, favorable physical, chemical and meteorological conditions for nucleation and chemical composition of nucleated particles are to be determined. ([Kulmala, 2004], http://www.atm.helsinki.fi/BACCI/). It is also not clear which mechanism leads to the formation of particles. Several approaches exist, which were introduced in Chapter 2, however it could not be clearly classified which mechanism is occurring. Model simulations of Quest 2 data indicated that kinetic processes [Laakso et al., 2004] or activated critical clusters [Kulmala et al., 2005] may lead to nucleation of particles.

The investigations are especially interesting during spring time, when the forest is very active and many organic components are released by the biosphere. Due to the large expanse of boreal forest regions, these newly formed particles are expected to have a remarkable impact on the Earths climate, [Bonn et al., 2005].

This work will mainly present the data from the BACCI4-QUEST campaign which took place in Hyytiälä at the Station for Measuring Forest Ecosystem Atmosphere Relations (SMEAR II) from 04th of April to 16th of May 2005. During this time sulfuric acid concentrations and parameters like light intensity, temperature, humidity, wind speed and wind direction were obtained continuously on 43 days by our group. This data was compared

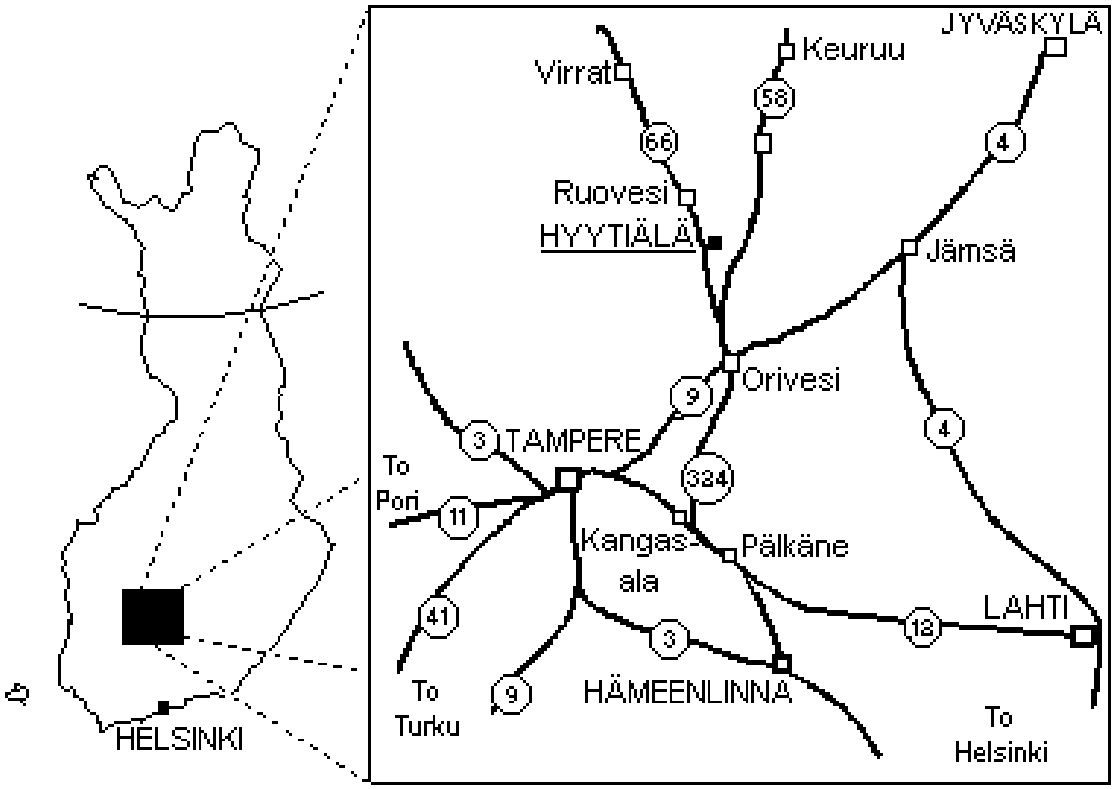

Figure 4.1: Map of Hyytiälä.

with the particle number concentration and the condensational sink which was derived from the aerosol size distribution measured by the University of Helsinki with a DMPS (Differential Mobility Particle Sizer), (explained in [Laakso et al., 2004]). H_2SO_4 measurements were never performed over such a long period at this site.

The Station for Measuring Forest Ecosystem Atmosphere Relations (SMEAR II) is located in Hyytiälä, Southern Finland ($61°51'N, 24°17'E$, 181 m asl[1]). A map is shown in **Figure 4.1**. The SMEAR II tower is surrounded by boreal coniferous forest which is dominated by the 40 year old Scots Pine (Pinus sylvestris) and homogeneous for about 200m in all directions, extending to the north for about 1.2km. For a more detailed description of SMEAR II and instrumentation, see [Kulmala et al., 2001], and www.honeybee.helsinki.fi/smear/. The instruments of the MPIK Heidelberg were situated near the SMEAR II tower in a hut merely next to a sawmill, see **Figure 4.2**. Thus relatively clean continental air was measured since few direct anthropogenic pollution sources were nearby. However, measurements could

[1]above sea level

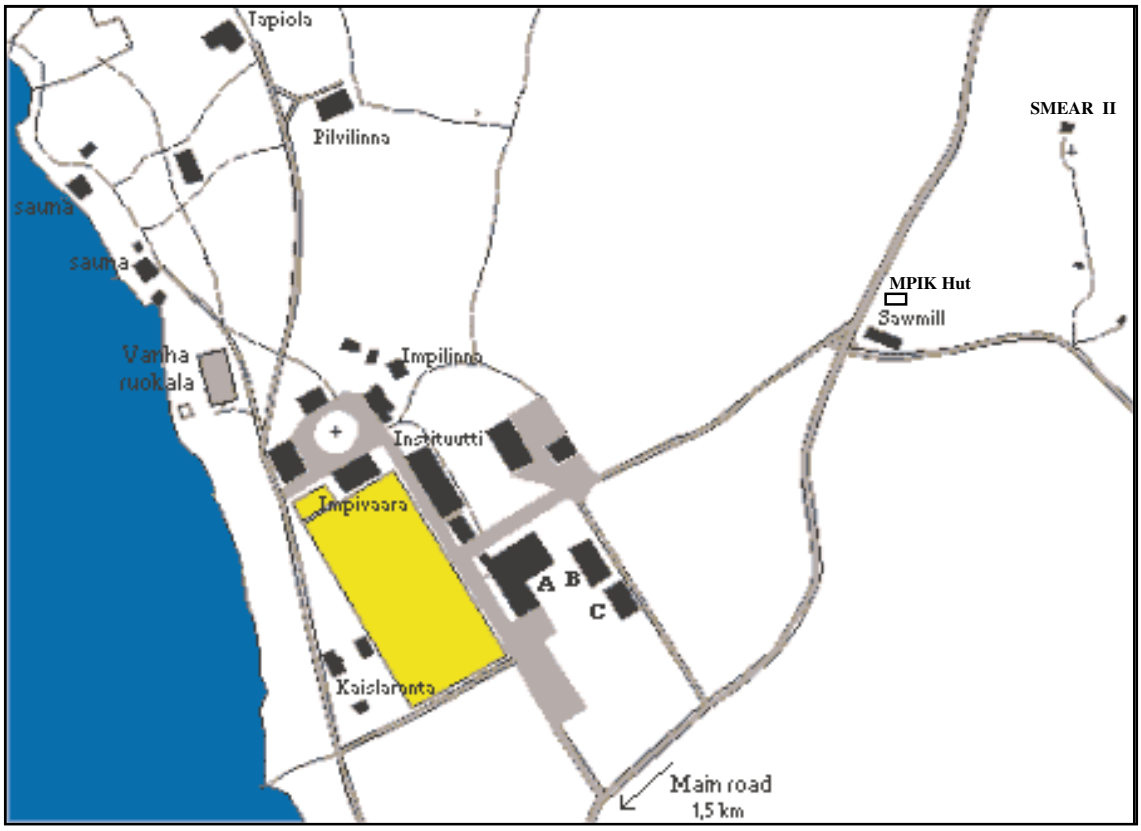

Figure 4.2: Site map of SMEAR II, the H_2SO_4-measurements were located near the sawmill.

temporarily be polluted by the station buildings, the sauna (0.5 km away) and the city of Tampere (60 km away), which are located in a west-south-west direction (215 - 265 degree) from the measurement site.

Seven European groups participated in the BACCI4-QUEST campaign to carry out extensive measurements on aerosol particle properties, trace gases, meteorological and radiation parameters as well as measurements on organic compounds. In recent years SO_2, particle size distribution and solar radiation were continuously obtained throughout the whole year at several European sites. Thus a great store of SO_2 and particle data is available. A model implementation of created H_2SO_4 concentration would be very helpful in order to retrospectively specify nucleation processes concerning the role of H_2SO_4. As elucidated in Chapter 2 the OH-concentration determines the production rate of H_2SO_4. Since OH-radicals are very reactive it is difficult to include all processes which determine the OH-concentration, especially in the presence of reactive compounds like organics. Therefore a specification of processes which contribute to OH-losses are expected to eventually enable the simulation of observed H_2SO_4 concentrations. The measurements accomplished during the BACCI4-QUEST campaign could promote these objectives.

Chapter 5

Experimental Setup and Calibration

In this chapter the experimental setup for the measurement of sulphuric acid concentrations and some other parameters during the BACCI4-QUEST campaign will be described: Atmospheric air streams through an inlet system into the flow reactor where the atmospheric sulfuric acid reacts with educt ions to product ions that are both detected in the mass spectrometer. The detailed measurement principle was described in Chapter 3. For the calibration, the setup had to be changed, this will be mentioned as well.

5.1 Experimental Setup

The principle setup during the BACCI4-Quest campaign used in Hyytiälä was very similar to the experimental setup during QUEST 2 which was described by Scholz [Scholz, 2004] and can be seen in **Figure 5.1**. This section will briefly review the most important parts.

Sulfuric acid has a very high affinity to stick to surfaces. In order to keep the losses of sulfuric acid to the walls of the instrument as low as possible the construction of the inlet system needs to fulfil certain requirements. On the one hand the inlet system needs to be very short, on the other hand it is important that the measured air has not been in contact with the walls of the container, so the inlet outside the container has to be long enough. If the probe is part of a parallel air stream, drifts against the walls and with it losses are minimized. Therefore a metal tube of 4 cm in diameter (KF40) inside a plastic tube of 20 cm in diameter was positioned on the roof of the container. With the help of a strong ventilation system that produced a flow of about 10^3 slm (standard liters per minute), the air was drawn through an ion cone with an aperture of 6 mm that closed the flow reactor (KF40-tube)

on the inlet side. The PITMAS side of the flow reactor was enclosed by a critical orifice of 1.5 mm in diameter. The flow reactor pump produced a continuous flow of about 19,9 slm. (Obtained with a calibration of the critical orifice.) Since the flow through the ion cone is limited, the pressure inside the flow reactor is slightly below the atmospheric value. Atmospheric pressure and downstream flow through the critical orifice result in a pressure of about $4{\cdot}10^3$ Pa behind the critical orifice, regulated with a butterfly valve in the exhaust tube. Inside the flow reactor temperature was measured as well. It was kept at 30°C by heating belts in order to have constant measurement conditions. The resolution of the mass spectrometermight also be improved [Scholz, 2004].

5.1.1 Inlet System, Ion Source and Flow Reactor

Opposite to the critical orifice in a distance of 0.5cm is the front plate of the PITMAS with a sampling orifice of 0.15 mm in diameter. A vacuum of $1 \cdot 10^{-5}$ Torr inside the PITMAS is achieved by its turbo pump. With the help of the flow reactor pump, a constant pressure in the spectrometer can be provided.
Other parameters like gas flow velocity, humidity and pressure were sampled in the exhaust tube (see **Figure 5.1**) in order to decrease possible disturbances in the flow reactor. The exhaust gas of the flow reactor pump and the mass spectrometer pump are disposed through an air cleaning system working with active coal. For a more detailed description, see Scholz [Scholz, 2004]. The setup with chosen length values during BACCI4 - QUEST can be seen in **Figure 5.1**.

In the upper part of the flow reactor is located the ion source. The educt ions $NO_3^-(HNO_3)_n$ were produced in a Polonium α-source (activity 63 MBq in February 2005, half-life 138.4 d), which is shown in **Figure 5.2**. This source has previously been developed by our group ([Scholz, 2004], [Hanke, 1999], [Uecker, 2002]) and is preferred to the glow-discharge ion sources because of its stable ion production and its clean educt ion spectrum, required for measurements of an ultra trace gas like sulfuric acid. A gas mixture of HNO_3 and N_2 (3 slm HNO_3 in N_2 of purity 5.0), the so-called source gas[1] was led into the ion source to produce ions which react with NO_2 (1.75 slm NO_2 in N_2(2500 ppmv) that was added straight after the source. The required educt ions $NO_3^-(HNO_3)_n$ are produced accordingly. Furthermore OH radicals which otherwise would react with atmospheric SO_2 and would cause an artificial H_2SO_4-signal are consumed. That means NO_2 acts as so-called quench gas, it eliminates the

[1]The gas mixture was produced in a permeation oven with a permeation tube by Dynacal and had a volume mixing ratio of 100ppbv.

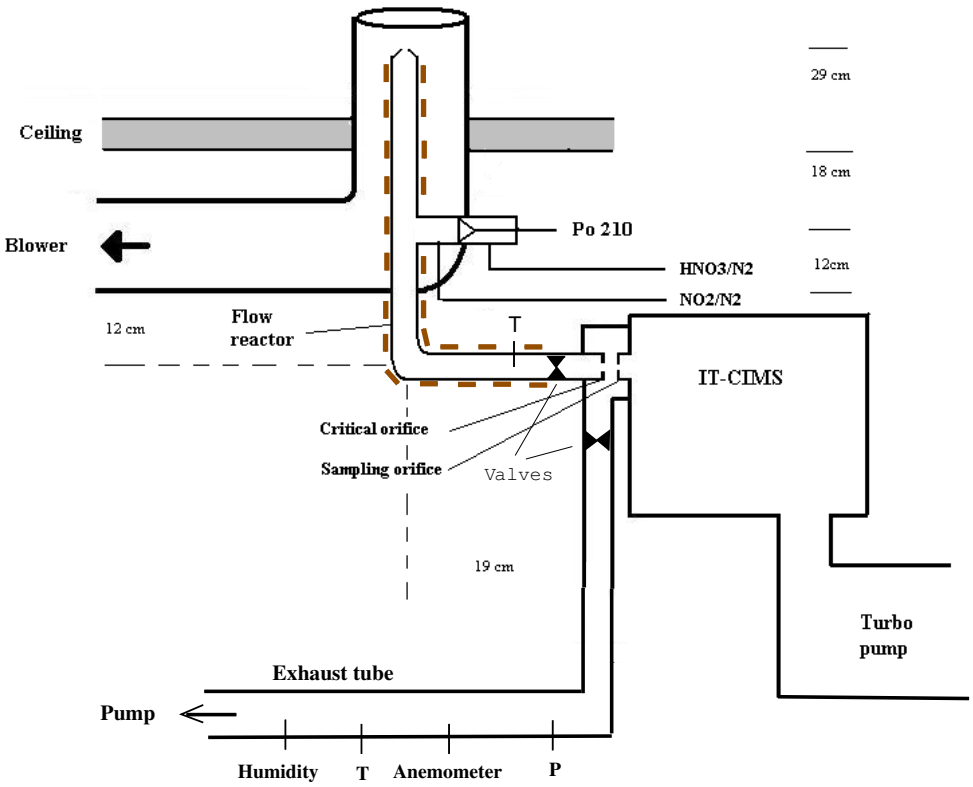

Figure 5.1: Schematic of the experimental setup. It comprises an inlet system with blower, a tempered flow reactor, an ion source (middle), sensors (exhaust tube) and an IT-CIMS instrument (PITMAS) for detection.

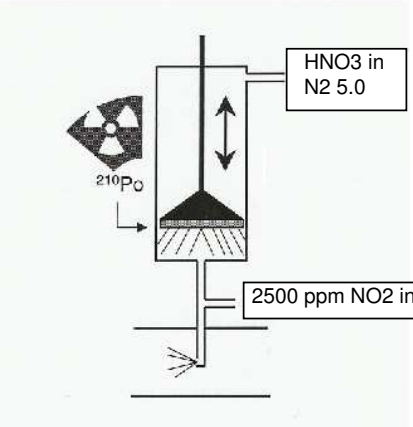

Figure 5.2: Schematic of the Polonium ion source, 3 slm (standard liters per minute) HNO_3 in N_2 are passed into as source gas and 1.75 slm NO_2 in N_2 were added in order to produce the educt ions.

artificial H_2SO_4-signal.

On the way to the spectrometer, a part of the $NO_3^-(HNO_3)_n$ ions react with the H_2SO_4 contained in the atmospheric air.

$$(NO_3)^-(HNO_3)_n + [H_2SO_4] \longrightarrow HSO_4^-(HNO_3)_n + HNO_3 \tag{5.1}$$

With a flow of 19.9 slm and a distance of 45 cm between ion source and spectrometer the ion residence time is about 1.7 s. During this time the reaction takes place until the ions are sampled by the sampling orifice of the PITMAS. The measured mole fractions of the analyte is proportional to the ratio of product ions and left over educt ions.

5.1.2 Data Accumulation

All instrumental values during operation were recorded with the software TUNE PLUS from Finnigan. A so-called HEADER, which shows all relevant values, is stored for each spectrum. The spectra are recorded with the Finnigan software LCQ. The acquired spectra have a resolution in time of 4 minutes. The maximum injection time constituted 8s, that means the ion trap was opened for sampling for 8s. The number of scans, which were averaged, was 30. Therefore the ion trap was opened 30 times 8 seconds in total, that means 240 seconds were needed until one spectrum is generated. The used AGC (Automatic Gain Control) function closes the ion trap automatically if a certain number of ions in the trap, in our case $4 \cdot 10^9$, is exceeded. That might happen if the sampling time is very long and suddenly a burst of ions streams into the trap.
During the campaign in Finland a rough data analysis (Quicklooks) was already made to control the instruments and to compare preliminary results with other groups.

5.1.3 Additional Data

The additional data was stored with the help of 2 personal computers. Pressure and temperature sensors were mounted at different points of the setup, see **Figure 5.1**. This data and those obtained from flow controllers and dew point sensors were recorded via a pulse code modulation (PCM) system, which is described in [Aufmhoff, 2004].

Additional meteorological data was acquired using a commercial weather station (WM 918 by Huger Electronics). This includes several quantities like temperature and humidity inside and outside plus wind measurements on the roof of the container. The data was collected via the software SBWeather. A LUX sensor for measurements of solar radiation was installed on the roof as well.

5.2 Calibration

The calibration source was originally built up by Reimann [Reimann, 2000] for calibration of OH-, HO_2- and RO_2-radicals. In his diploma - thesis a detailed description can be found. This section will show the principles and the calculation of the calibration factor during our measurements. All formulas are taken from [Reimann, 2000].
The calibration is based on the artificial production of a defined amount of sulfuric acid that is measured with the mass spectrometer and compared with each other.
In irradiating humid air with an UV lamp, OH radicals are produced via the photolytic dissociation of water.

$$H_2O + h\nu \longrightarrow H + OH \qquad \lambda < 185\text{nm} \tag{5.2}$$

These OH-radicals can further react with the added SO_2 and form H_2SO_4. One OH forms exactly one H_2SO_4-molecule and if the reaction time is long enough ($> 10^{-3}$ s) all OH-radicals will react. Therefore the OH-concentration determines the H_2SO_4-concentration. The OH-concentration [OH] can be calculated from

$$[OH] = [H_2O]_0 \, \sigma_{H_2O} \, \Phi_{OH} \, \Psi \, \tau = [H_2SO_4] \tag{5.3}$$

where $[H_2O]_0$ represents the water vapor concentration, σ_{H_20} the photo dissociation cross section of water at 185 nm, Φ_{OH} the quantum yield, Ψ the photon flux and τ the irradiation time.

The principal setup can be seen in **Figure 5.3**. Humid air is passed through a suprasil tube and along the way irradiated by UV-light, the photo current is measured via a photo diode. Between the UV lamp and the tube an interference filter is mounted to obtain a single wavelength of 185nm. The originated OH radicals stream then into the flow reactor where they react with the added SO_2 to H_2SO_4. Since the suprasil tube was placed on the roof of the container, the temperature and pressure in the tube correspond to the values outside measured by the Weather Station.

5.2.1 Calculation of the Calibration Factor

The OH-concentration is calculated according to Equation 5.3. All determining parameters can be obtained from the measured quantities during calibration.
The *water vapor concentration* is

$$[H_2O]_0 = \frac{p_{H_2O}}{p_0} \cdot \frac{T_0}{T_{sr}} \cdot \frac{N_A}{V_0} \tag{5.4}$$

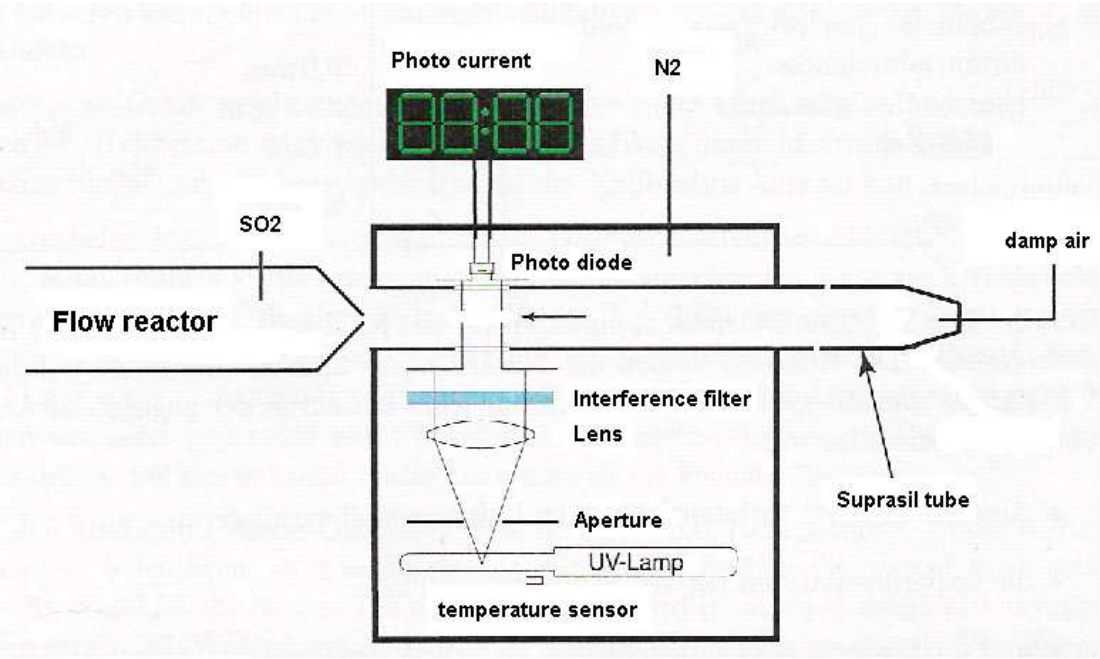

Figure 5.3: Schematic of the experimental setup during calibration: Calibration source (right) and flow reactor (left) with SO_2-injection. The source consists of a UV-lamp, photo diode and suprasil tube where humid air is irradiated.

so with

p_{H_2O}	=	475.05 Pa $\pm 14\%$	Water Vapor Partial Pressure[2]
T_0	=	273.15 K	Standard temperature
N_A	=	$6.022045 \cdot 10^{23}$ mol^{-1}	Avogadro constant
p_0	=	$1.01325 \cdot 10^5$ Pa	Standard pressure
T_{sr}	=	284.35 K	Suprasil tube temperature
V_0	=	$2.241383 \cdot 10^{-2}$ m^{3}mol^{-1}	Standard volume

we get

$$[\mathrm{H_2O}]_0 \approx 8.7 \cdot 10^{22}\ m^{-3} \tag{5.5}$$

with

the *absorption cross-section of water* at 185 nm	σ_{H_2O}	=	$7.14 \cdot 10^{-24}\ m^2$
the *quantum yield*	Φ_{OH}	=	$1.0 \pm 1\%$

and the *photon flux*

$$\Psi = \frac{I\lambda}{sAhc} \cdot k_d \cdot k_t \cdot (e^{k_\sigma} + \rho \cdot e^{-k_\sigma}) \tag{5.6}$$

with

$$k_\sigma = (\sigma_{O_2}[\mathrm{O_2}] + \sigma_{H_2O}[\mathrm{H_2O}]_0) \cdot R \tag{5.7}$$

[2]Calculated with approximation (7.16) in [Reimann, 2000].

and with the following measured values and constants

I	=	$3.0 \cdot 10^{-8}$ A $\pm$ 3.3%	Photocurrent
λ	=	$1.849 \cdot 10^{-7}$ m	Wavelength
s	=	0.097 A/W $\pm$ 2.7%	Spectral sensitivity
A	=	$1.3 \cdot 10^{-5}$ m^2	Sensitive surface area of the photodiode
h	=	$6.626 \cdot 10^{-34}$ Js	Planck-constant
c	=	$2.998 \cdot 10^{8}$ m/s	Light velocity
k_d	=	$1.380 \pm 1.4\%$	Correction factor for beam divergency
k_t	=	$1.293 \pm 0.8\%$	Correction factor for transmissivity
ρ	=	$0.085 \pm 1.4\%$	Reflection ability
σ_{O_2}	=	$1.4 \cdot 10^{-24}$ m$^2 \pm 22\%$	Absorption coefficient of O_2 at $\lambda = 185$ nm
σ_{H_2O}	=	$7.14 \cdot 10^{-24}$ m$^2 \pm 2.8\%$	Absorption coefficient of H_2O at $\lambda = 185$ nm
$[O_2]$	=	$5.0 \cdot 10^{24}$m^{-3}	Oxygen concentration in suprasil tube[3]
$[H_2O]_0$	=	$8.7 \cdot 10^{22}$m^{-3}	Water vapor concentration from above
R_s	=	0.01 m	Radius of the suprasil tube

we get

$$\Psi \approx 4.6 \cdot 10^{16}\ s^{-1}m^{-2} \tag{5.8}$$

as a value for the photon flux.

The *irradiation time* is

$$\tau = \frac{k_l\, b\, p_{sr}}{\chi_r\, p_0} \cdot \frac{T_0}{T_{sr}} \cdot \pi R^2 \cdot \left(1 - \sqrt{1 - \frac{\chi_r}{\chi_R}}\right) \tag{5.9}$$

[3]Calculated with ideal gas law ($0.2 \cdot pN_A/RT$).

with the values

k_l	=	$1.078 \pm 5\%$	Correction factor for the length of the irradiation zone
b	=	0.015 m	Aperture width
p_{sr}	=	$9.90 \cdot 10^4$ Pa $\pm 0.4\%$	Pressure in the suprasil tube
χ_r	=	13.65 slm $\pm 10\%$	Flux soaked up by the flow reactor
χ_R	=	18.4 slm $\pm 10\%$	Total flux in the suprasil tube

we obtain

$$\tau \approx 1 \cdot 10^{-2} s \tag{5.10}$$

Now with the equations (5.4) to (5.9) equation (5.3) can be solved yielding a sulphuric acid concentration of

$$[H_2SO_4] = [OH] = 2.1 \cdot 10^{14} \text{ m}^{-3} \pm 30\% \tag{5.11}$$

and we obtain for the calibration factor according to CF= $[H_2SO_4]/ln(1 + R)$ with R measured, a value of

$$\text{CF} = 2.12 \cdot 10^{15} \text{ m}^{-3} \pm 30\% \tag{5.12}$$

The calibration procedure was carried out several times throughout the day with varying temperature, pressure and different fluxes (18.1 - 20.3 slm). Thus several calibration factors were obtained. With 5 of them taken into account according to the maximum stable conditions, the average was calculated, yielding for the

$$\textbf{Calibration Factor} \qquad \textbf{CF} = 2.07 \cdot 10^{15} \text{ m}^{-3} \pm 30\% \tag{5.13}$$

which was used in the evaluation of the sulphuric acid measurements.

Chapter 6

Measurements

Besides the calibration factor, discussed in the previous chapter, further corrections have to be made in order to obtain the atmospheric H_2SO_4 concentration. This and the corrected data acquired during the Bacci4-Quest campaign in Hyytiälä will be presented in the following chapter and compared to other measured and derived parameters.

6.1 Further Considerations

6.1.1 Background

According to the ACIMS - formula the concentration of the analyte (trace gas) is determined by the ratio R of product to educt ions, which is in this case the ratio of measured $HSO_4^-(HNO_3)$ (mass 160) to measured $NO_3^-(HNO_3)$ (mass 125). Since mass lines of clusters with 0 or more than 1 nitric acid molecules can be neglected [Uecker, 2002], only these dominant two lines were taken into account. This ratio R has to be corrected according to the background signal of the measurement device, which is caused by e.g. electronic noise or $H_2SO_4^-$ stuck on the walls of the measurement device. Possible ways of $H_2SO_4^-$ formation are:

$$(HO_2)^-(CO_2)_n + [SO_2] \longrightarrow HSO_4^- + CO_2 \tag{6.1}$$

$$(HSO_4)^- + [HNO_3] \longrightarrow HSO_4^- + HNO_3 \tag{6.2}$$

To determine the background value a filter made of several layers of paper was assembled on top of the inlet system instead of the ion cone. Since atmospheric H_2SO_4 is absorbed on this filter the measured signal then results only from the background. A more detailed description can be found in [Scholz, 2004]. These background measurements were carried out on most days for about one hour either early in the morning or after sunset in the evening. Similar

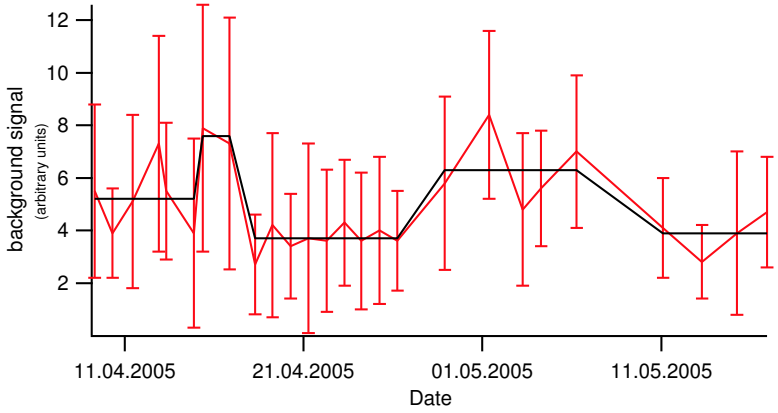

Figure 6.1: Measurements of the background: The background value of the mass line 160 ($HSO_4^-(HNO_3)$) with error bars is plotted in arbitrary units versus time.

to the background measurements carried out in Heidelberg [Fiedler, 2004] the signal was not constant in time but changed during the campaign every few days, the values were at around $5 \cdot 10^5$ cm^{-3}. The time series of background values is shown in **Figure 6.1**. As indicated in the figure several time intervals were found. For each interval an average background value was obtained according to which the H_2SO_4 measurements on each day were corrected.

The background signal was, as shown in [Fiedler, 2004], independent of the educt ions concentration with mass 125, that means only the product ion concentration has to be corrected. This indicates, that neither artificially created H_2SO_4 nor atmospheric H_2SO_4 stuck on the walls, seems to be the major source for the background signal. Otherwise with an increased mass of 125 amu we would also detect more product ions. Most of the background apparently originates from electronic noise or artificially created HSO_4^- in the trap.
The background signal is reflected in the detection limit of approximately $5 \cdot 10^5$ cm^{-3}.

6.1.2 Temperature factor

Since the flow reactor is tempered in order to maintain stable conditions during detection. Atmospheric sulfuric acid is detected at a temperature of 10°C to 30°C degrees higher than under outdoor conditions. Due to an expansion of a sample air parcel which flows through

the reactor, less molecules per cm^{-3} can be found than at a lower temperature while the existent concentration is the same. Therefore, a further correction has to be applied and the H_2SO_4 concentration values multiplied with a factor F_{Temp} to compensate this discrepancy.

$$F_{\text{Temp}} = \frac{T_{fl}}{T_{out}} \tag{6.3}$$

with

T_{fl} Temperature in the flow reactor

T_{out} Outdoor Temperature

The total error of the measured H_2SO_4 concentration was in the range of $1 \cdot 10^6$ cm^{-3}. The total error consists of the absolute error, which is given by the fluctuating background signal and the relative error. The relative error is composed of the systematic and the statistic error of the calibration factor, which was in total $\pm$ 30 %. The absolute error is dominant for small concentration values, for large values the relative error is mainly determining.

6.2 Experimental Data

6.2.1 Sulfuric Acid

During the BACCI4-QUEST campaign in Hyytiälä from 04th of April to 16th of May, H_2SO_4 was constantly measured during the day and also during cloud free nights. These data are shown in the appendix, Figure A.1, A.3 - A.36. On the following pages some selected days are presented, two event-days (**Figures 6.2 and 6.4**) and two non-event days (**Figures 6.5 and 6.6**). The values are corrected according to the background and the temperature difference between an sampled air stream and the tempered flow reactor, as mentioned above. In the graphs time gaps can be seen, which are caused by periods of calibration, background measurements or are due to no operation of the instrument during nights. Occasionally they can result from cloudy or rainy weather. If the H_2SO_4 concentration is very low and background corrected negative values can sometimes be obtained. This data refers to H_2SO_4 abundances below the detection limit of the instrument.

6.2.2 Additional Data

For each day the H_2SO_4 concentration was compared to relevant parameters to be able to understand the processes of particle formation and growth. Definitions and explanations of these parameters will be given in this section. The diurnal courses will be analyzed to characterize the favorable conditions for nucleation. Thereby we will concentrate exemplary on typical days.

In **Figure 6.2** the H_2SO_4 number concentrations, as well as particle and weather parameters are shown. Light intensity, relative humidity, temperature and atmospheric gaseous H_2SO_4 are important factors which determine the formation of particles. These quantities were measured by our group and are shown in the first three panels. Concentrations of small particles (between 3 nm and 6 nm (N3-N6) and particles between 6 nm and 12 nm (N6-N12)) as well as the condensation sink are illustrated in the forth and fifth panel. Measurements of the particle number concentrations were carried out by Pasi Aalto, University of Helsinki using a Differential Mobility Particle Sizer (DMPS).
The DMPS samples the number concentrations of particles between 3 and 800 nm diameter, divided in 40 different size classes, with 10 minutes time intervals. From these data the Condensation Sink was derived, which will be explained in more detail further down. A more detailed description of a DMPS is given in [Laakso et al., 2004].

On 15 days out of 43 days, nucleation events with class 1 or 2 were observed. A classification of events can be found in the work of V. Fiedler, [Fiedler, 2004]. Class 1 means a distinct formation of new 3 nm particles with subsequent extended growth, on the DMPS plot it appears as a typical 'banana' shape. For class 2, clear formation but less distinctive growth can be seen and class 3 events show some formation, but very poor growth. In the nucleation analysis only class 1 and 2 events were taken into account.
In **Figure 6.2** the measured H_2SO_4 concentration and relevant parameters are shown for the 13th of April, an exemplary event day of class 1.

Light Intensity

The light intensity was detected with a LUX sensor, that was installed on the roof next to the inlet system. The sensitivity maximum lies between a wavelength of 500nm to 600nm which corresponds to the range of visible light. UV radiation with wavelength $\lambda \leq 320nm$ is responsible for the formation of $O(^1D)$ via photolysis of ozone and thus provides the opportunity that H_2SO_4 can be created from SO_2. The visible light gives an adequate estimate

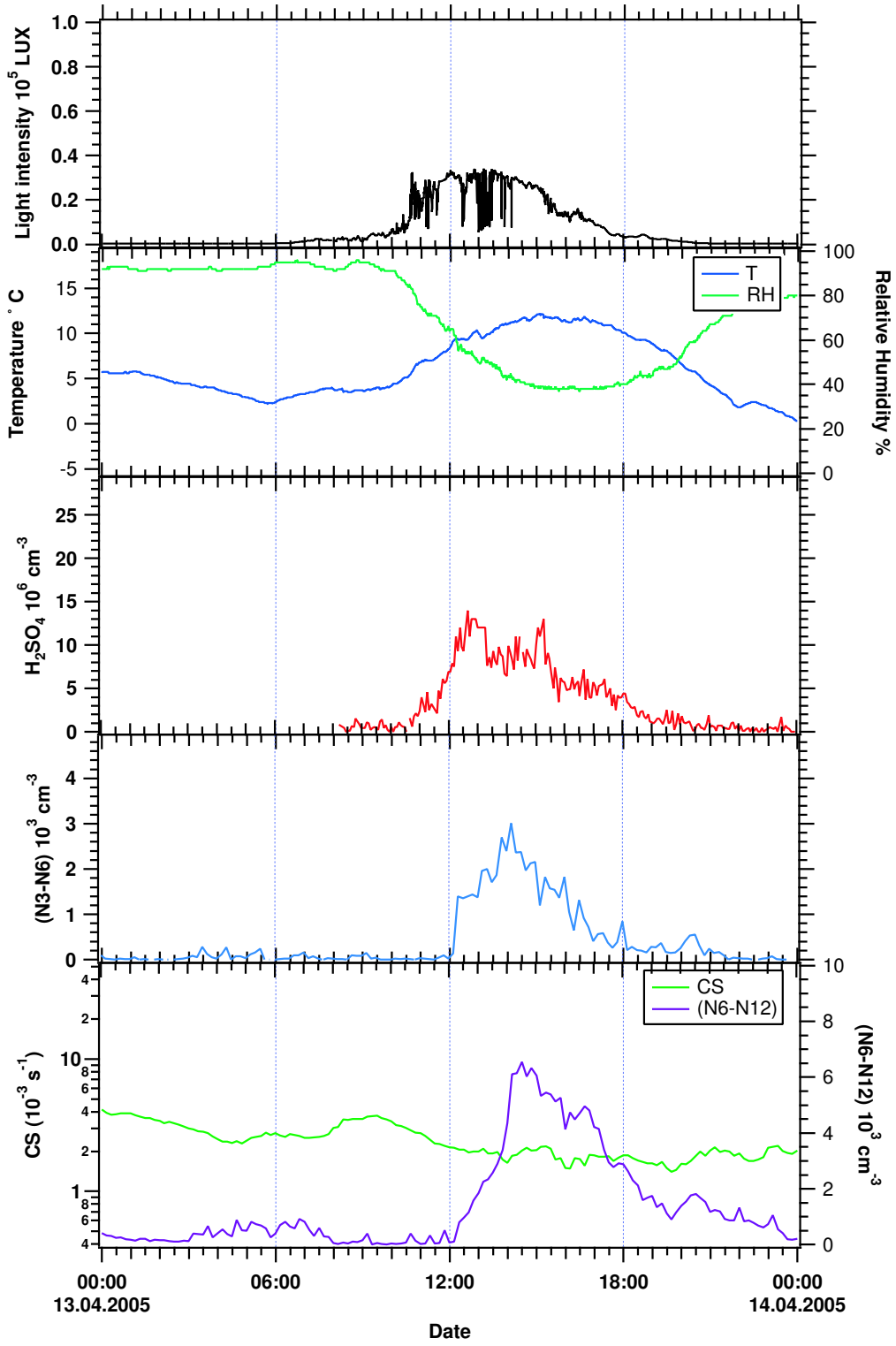

Figure 6.2: Relevant parameters measured on the 13th of April (Event-day). Sulfuric acid number concentrations are compared to particle and meteorological parameters. Significant increase of H_2SO_4 was observed around noon. In the morning relative humidity was high and the temperature relatively low. A distinctive nucleation event with subsequent growth was recorded in the early afternoon.

for UV-B radiation, since the course is very similar except in the morning and evening, when short wavelengths are filtered out due to the longer pathway through the atmosphere [Roedel, 2000]. On the 13th of April the H_2SO_4 concentration nearly follows the course of the visible light. It was a sunny day in the morning with some clouds around 1pm, correspondingly we can see a small gap from 1pm to 3pm.

Temperature, Relative Humidity

These data were accomplished with a Commercial Weather station, mentioned in chapter (5). The typical diurnal courses can be seen on this day. The temperature increases during the day and correspondingly decreases the relative humidity. It was a cold and clear day with a relative humidity of more than 90 % in early morning and about 60 % before nucleation. The admixture of water vapor to gaseous sulphuric acid diminishes the saturation vapor pressure, such that condensation and with it particle formation is favored due to a decreased condensation barrier. Concerning temperature, lower values are more favorable for nucleation since evaporation of molecules from forming clusters is less probable, thus particles grow easier. If the temperature is too low, sometimes the air becomes very dry as on the 19th or 20th of April, (see A.11, A.12 in the appendix.)

Particle Number Concentration (N3-N6) and (N6-N12)

From the DMPS measurements, which samples relative number concentrations of particles, the absolute particle concentration was calculated. (N3-N6) is the number concentration of particles between 3 nm and 6 nm. Freshly formed particles with diameters around 1 nm cannot be detected immediately due to the instrumental limitation of the DMPS. Newly formed particles first need to grow to a detectable size of 3nm. Since sulphuric acid is the main precursor gas and key compound for new particle formation, usually the shape of the time series of both curves is similar but the N3 curve is delayed, it follows the H_2SO_4 curve with a certain time lag. In the next chapter we will go into the timeshift analysis, which is used in case correlations between the two curves are observed. On 13th of April a time lag of about one hour can be seen. Particles seem to grow very fast, reflected in the steep slope of the N3 curve. In the next panel (N6-N12), particles between 6 nm and 12 nm are plotted (right axis) to observe the subsequent growth of these originated particles. These two curves exhibit a similar pattern, that means growth as expected for a class 1 event follows. **Figure 6.3** shows a DMPS - plot for this day. With the typical shape it corresponds to the (N3-N6) and the (N6-N12) curve in **Figure 6.2**.

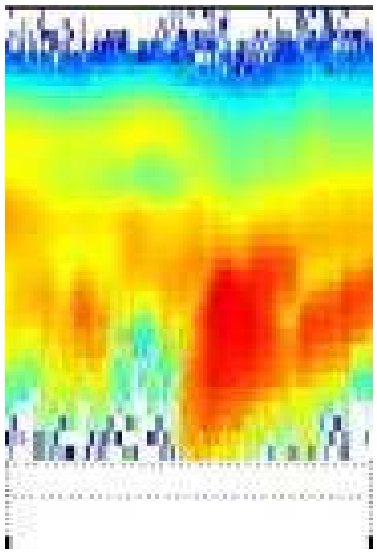

Figure 6.3: DMPS plot for the 13th of April. It shows the particle data obtained with an Differential Mobility Sizer and comprises the particle diameter versus time and the particle number concentrations as color-code. The typical shape for an event day can be seen. Small particles are formed and grow to larger sizes.

Condensation Sink

The aerosol condensation sink (CS) reveals how rapidly molecules will condense onto aerosols [Kulmala et al., 2005] and is determined from size spectra measurements. The dimension is s^{-1} and it can be interpreted as the inverse lifetime of the gaseous H_2SO_4 molecules. The CS - value can be calculated from

$$\mathrm{CS} = 4\pi D \int_0^\infty r\beta_M(r)n(r)dr = 4\pi D \sum_i \beta_M r_i N_i \tag{6.4}$$

with D being the diffusion coefficient (in our case the diffusion coefficient of sulphuric acid), β_M the transitional correction factor, N_i and r_i are the number concentration and the radius of the particles in the i'*th* size class measured with a DMPS system at dry relative humidity.

Higher values of CS indicate a higher concentration of particles, that means a higher degree of pollution. For nucleation clean air, corresponding to a low CS-value is more favorable, since the possibility for condensation on existing particles is smaller. Actually on many event days, as on the 13th in (**Figure 6.2**), a small drop of CS can be seen before nucleation occurs. That agrees with the observations of Fiedler that mostly clean air masses reached the measurement site before particle formation was observed [Fiedler et al., 2005]. Strong

variations in the CS-curve reflect the influence of anthropogenic pollution sources. During this campaign the CS-curve was relatively smooth with little variations except one week from 25th of April to 29th of April, where strong pollution can be seen mostly in the night. During these days particle formation was much lower. Due to a decreasing CS-value during the day, events of class 2 still occurred. These observations illustrate the sensitivity of new particle formation to the value of CS.

To clarify the key compounds for nucleation, another event day, but of class 2 and two non-event days are shown on the following pages in (**Figures 6.4, 6.5 and 6.6**). In **Figures 6.4** the H_2SO_4 concentration is in the same range as on the 13th of April corresponding to high light intensity. However an event of class 2 occurred, which may be explained by the high CS values suppressing the growth of freshly formed particles to detectable sizes. Thus relatively low concentrations of (N3-N6) were measured, also subsequent growth turned out less distinctive.
In **Figures 6.5** a non-event day is illustrated. The H_2SO_4 concentration was too low attended with a very low light intensity, caused by a high cloud cover on this day. In addition the Relative Humidity ranged between 40 % and 70 %, which is comparatively low. On the 5th of May, see (**Figures 6.6**) the Relative Humidity was quite high, but the weather was bad with low light intensity. Additionally high CS values were obtained which indicates a higher degree of pollution. Therefore only very little H_2SO_4 was created and no particle formation can be seen.

The remaining data measured during the BACCI4-Quest campaign is shown in the appendix. Divided into event and nonevent days, these quantities exhibit quite similar diurnal variations. Comparatively high amounts of H_2SO_4 were obtained during this campaign, on many days the concentrations ranged around $1.0 \cdot 10^7 cm^{-3}$ to $1.5 \cdot 10^7 cm^{-3}$ and even reached a peak value of $2.9 \cdot 10^7 cm^{-3}$. During the QUEST2-campaign in 2003 which took place at the same site the measured H_2SO_4 concentrations were very similar, but a little lower [Scholz, 2004]. In Heidelberg during QUEST3 the concentrations were also lower, up to $1.6 \cdot 10^7 cm^{-3}$, [Hoffmann, 2004].

From the comparison of H_2SO_4 particle and meteorological parameters can be concluded that a minimum concentration of H_2SO_4 seems to be required and a low number of preexistent particles may favor nucleation. The H_2SO_4 concentrations were mostly high when a nucleation event was recorded. However there were also some days, especially in the end

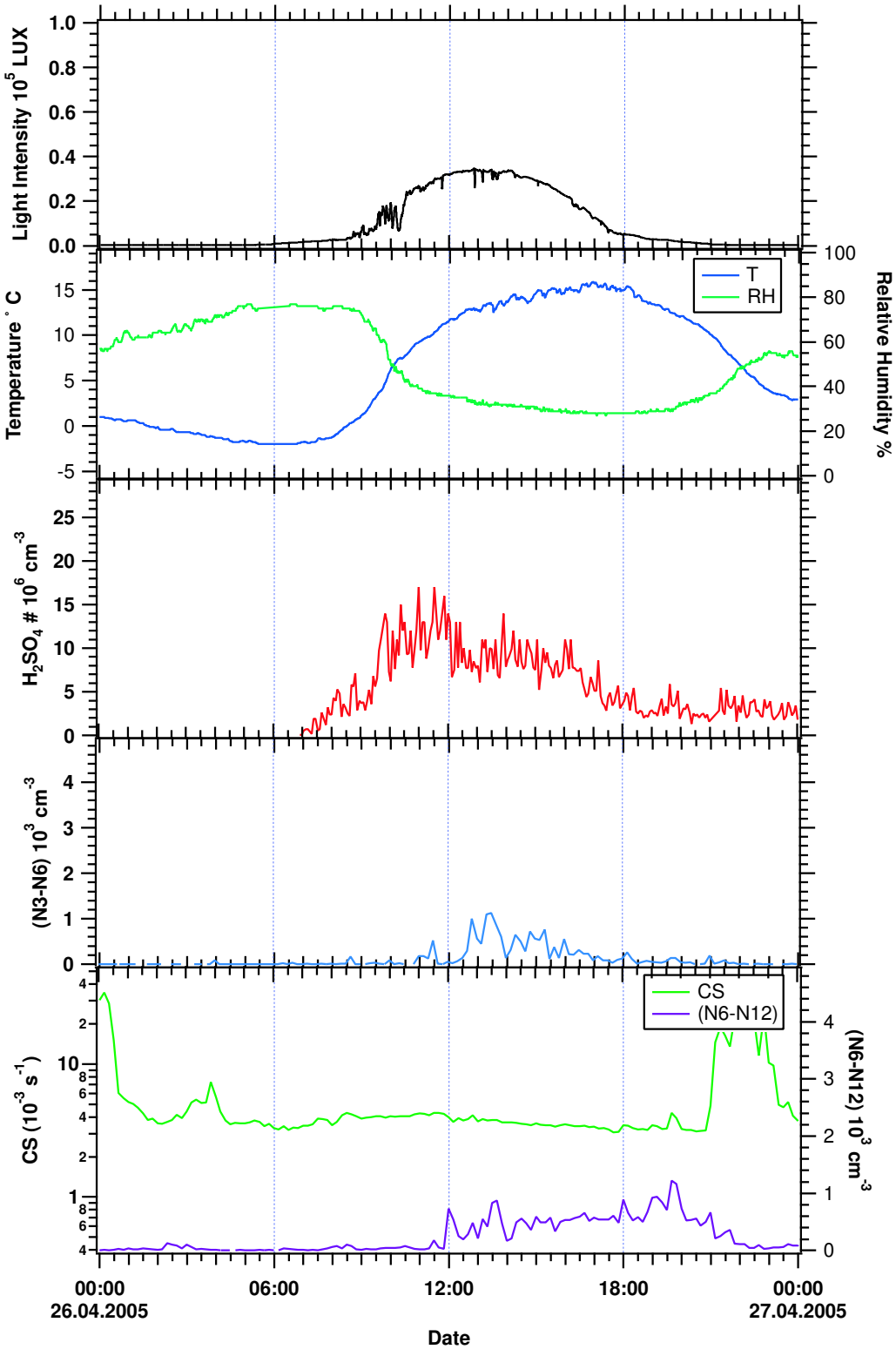

Figure 6.4: Relevant parameters measured on the 26th of April (Event day). Sulfuric acid number concentrations are compared to particle and meteorological parameters. Relatively high H_2SO_4 concentrations but comparatively modest particle concentration was observed. The CS values were very high during the nights.

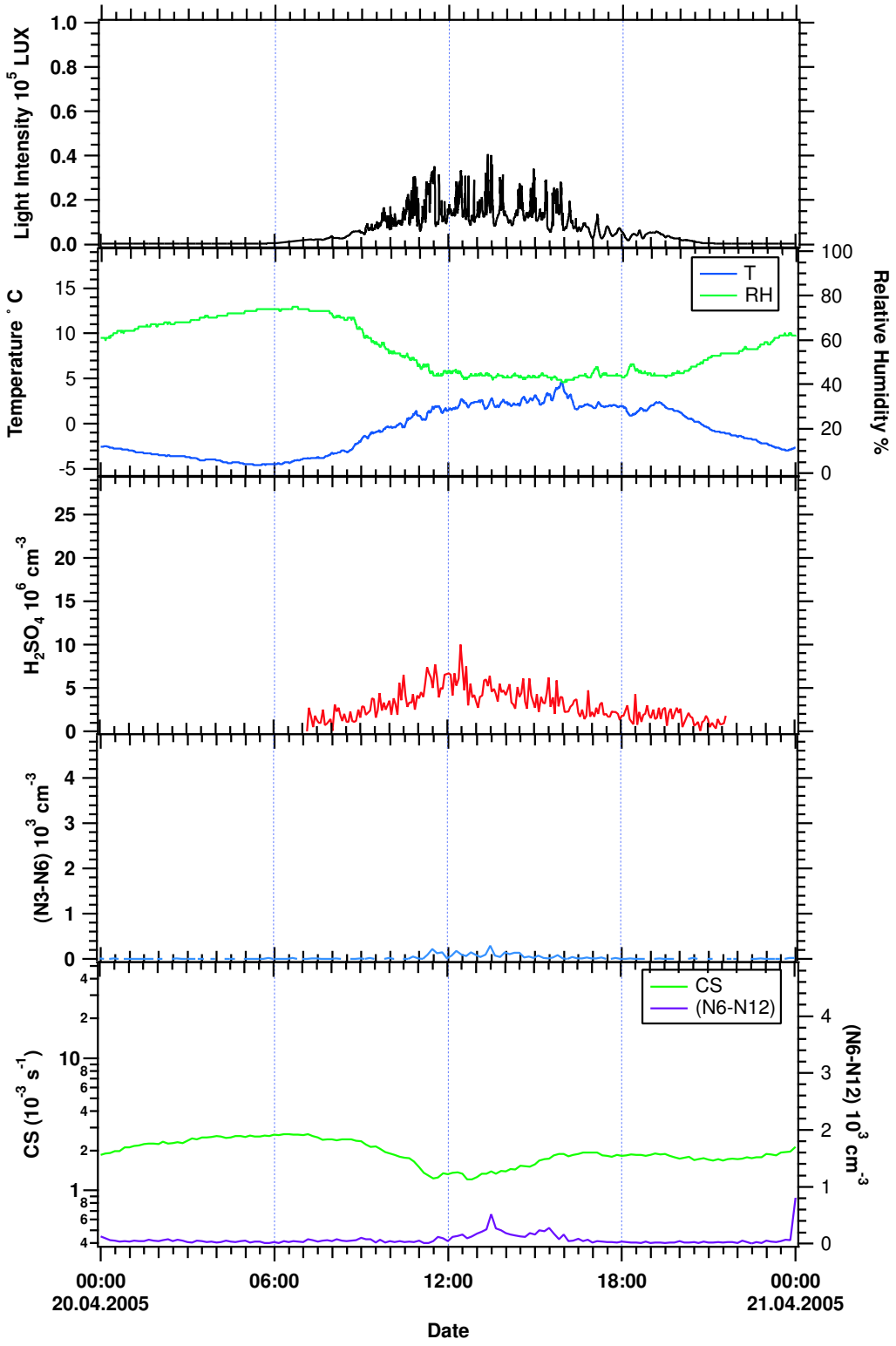

Figure 6.5: Relevant parameters measured on the 20th of April (Non-event day). Sulfuric acid number concentrations are compared to particle and meteorological parameters. Low light intensity, temperatures and relative humidity were measured. Also no distinct formation of small particles occurred.

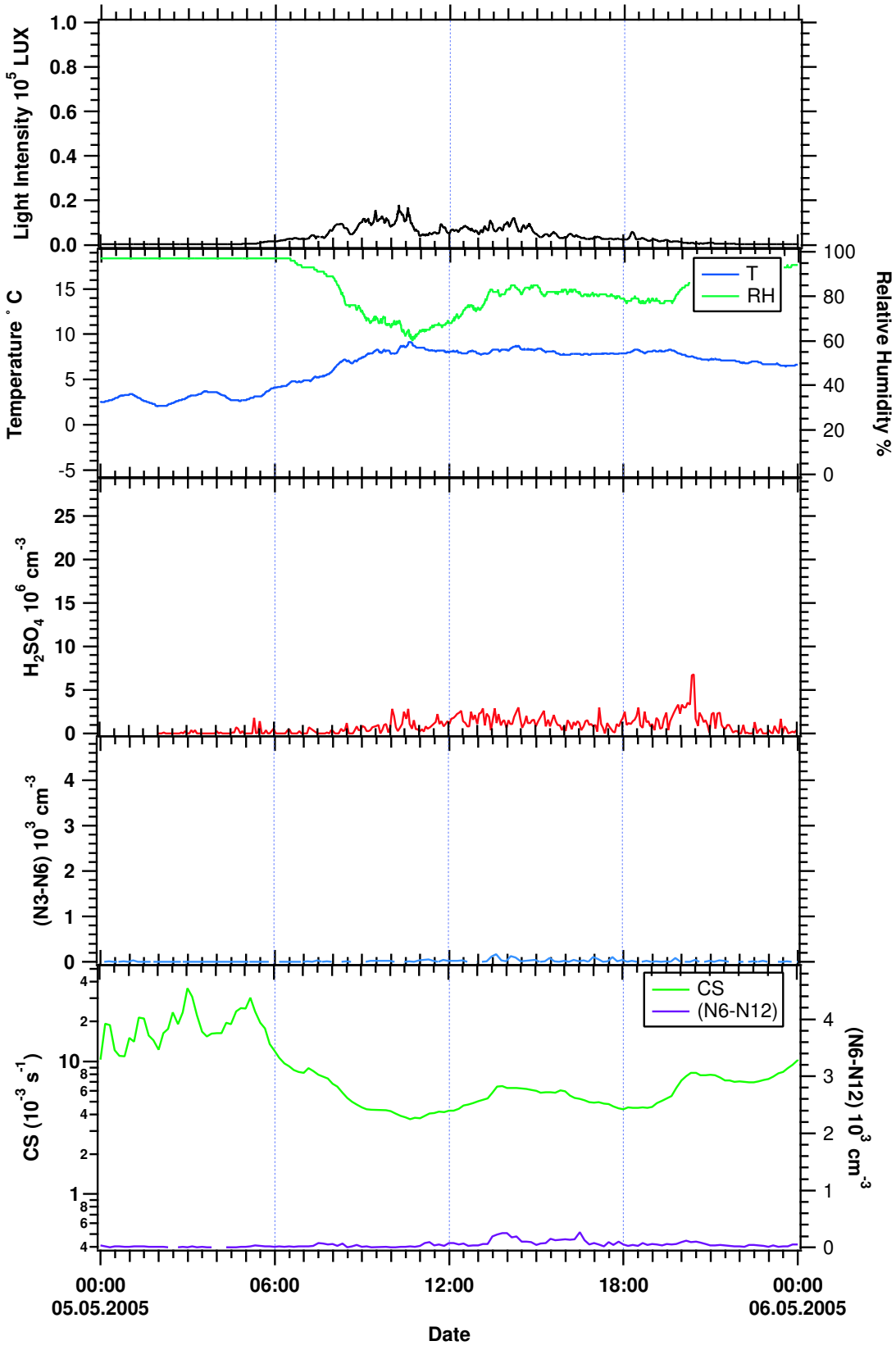

Figure 6.6: Relevant parameters measured on the 5th of May (Non-event day). Sulfuric acid number concentrations are compared to particle and meteorological parameters. Corresponding to a very low light intensity small amounts of gaseous sulfuric acid were produced.

of the campaign in middle of May, on which the H_2SO_4 concentration was relatively low, but still comparatively high particle concentration was observed. Are these days included, the threshold amount of H_2SO_4 seems to be at $(0.2 - 0.4) \cdot 10^7 cm^{-3}$. These low H_2SO_4-concentration values might result from an overcorrection according to the background, that means through averaging, the values might be overestimated during the last days of this campaign. Another reason could be that due to a higher temperature and an increased release by the forest organic vapors become more important during this time. There is evidence that aerosol formation might also be initiated by oxidation products from biogenic VOCs as discussed in [Bonn et al., 2005]. This nucleation mechanism seems to compete with sulfuric acid induced processes. Due to a higher concentration of VOCs biogenic induced nucleation might occur more often. However this process and the role of VOCs is not yet completely understood [Bonn et al., 2005].

Chapter 7

Results and Discussion

The formation of ultrafine particles has been frequently observed in the continental boundary layer. These measurements indicate that the concentration of particles with a diameter between 3nm and 6nm (N3-N6) clearly depends on the atmospheric H_2SO_4 concentration. However, the question remains to what extent sulfuric acid plays a role in formation of these nano-sized particles. Previous measurements during Quest2 reveal a power-law dependency with an exponent in the range of 1-2 [Kulmala et al., 2005]. In order to address this problem in detail, two different theoretical approaches exist as shown in Chapter 2. At first, the kinetic approach which describes the process of nucleation on the basis of gas-phase-kinetics. It assumes, that particles emerge by collision of ammonia - bisulphate - clusters. A quadratic dependency of the nucleation rate on the ambient sulfuric acid concentration results if a corresponding critical cluster consists of only two acid molecules.
The second theory, describing the so-called activation mechanism presumes that critical clusters only contain one H_2SO_4 molecule among several water and organic molecules. Above a critical size, coagulation and condensation leads to further growth. The formation rate of 3nm particles, derived on the basis of the activation theory shows a linear dependency on the H_2SO_4 concentration.
In the following chapter both theories will be used to describe new particle formation observed during the field campaign BACCI4-QUEST. In order to assess which mechanism (activation or kinetic) is involved in the particle nucleation observed, we will investigate the measured (N3-N6) and sulfuric acid concentration. In case the (N3-N6) shows a linear dependency on the amount of H_2SO_4, activation theory holds. An observed quadratic dependency would favor the kinetic approach.

7.1 Sulfuric Acid Dependency of the Particle Concentration

The diurnal time series of the measured gaseous H_2SO_4 concentration will be compared to the concentration of particles between 3nm and 6nm. This is attained by matching the (N3-N6) to the linearly as well as quadratically plotted H_2SO_4 concentration. As described above, a classification of the exponent as either one or two would then be taken to refer to the respective underlying mechanisms in the nucleation process.

7.1.1 Timeshift Analysis

In order to be able to compare the measured sulfuric acid and the (N3-N6) time series, the time lag between both curves as it is shown in **Figure 7.1** needs to be considered. This lag results from the small size of freshly formed particles being below the detection limit of typically 3nm which instrumentally cannot be accessed. Therefore some time is needed for the particles to grow until they reach detectable sizes. This effect can be corrected by explained in more detail in [Fiedler, 2004].
The span of time particles need until they are grown to a detectable size is determined by the time segment Δt which is obtained from comparing the average slopes of the first increase of both curves as indicated in **Figure 7.1**.

Next, the sulfuric acid time series is shifted according to the derived time lag such that, in a third step, the time series of sulfuric acid and (N3-N6) can be plotted against each other. The resulting scatter plot now provides information on the relationship between formation of small particles and sulfuric acid concentration. This information may then, in a final step, be used to decide whether in fact the kinetic or activation mechanisms are underlying the observed particle nucleation.

Results of the Timeshift-Analysis

H_2SO_4 was consistently observed to precede significant increases of (N3-N6) and is therefore likely to play a role in initiation of particle nucleation. It is assumed that during this time particles grow from 1nm to 3nm. In some cases we also found that periods of increased sulfuric acid concentrations overlap periods of high (N3-N6) on both sides, resulting in a greater overall duration. This behavior is illustrated in (**Figure 7.3, upper panel and Figure 7.2, upper panel**). Apparently, to determine the time lag from the particle and sulfuric acid time profile implies several difficulties. It can also be seen from the figures, that on some days the major peaks appeared without any time lag and that the applied time shift (lower

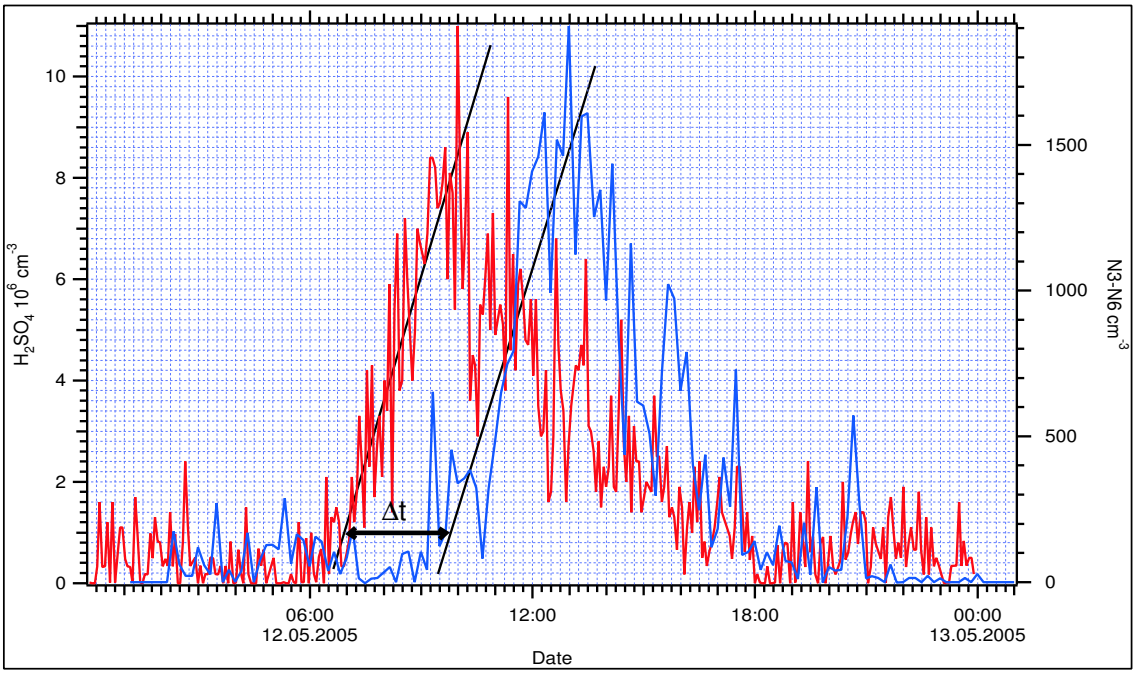

Figure 7.1: Number concentration of particles in the size range between 3nm to 6nm (N3-N6) and H_2SO_4 concentration for a typical observation day in Hyytiälä. The slopes indicated are used to specify the time lag Δt between both curves.

DATE	TIME LAG (min)
12.04.2005	0
13.04.2005	45
14.04.2005	0
18.04.2005	200
25.04.2005	180
26.04.2005	165
27.04.2005	0
30.04.2005	0
02.05.2005	0
03.05.2005	0
11.05.2005	120
12.05.2005	165
13.05.2005	0
14.05.2005	0

Table 7.1: Assessed time lags for each event day when significant particle growth in addition to enhancements in the sulfuric acid concentration was observed.

panel of both figures) would lead to some bias. Therefore the H_2SO_4 curve was not shifted on these days.

In **Table 7.1** the time lag for each event day is listed, when significant particle growth in addition to enhancements in the ambient gaseous sulfuric acid concentration was observed. As in previous measurements a time lag was not always assessed. On 8 out of 14 event days this was the case. This could lead to the conclusion that on these days H_2SO_4 was not required for the formation of particles and the major peaks of the H_2SO_4 concentration and the (N3-N6) were coincidentally recorded at the same time since the nucleation event occurred within the diurnal variation of H_2SO_4, which is triggered by sunlight induced OH production.

However, it could also be explained by a very fast growth rate of the newly formed particles. If the growth rate is below the time resolution of the DMPS, which accounts for 10 minutes, the observed "instant growth" in our measurements could be explained. Newly formed particles grow to detectable sizes by condensation, where organic compounds are supposed to contribute to large extents. When biological growth starts in spring due to increasing temperatures, higher amounts of volatile organics (VOCs) are likely to be found in the atmosphere, since they are generally released by trees. A higher concentration of VOCs may lead to enhanced growth rates and thus to an acceleration of the condensational growth of aerosol particles. The Bacci4-Quest campaign took place from April until mid May, when

the biosphere is already very active.

7.1.2 Identification of Kinetic or Activation Approach

Whether the observed particle concentrations during a day can be explained by kinetic nucleation or activation theory was investigated by plotting the particle concentrations versus the measured sulfuric acid concentrations. As previously mentioned the activation approach predicts one sulfuric acid molecule in a critical cluster, whereas kinetic theory favors two sulfuric acid molecules. This in turn leads to the earlier described linear (activation) or quadratic (kinetic) relation of the particle concentration described earlier. Thus **Figure 7.4 - Figure 7.7** show the (N3-N6) plotted against the linear and quadratic H_2SO_4 concentrations. Beside these scatter plots the graphs also include time series of H_2SO_4 and particle concentrations for selected event days. Further graphs of other days are shown in the appendix, (B.1 - B.10). Days on which the timeshift analysis was applied are labeled as "indirect correlation", days which were not processed according to the time lag between H_2SO_4 and (N3-N6) are categorized as "direct correlation".
The black straight line in all scatter plots represents a linear fit. The criterion for a classification with respect to activation or kinetic theory was the calculated correlation coefficient of the fit. The data points considered for the calculation of the correlation coefficient were chosen by an individually derived threshold. This threshold was set to be at the first significant increase of the measured sulfuric acid concentration. For example early morning or evening time periods, when H_2SO_4 concentrations are close to the detection limit, were omitted because the relative error of gaseous H_2SO_4 is very high in this range.

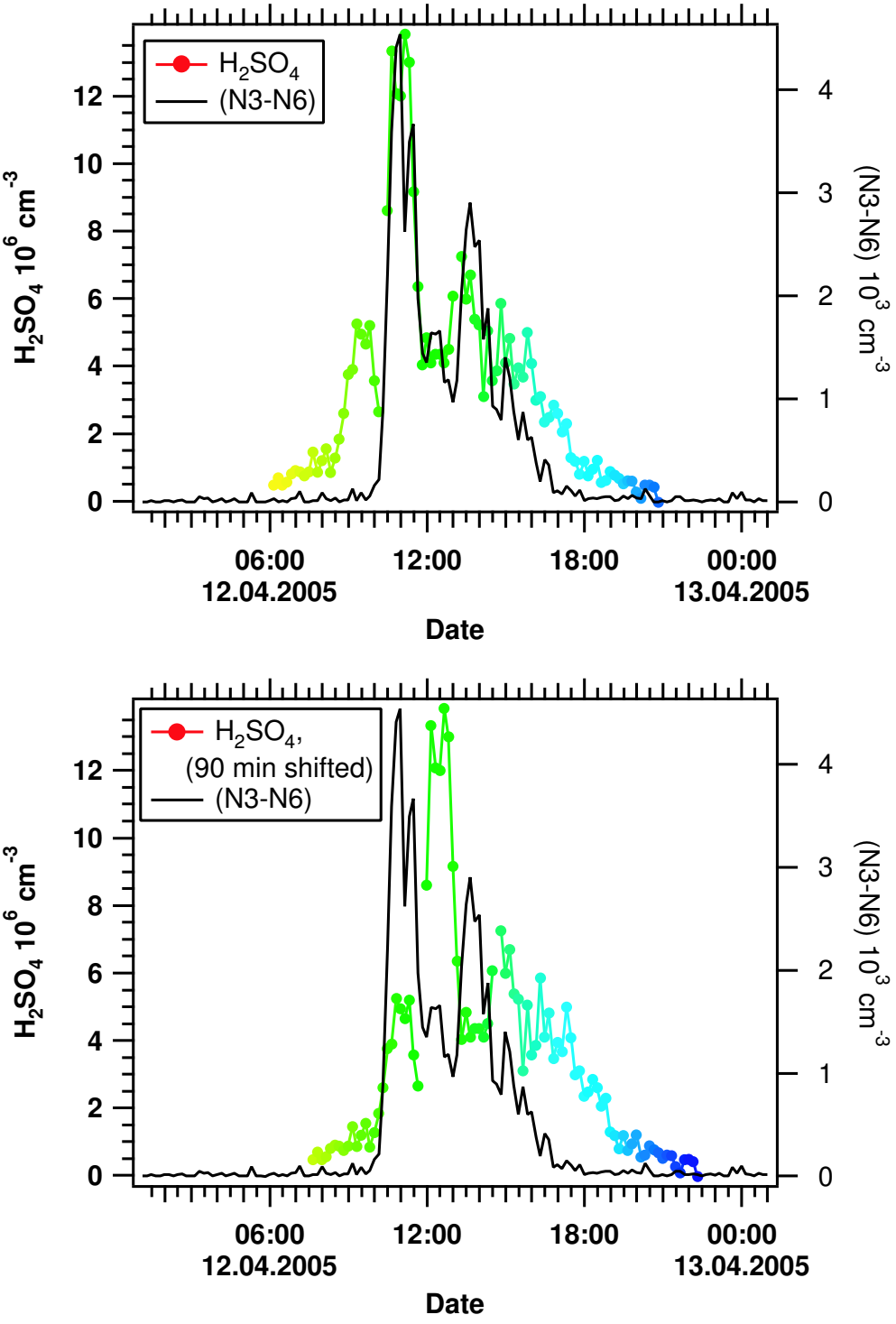

Figure 7.2: H_2SO_4 and (N3-N6) versus time for the 12th of April. In the upper graph the timeshift analysis was not applied, in the lower graph the H_2SO_4 concentration curve was shifted 90 minutes ahead.

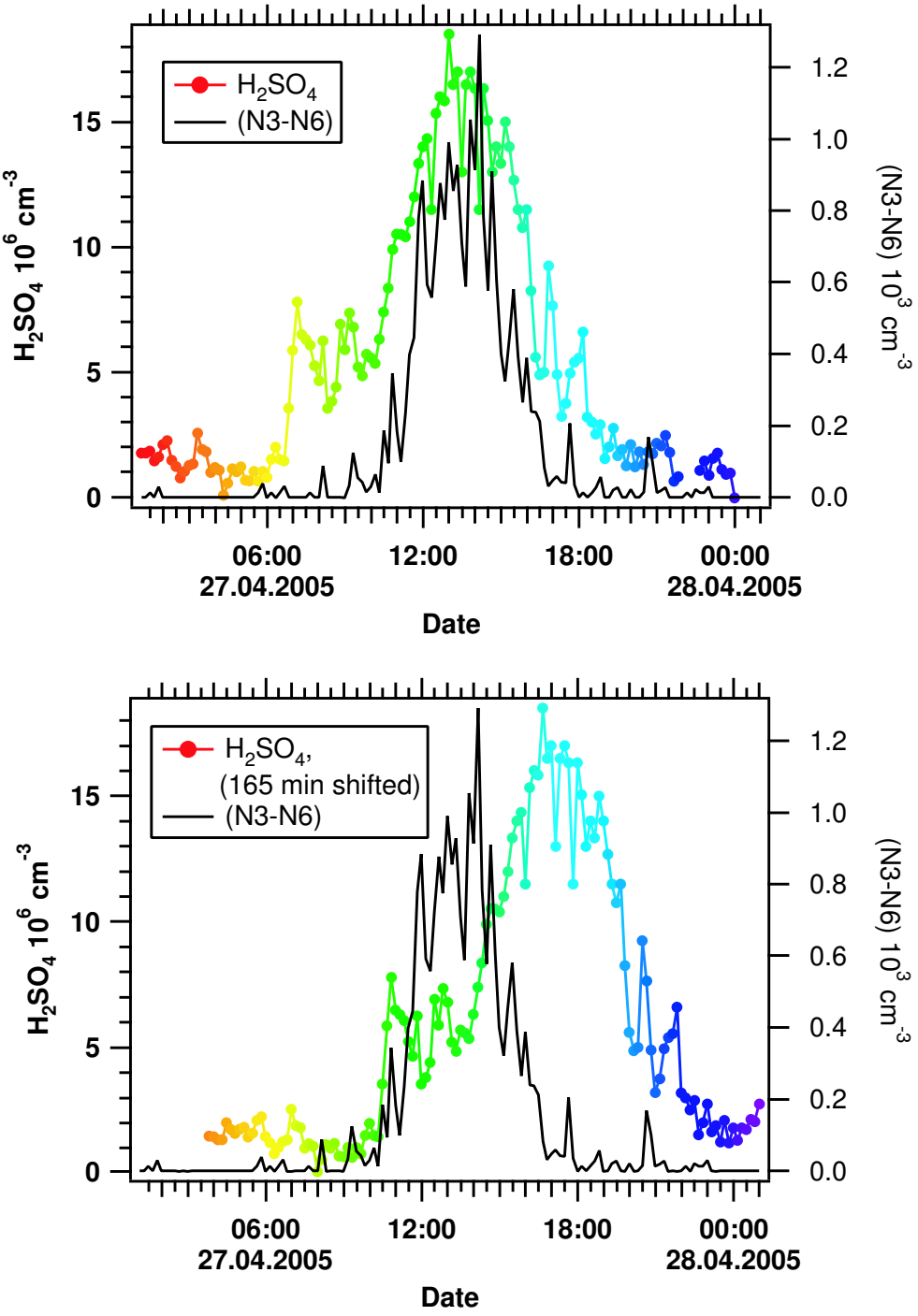

Figure 7.3: H_2SO_4 and (N3-N6) versus time for the 27th of April. In the upper graph the timeshift analysis was not applied, in the lower graph the H_2SO_4concentration curve was shifted 165 minutes ahead.

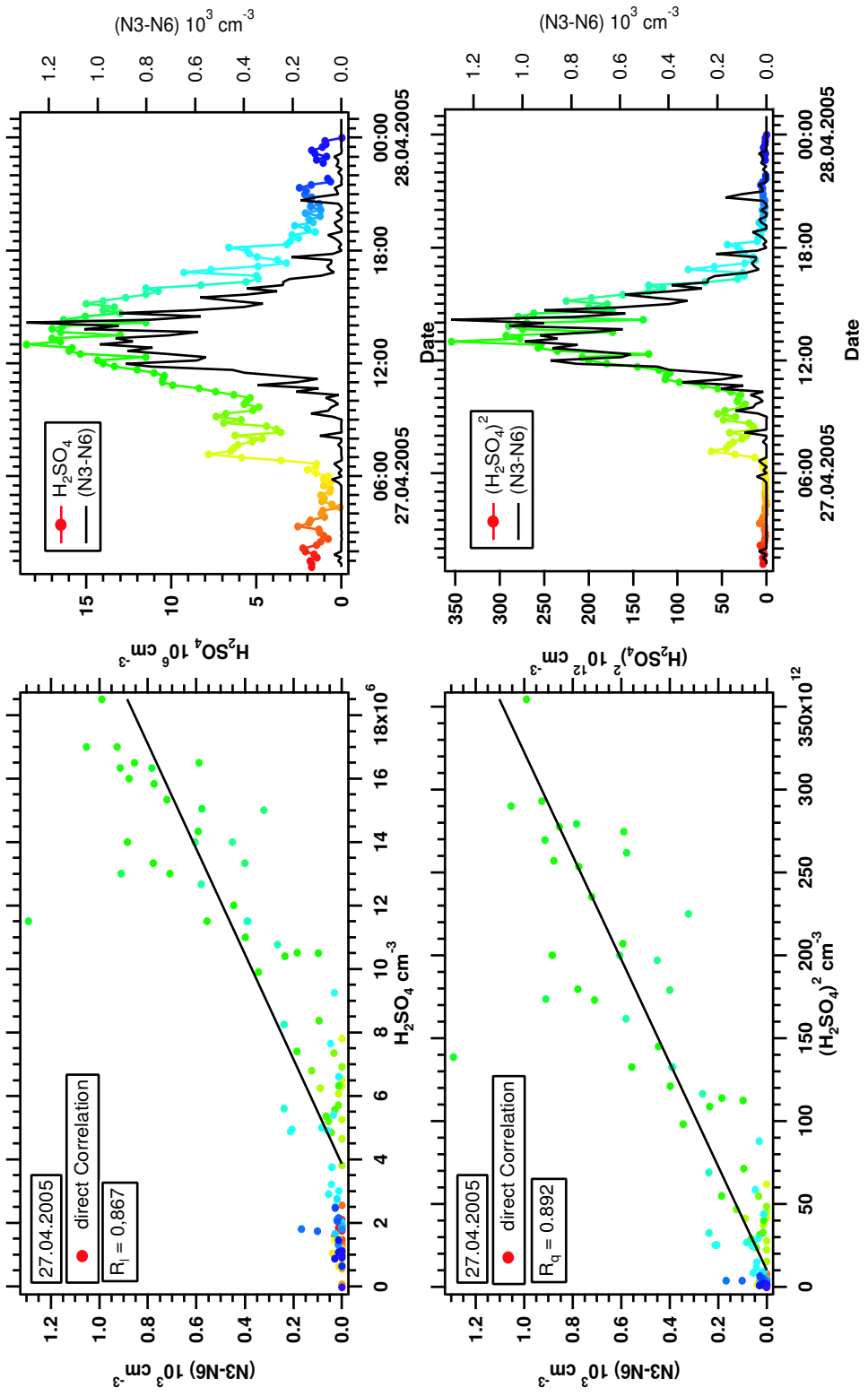

Figure 7.4: Direct correlation plots for the 27th of April. (Timeshift analysis was not applied). On the left side time series of (N3-N6) and of H_2SO_4 concentration (linear and squared) are compared. On the left side the corresponding scatter plots are shown.

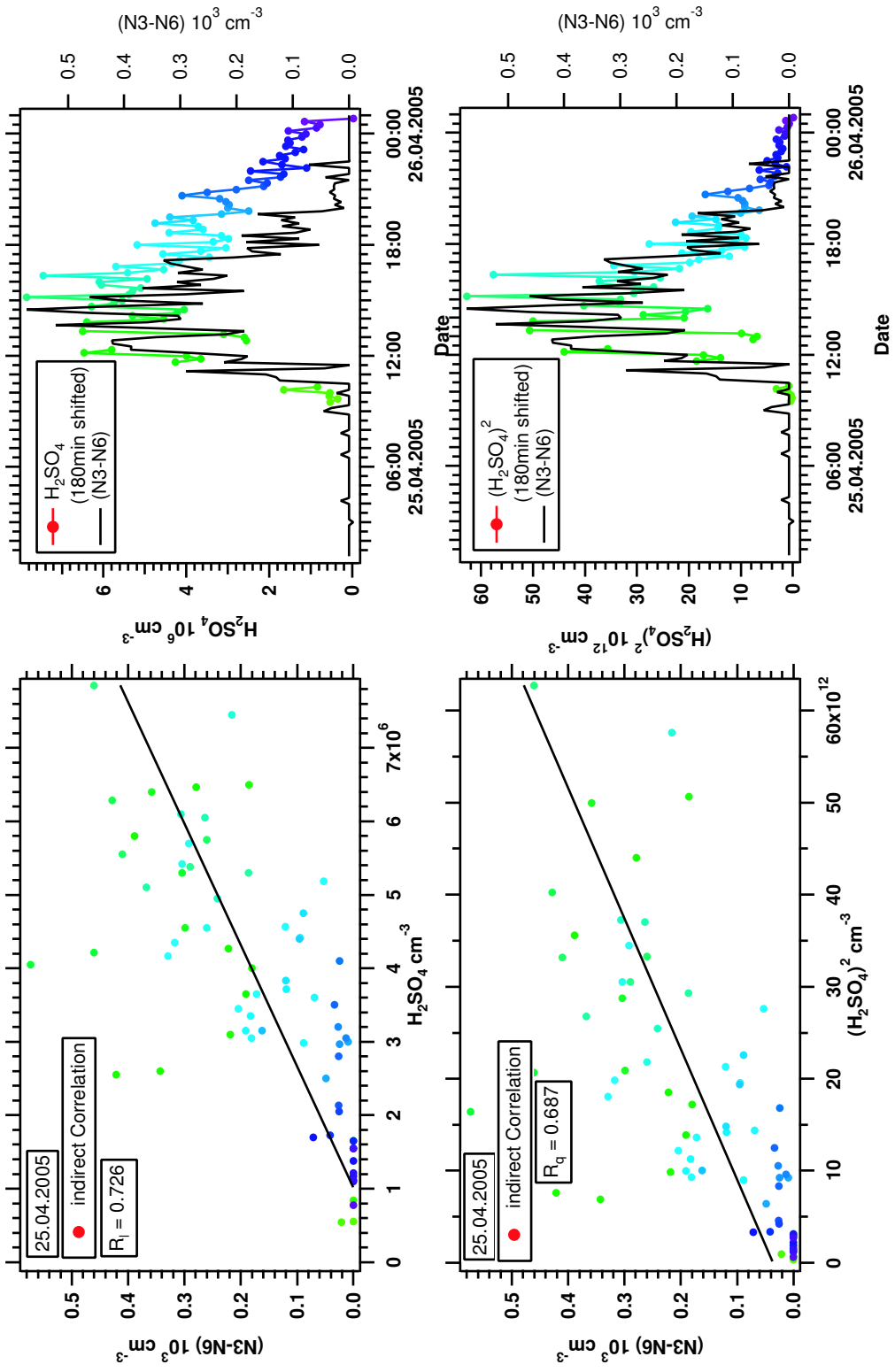

Figure 7.5: Indirect correlation plots for the 25th of April. (The H_2SO_4 curve was 180min shifted ahead). On the left side time series of (N3-N6) and of H_2SO_4 concentration (linear and squared) are compared. On the left side the corresponding scatter plots are shown.

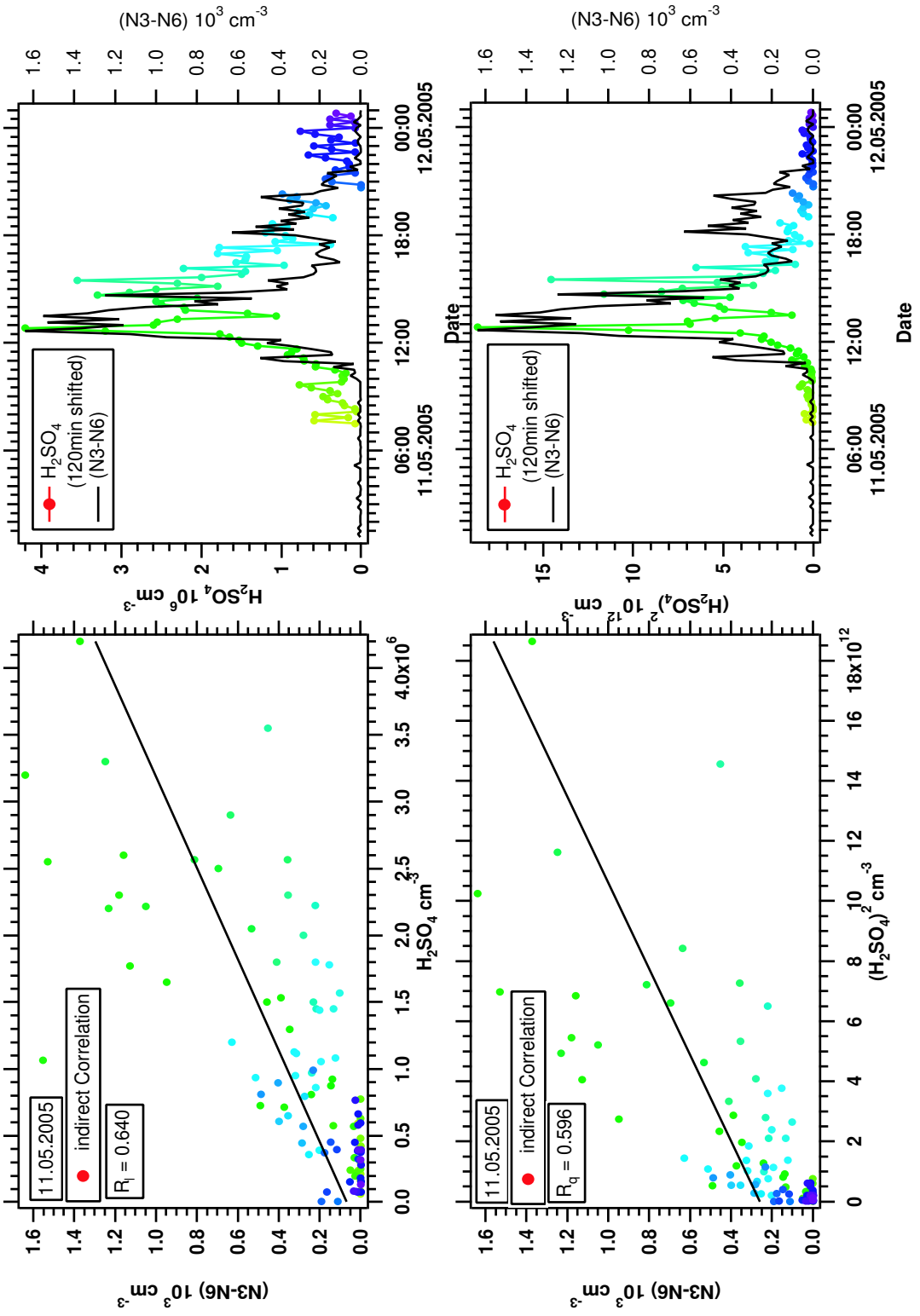

Figure 7.6: Indirect correlation plots for the 11th of May. (The H_2SO_4 curve was 120min shifted ahead). On the left side time series of (N3-N6) and of H_2SO_4 concentration (linear and squared) are compared. On the left side the corresponding scatter plots are shown.

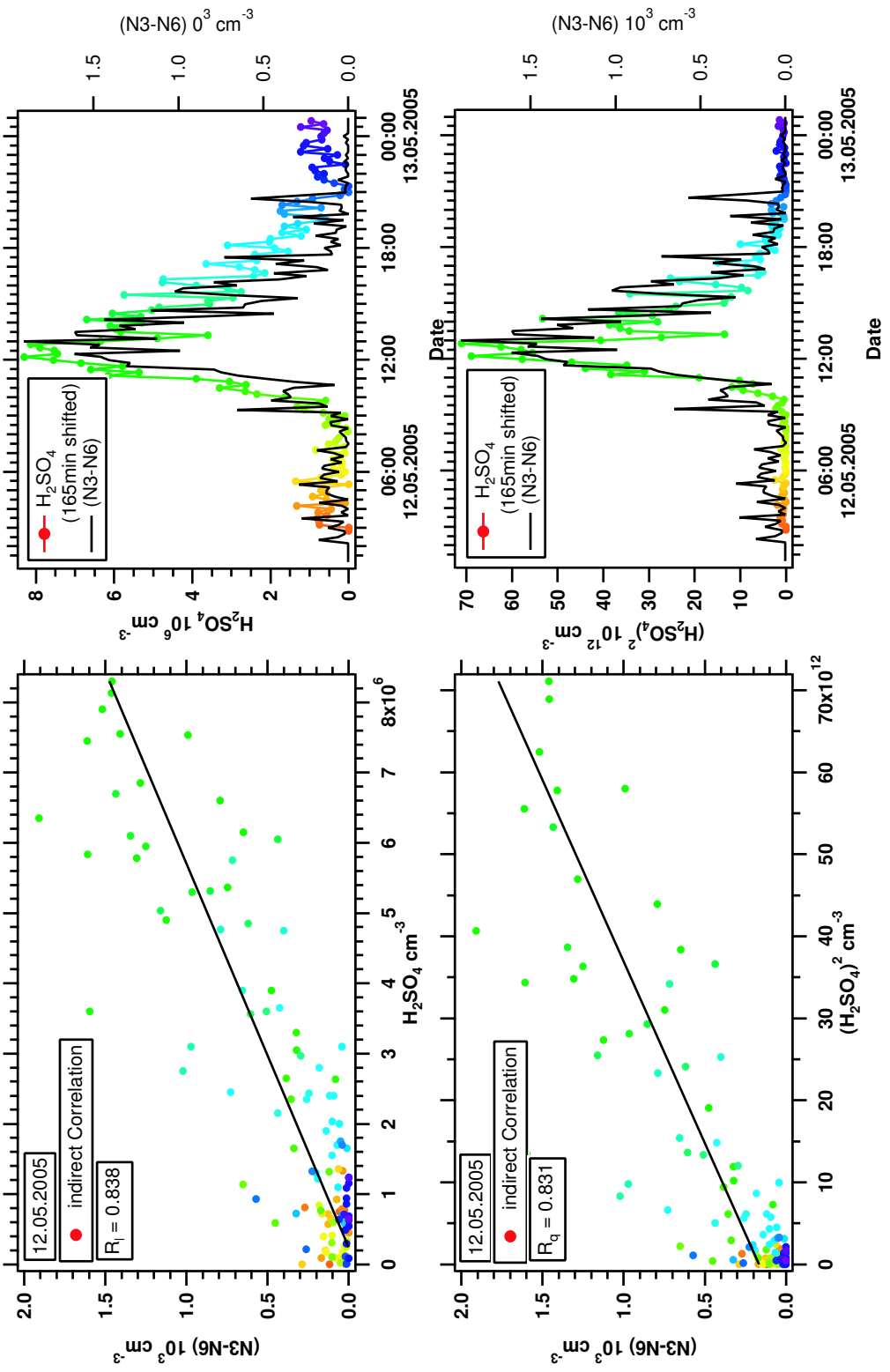

Figure 7.7: Indirect correlation plots for the 12th of May. (The H_2SO_4 curve was 165min shifted ahead). On the left side time series of (N3-N6) and of H_2SO_4 concentration (linear and squared) are compared. On the left side the corresponding scatter plots are shown.

Figure 7.4 illustrates linear and quadratic relationships for the 27th of April. The quadratic dependency yields a very good description, as can be seen from the time series. That means the observations on this day support a kinetic approach to explain the particle nucleation mechanism. The correlation coefficient in case of the squared sulfuric acid concentration reflects a similar tendency.
The diurnal courses of the 27th of April are shown in the appendix (A.19). Interestingly, relatively high concentrations of sulphuric acid, up to $2.2 \cdot 10^7$ cm^{-3} were reached during this cloud free day, but comparatively few new particles were formed. Thus, newly formed particles were either scavenged by larger particles or quickly grew to sizes of such order not to be contained in the (N3-N6) size bins. The latter seems to be likely since a "direct correlation" was observed indicating a high present concentration of VOCs. Another aspect is whether the conditions for particle nucleation were favorable. Sufficiently high amounts of water vapor in the atmosphere are necessary for nucleation and low temperatures diminish the thermal destruction of newly formed molecular clusters. In the mornings the relative humidity was around 70% - 80% and the temperature was about 0°C. At this time no (N3-N6) was observed. As soon as the CS term diminishes, the amount of sulfuric acid further increases and (N3-N6) enhancement commences. It is likely that the sulfuric acid concentration before was slightly too small to cause significant formation of new particles, either due to the large CS term or because the new particles were directly scavenged by larger ones. It is also possible that freshly formed particles grew very slow in the morning. Temperature influences indirectly the amount of volatile organic compounds (VOCs). A rise in temperature throughout the day, up to 15°C, leads to an increased release rate of these compounds from trees and therefore may support a fast growth of small particles to larger ones.

Figure 7.5 shows the diurnal variations of (N3-N6) and H_2SO_4 for the 25th of April. According to the time series and the correlation coefficients, it cannot be decided whether kinetic or activation theory explains the observed amount of small particles. The correlation coefficients are R_l= 0.726 (linear) and R_q= 0.687 (quadratic). Comparing the time series, the quadratic relation seems to be more suitable. Interestingly the 25th and 27th of April show very similar conditions, except for the sulfuric acid concentration, which was 3 times smaller. Correspondingly the amount of (N3-N6) was lower as well, in this case by a factor of 2, (see appendix, A.17).

On the 11th of May (**Figure 7.6**) the particle production can be described by activation (n = 1). The correlation coefficients constitute $R_l = 0.640$ (linear) and R_q= 0.596 (quadratic).

Due to high cloud cover[1] only a H_2SO_4 concentration of about $0.5 \cdot 10^7$ cm^{-3} existed. Relative humidity of about 50 % - 60 % was measured and particle formation was modest with a concentration of 1600 cm^{-3} (see A.31 in appendix). Despite these rather unfavorable conditions, an event of class 1 still occurred.

The 12th of May (**Figure 7.7**) does not show any distinct power-law dependencies. R_l= 0.838 is basically equivalent to R_q= 0.831. However both correlation coefficients are relatively high reflecting the similarities in the time series of (N3-N6) and H_2SO_4 for the linear as well as the quadratic case. This might be interpreted as a power-law dependency between one and two. As on the 11th of May, the H_2SO_4 concentrations were again relatively low, about 0.5 - 1 $\cdot 10^7$ cm^{-3},(see A.32 in the appendix), but surprisingly a very distinctive nucleation event (class 1) was detected again.

Towards the end of the campaign this phenomenon was observed more frequently. As the medium temperatures were rising throughout the campaign and reached up to 20°C in mid May which leads to an increased release of organic compounds by the biosphere, it seems likely that other components were mainly involved in the nucleation process. Modeling could bring more clarity into this issue concerning the contribution of other compounds than H_2SO_4.

Table 7.2 gives an overview of the discussed event days, classified by the analyzed parameters. It is also listed which theoretical approach is likely to explain the observed nucleation.

[1] low photochemical OH production rate leads to a small H_2SO_4 concentration

Date	event class	correlation	R_l	R_q	R_l - R_q	nucleation mechanism	max.GSA	max.(N3-N6)	Temp
12.04.2005	2	direct	0,841	0,794	0,048	activation theory	1,6	4,5	0 - 4
13.04.2005	1	indirect	0,864	0,834	0,030	activation theory	1,4	3	4 - 9
14.04.2005	1	direct	0,671	0,792	-0,121	kinetic nucleation	1,45	7	0 - 10
18.04.2005	2	indirect	0,545	0,527	0,018	activation theory	1,1	2	-3 - 5
25.04.2005	2	indirect	0,726	0,687	0,039	activation theory	0,95	0,6	1 - 10
26.04.2005	2	indirect	0,576	0,593	-0,017	kinetic nucleation	1,7	1,2	-1 - 12
27.04.2005	2	direct	0,867	0,892	-0,025	kinetic nucleation	2,2	1,3	0 - 11
30.04.2005	2	direct	0,410	0,373	0,038	activation theory	0,45	0,3	4 - 9
02.05.2005	1	direct	0,374	0,353	0,021	activation theory	2,3	21	4 - 9
03.05.2005	1	direct	0,619	0,634	-0,015	kinetic nucleation	2,9	9	4 - 9
11.05.2005	1	indirect	0,640	0,596	0,044	activation theory	0,5	1,6	4 - 9
12.05.2005	1	indirect	0,838	0,831	0,007	activation theory	1,1	2	4 - 9
13.05.2005	1	direct	0,290	0,304	-0,013	kinetic nucleation	0,4	1,2	4 - 9
14.05.2005	2	direct	0,690	0,799	-0,109	kinetic nucleation	0,6	3,7	4 - 9

Table 7.2: Overview of event days. Class of events, correlation parameters and deduced nucleation mechanism are compared to the maximum sulfuric acid concentration, the maximum (N3-N6) and temperature.

Evaluation of the correlation method

The correlation method holds several problems. First it is difficult to derive an error estimate for the calculated correlation coefficients, since the time interval for the correlation is chosen individually by a threshold. The same threshold should be applied to all curves. Second, the correlation coefficients are often not unique to decide which theoretical approach should be chosen. Most often the time series carry more information. Another way to extract the information is to calculate the slope of the logarithmic plotted H_2SO_4 concentration and (N3-N6). The slope then directly corresponds to the number of sulfuric acid molecules in the critical cluster. It can be approximated by curve fitting a linear function to the scatter plot. The CHI^2-method of the curve fit also offers an error estimate. It can then be decided within an error interval which theory, kinetic or activation, matches the observed nucleation. It has to be left to further investigations to examine whether this method may actually be superior.

Chapter 8

Summary and Perspectives

This diploma thesis presented measurements of atmospheric gaseous H_2SO_4 which were obtained in the boreal forest region of Finland during the EU-funded BACCI4-QUEST campaign. The measurements were conducted with an Ion Trap Mass Spectrometer using the CIMS (Chemical Ionization Mass Spectrometry) Method as described in this work. To determine the systematic error of the measurement device a calibration on the basis of OH-induced H_2SO_4 production from SO_2 was carried out. The measured H_2SO_4 concentration was then corrected according to the experimentally obtained calibration factor, the instrumental background and the temperature difference between the sampled air stream and the tempered flow reactor. The processed H_2SO_4 data was presented in comparison to particle concentration, weather parameters and condensational sink in order to depict the favorable and unfavorable conditions for nucleation.

Additionally the relation of the H_2SO_4 concentration and concentration of aerosol particles between 3nm and 6nm in diameter was discussed. The objective was to determine which theoretical approach is best suited to describe the observed formation of new particles. Mainly two theories were taken into consideration, the kinetic and the activation approach.

The time series obtained were modified by the so called "time-shift analysis". Correlation coefficients derived from scatter plots served to distinguish between the respective models. In this framework correlations between (N3-N6) and the H_2SO_4 concentration were often observed. On some days this was even the case without shifting the H_2SO_4 curve by the time particles needed to grow from 1nm to 3nm (direct correlation). Reasons for a direct correlation are perhaps fast growth, below the time resolution of the particle counter, caused by a high amount of VOCs. The process is thus triggered by the ambient temperature which influences the release rate of the organic compounds of trees.

Regarding the power-law-dependency, a linear as well as a quadratic relationship between the H_2SO_4 concentration and the (N3-N6) was observed which indicates that both mechanisms account for the occurrence of nucleation events. Thus, our investigations reveal that there is no unique preference of nucleation by activation or by a purely kinetic mechanism and both theories are needed to explain the experimentally investigated nucleation in the boreal region of Finland. As the exponent varies mostly between 1 and 2, they are in accordance with earlier observations made by our group [Kulmala et al., 2005].

Difficulties emerged in trying to uniquely classify which mechanism led to new particle formation. The comparison of time series of (N3-N6) to the linearly and quadratically plotted H_2SO_4 concentration plus scatter plots provide a good estimate. A single criterion according to which the best fitting dependency can be assessed would, however, be helpful. In general correlation coefficients provide this information, but since they diverge only slightly from each other in some cases, an error estimate for the coefficients needs to be derived.
A uniform method in this context would generate the necessary guidelines. For example, always the same threshold should be applied when the time interval for the calculation of the correlation coefficients is selected. Then it could be decided within an error interval which theory verifies the observed nucleation.

Further investigations will have to include a statistical evaluation. Therefore the number of data points considered in the correlation analysis has to be taken into account in order to allow a conclusion about the significance of the observed relationship. Another possibility is to calculate the slope of the logarithmic plotted H_2SO_4 concentration and (N3-N6) which corresponds to the number of sulfuric acid molecules in the cluster. An error estimate can be obtained from the curve fit, which provides the opportunity to proceed systematically in deciding which mechanism was operant.

In future experimental observations a further specification of the role that volatile organics play for nucleation and growth of freshly formed particles would be desirable. Since the activity of the biosphere in general and therewith the emission of VOCs varies with temperature, it is recommended to carry out H_2SO_4 measurements and examine the relationship of (N3-N6) and H_2SO_4 concentrations during different seasons throughout the year.
In addition, if a model of the H_2SO_4 production was developed, H_2SO_4 concentrations could be reproduced from the measured SO_2 data of recent years, such that the systematic study of the dependency of particle nucleation on sulfuric acid concentration would become possible.
An experimental approach to determine additional, important components for nucleation

and growth of freshly formed particles are provided by the CIMS - Method devised by [Arnold, 1978, Arnold and Fabian, 1980, Arnold and Viggiano, 1980, Knop and Arnold, 1985] and further developed by [Eisele and Tanner, 1993] which makes very selective and sensitive measurements possible. In Finland test measurements concerning this matter were already carried out with the LIOMAS (Large Ions Mass Spectrometer), explained in [Wilhelm et al., 2004] and [Eichkorn et al., 2002]. In particular, sulfuric acid-water-ion clusters were artificially produced and subsequent reactions in ambient atmospheric air examined. Since the artificially created sulfuric acid-water clusters are expected to grow and react as in the atmosphere, the detection of the product ions would provide information about the masses and eventually allow an identification of the compounds which condensed on the clusters. This principle is still in development and due to instrumental restrictions not realized yet, but could in general promote the understanding of nucleation processes remarkably.

Appendix A

Experimental Data

Event Days
12.04.2005
13.04.2005
14.04.2005
18.04.2005
25.04.2005
26.04.2005
27.04.2005
30.04.2005
02.05.2005
03.05.2005
11.05.2005
12.05.2005
13.05.2005
14.05.2005

Table A.1: Event days during the BACCI4-QUEST campaign, classified on the basis of DMPS plots.

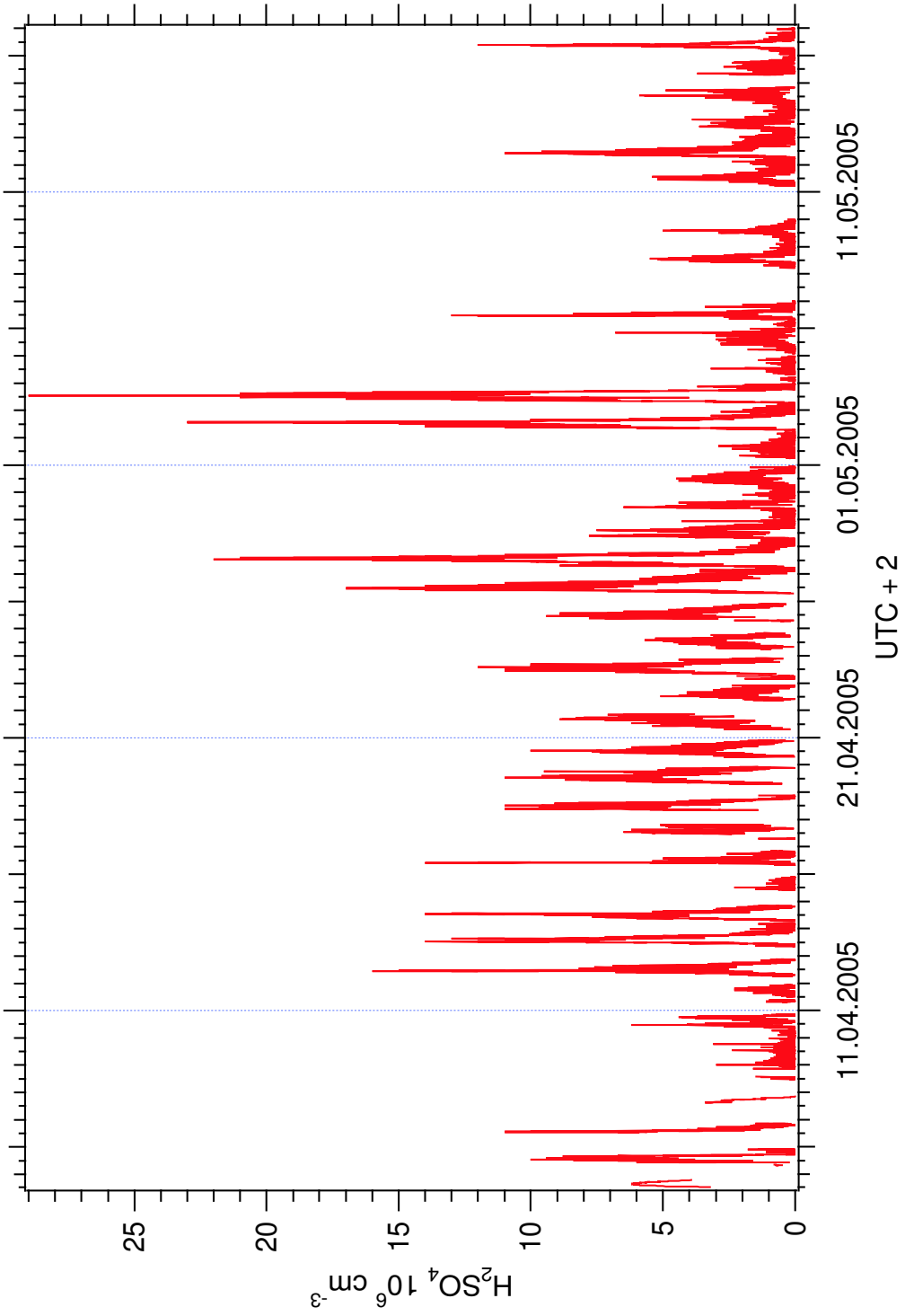

Figure A.1: Overview of sulfuric acid number concentrations during the whole measurement period of the BACCI4-QUEST campaign.

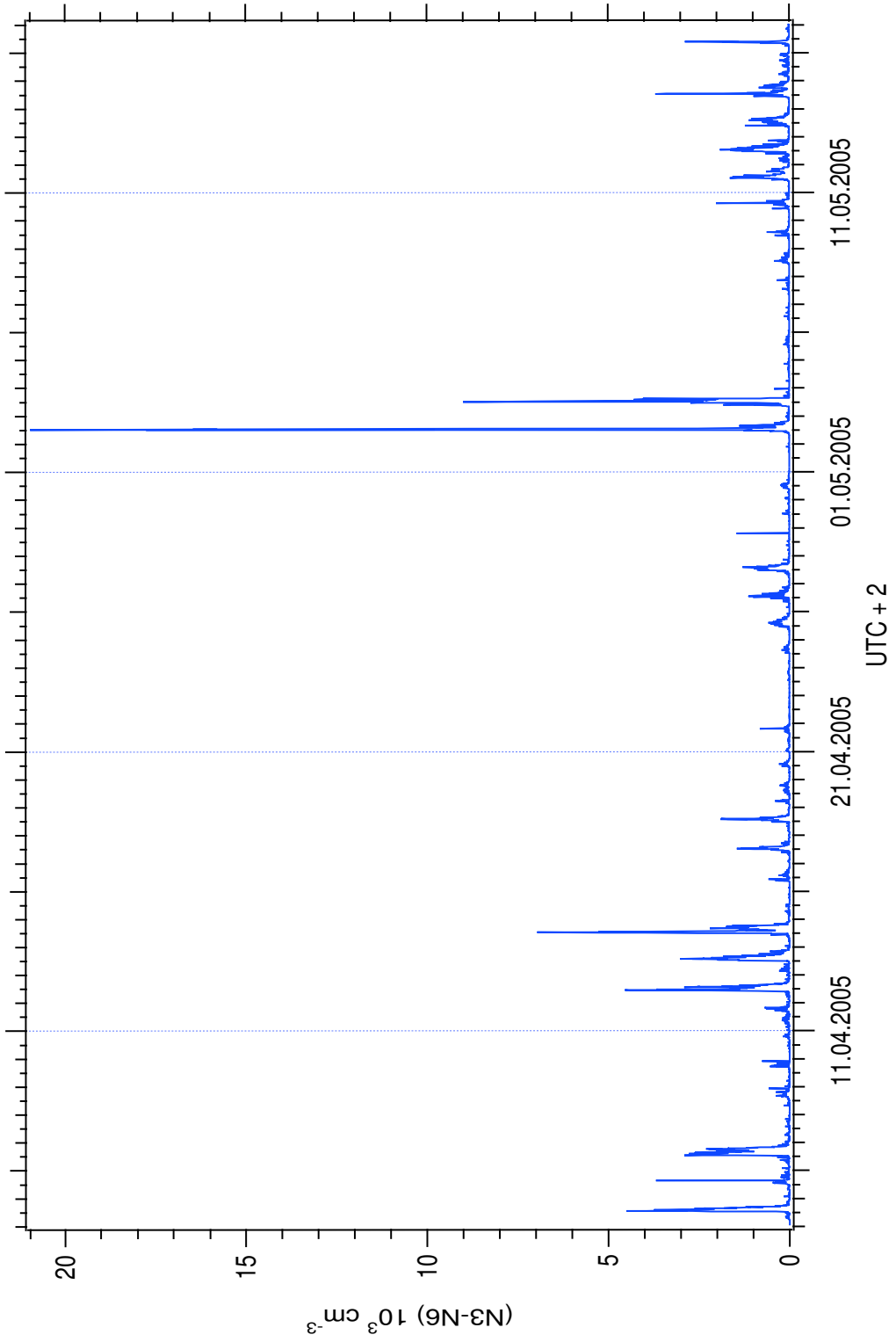

Figure A.2: Overview of particle number concentrations during the whole measurement period of the BACCI4-QUEST campaign.

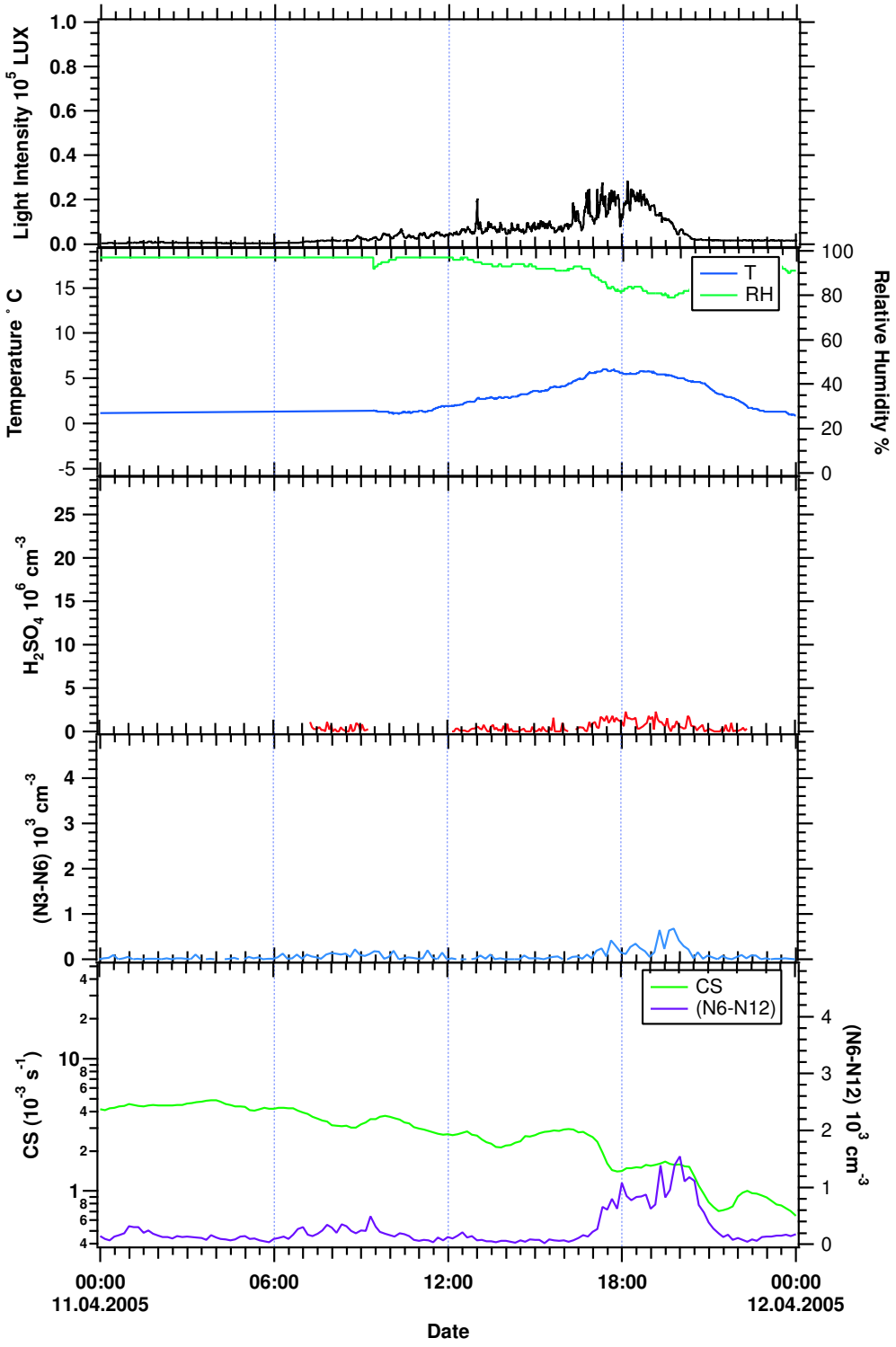

Figure A.3: Measured Data on the 11th of April (Non-event day). Sulfuric acid number concentrations are compared to other relevant parameters.

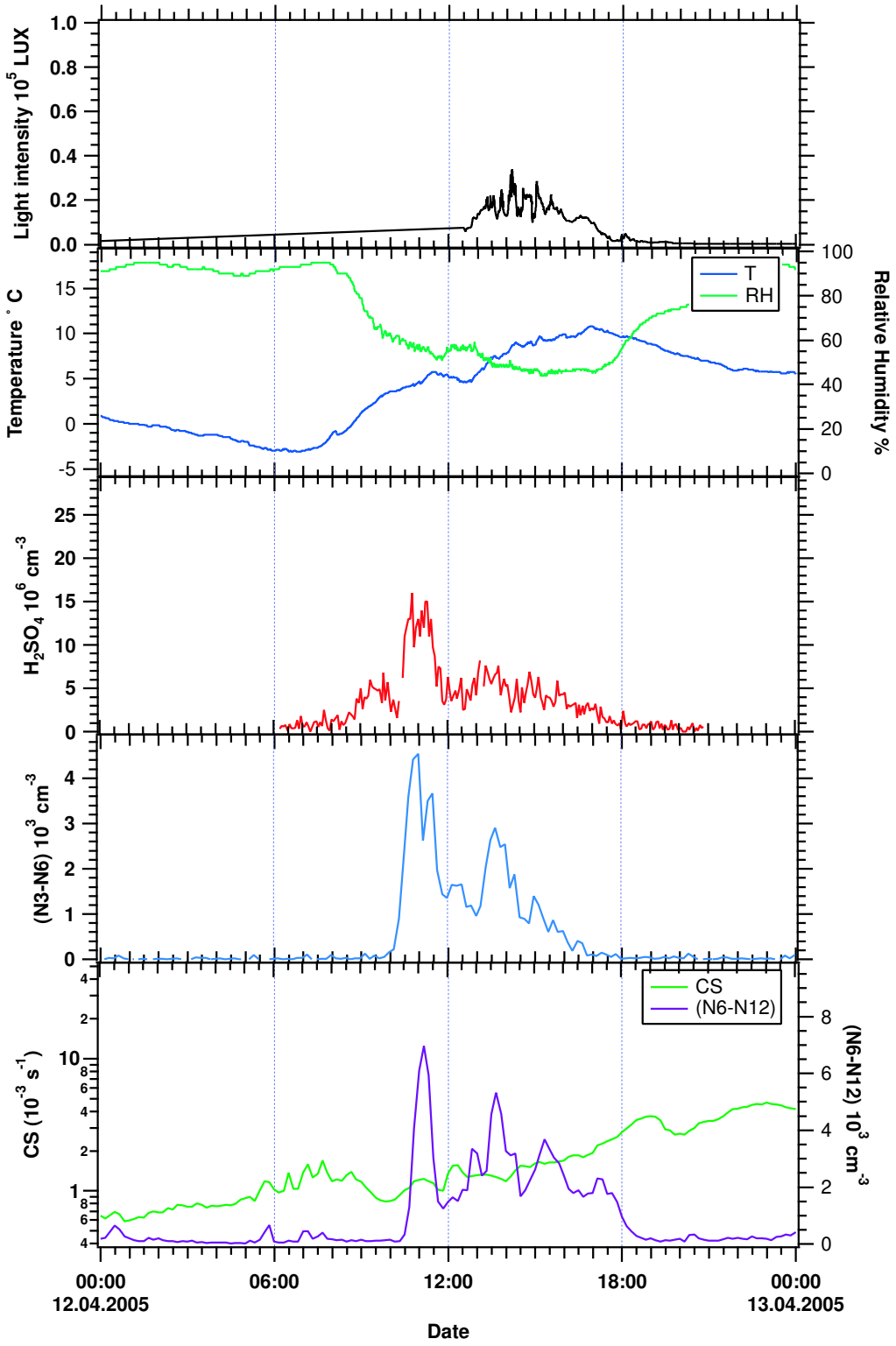

Figure A.4: Sulfuric acid number concentrations compared to particle and meteorological parameters measured on the 12th of April (Event day).

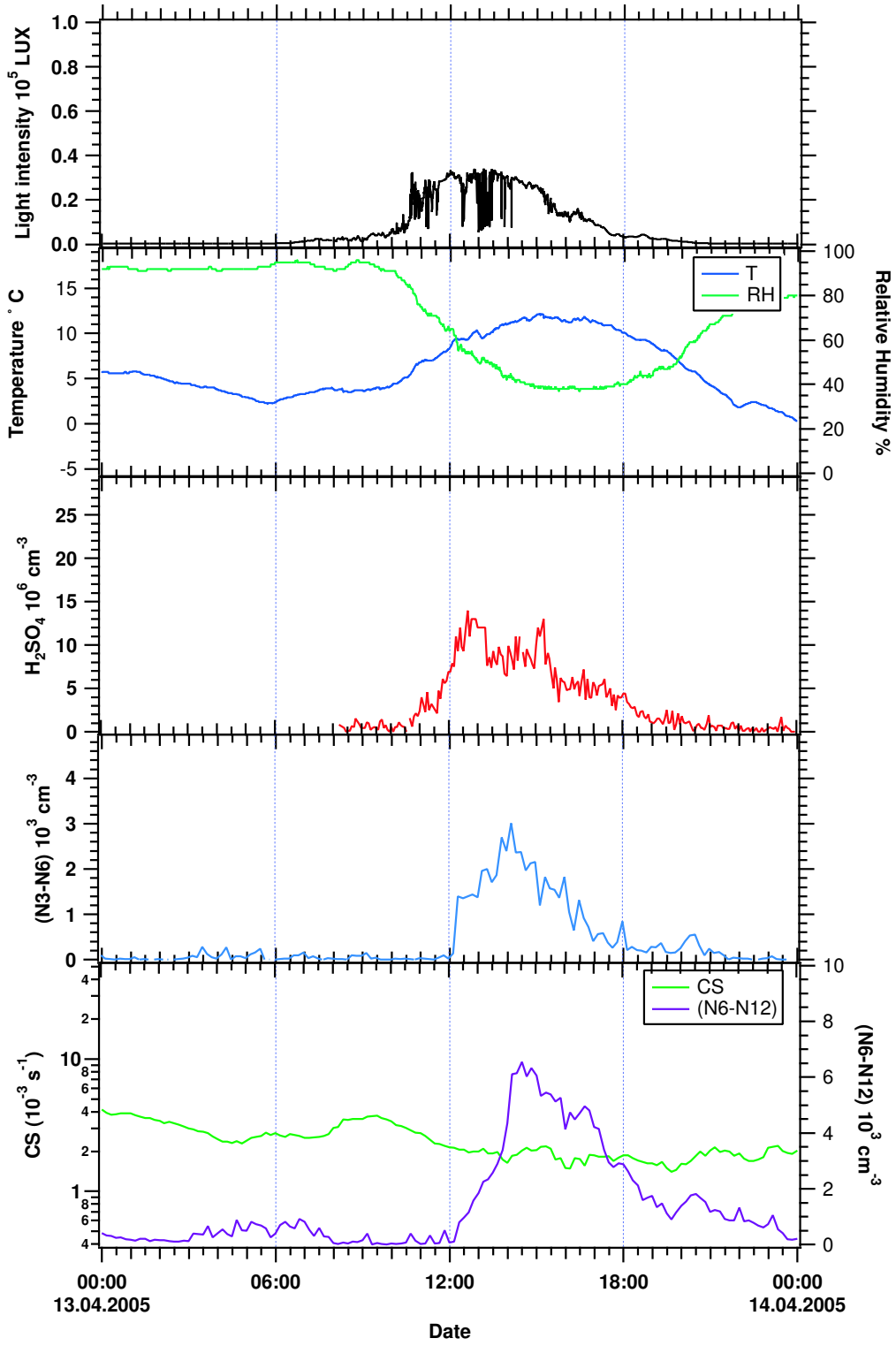

Figure A.5: Sulfuric acid number concentrations compared to particle and meteorological parameters measured on the 13th of April (Non-event day).

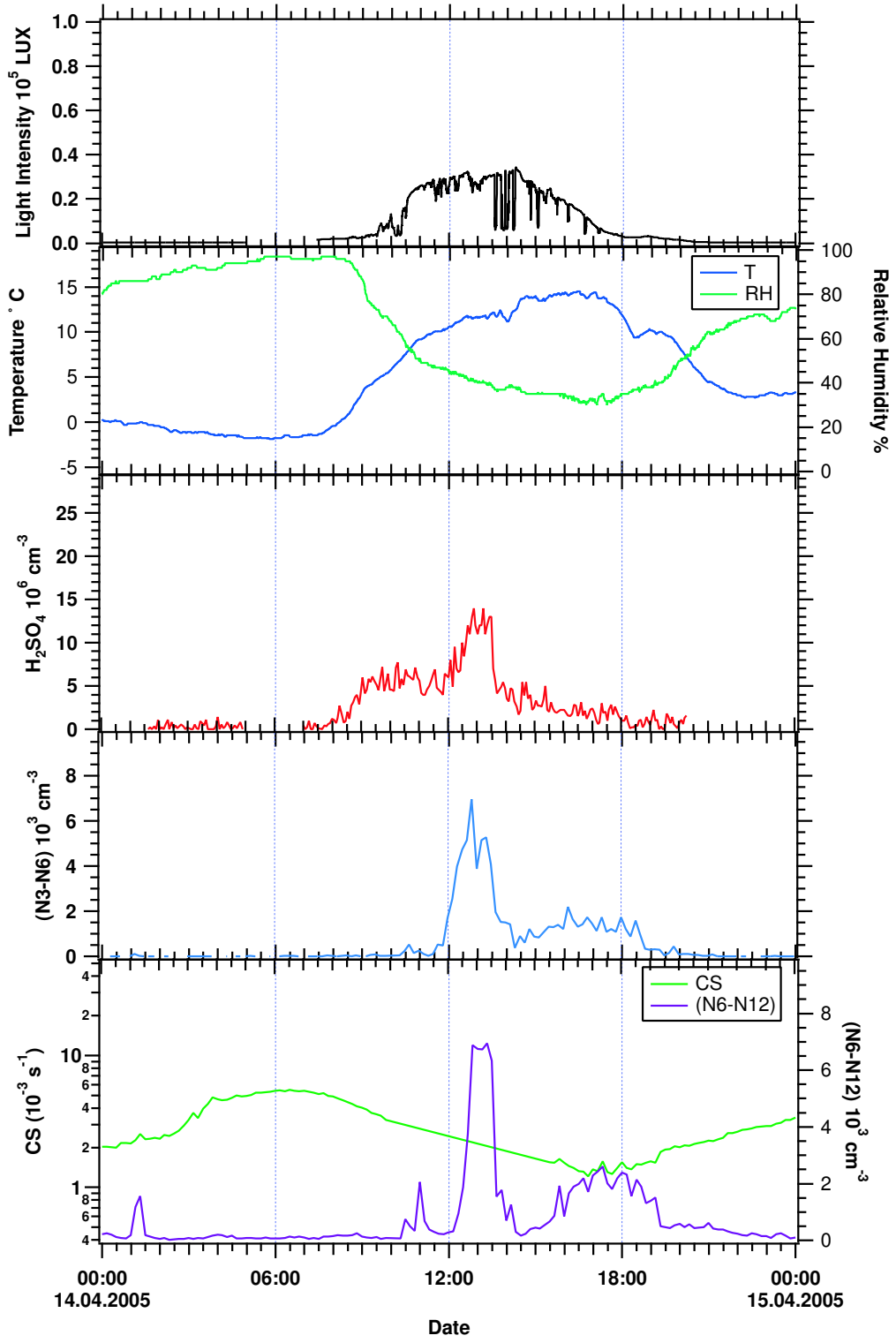

Figure A.6: Sulfuric acid number concentrations compared to particle and meteorological parameters measured on the 14th of April (Event day).

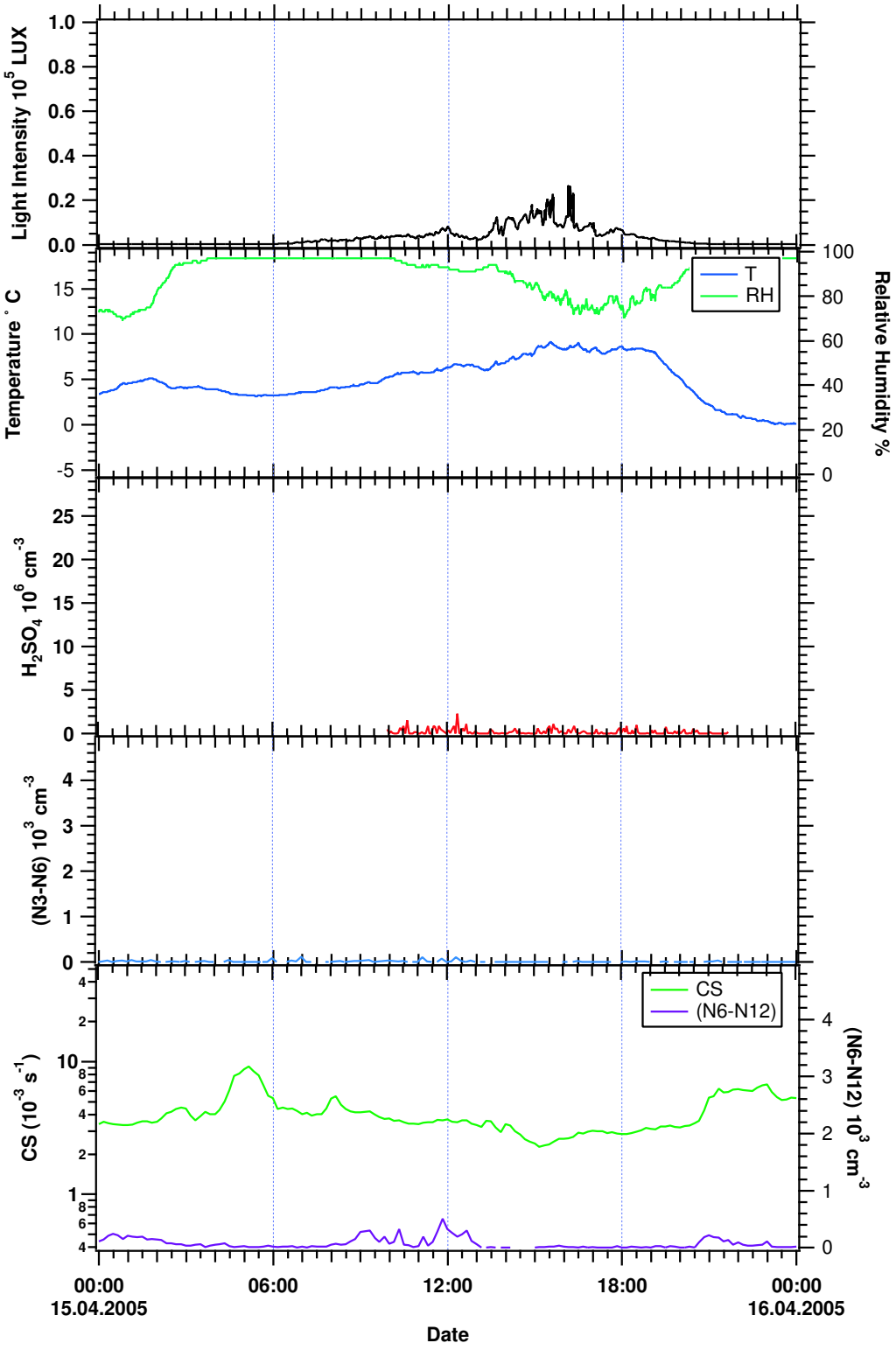

Figure A.7: Sulfuric acid number concentrations compared to particle and meteorological parameters measured on the 15th of April (Non-event day).

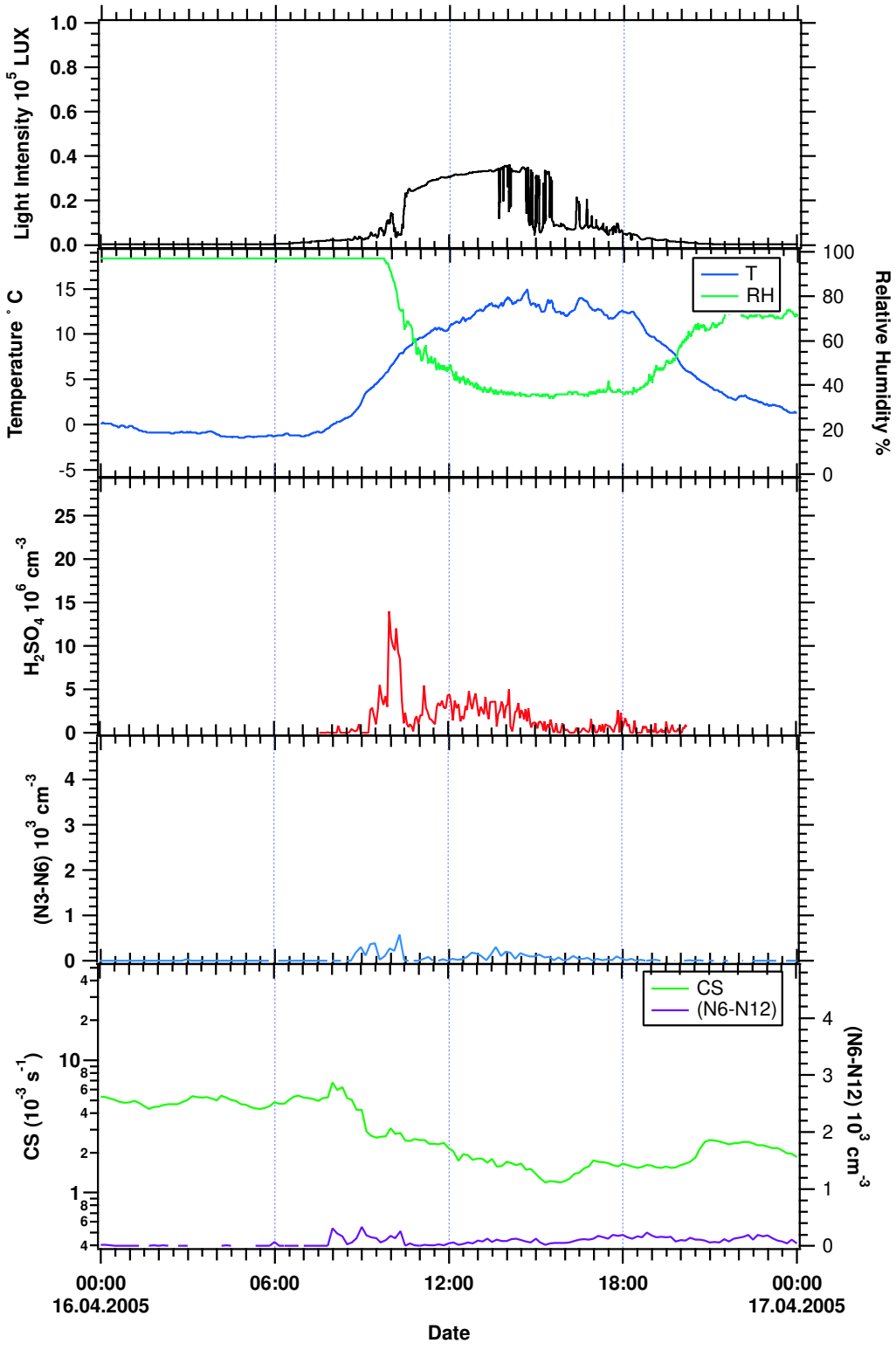

Figure A.8: Sulfuric acid number concentrations compared to particle and meteorological parameters measured on the 16th of April (Non-event day).

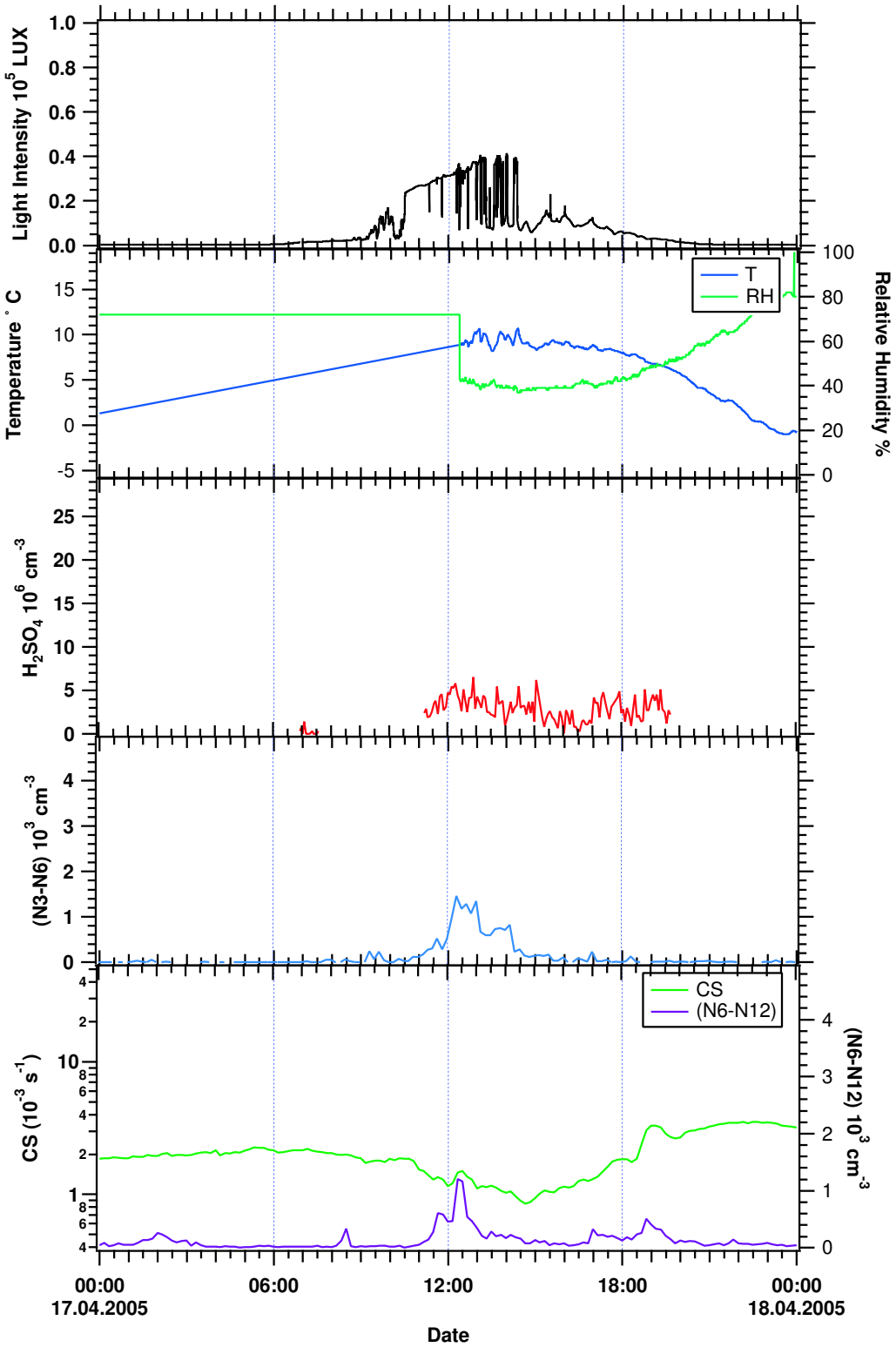

Figure A.9: Sulfuric acid number concentrations compared to particle and meteorological parameters measured on the 17th of April (Non-event day).

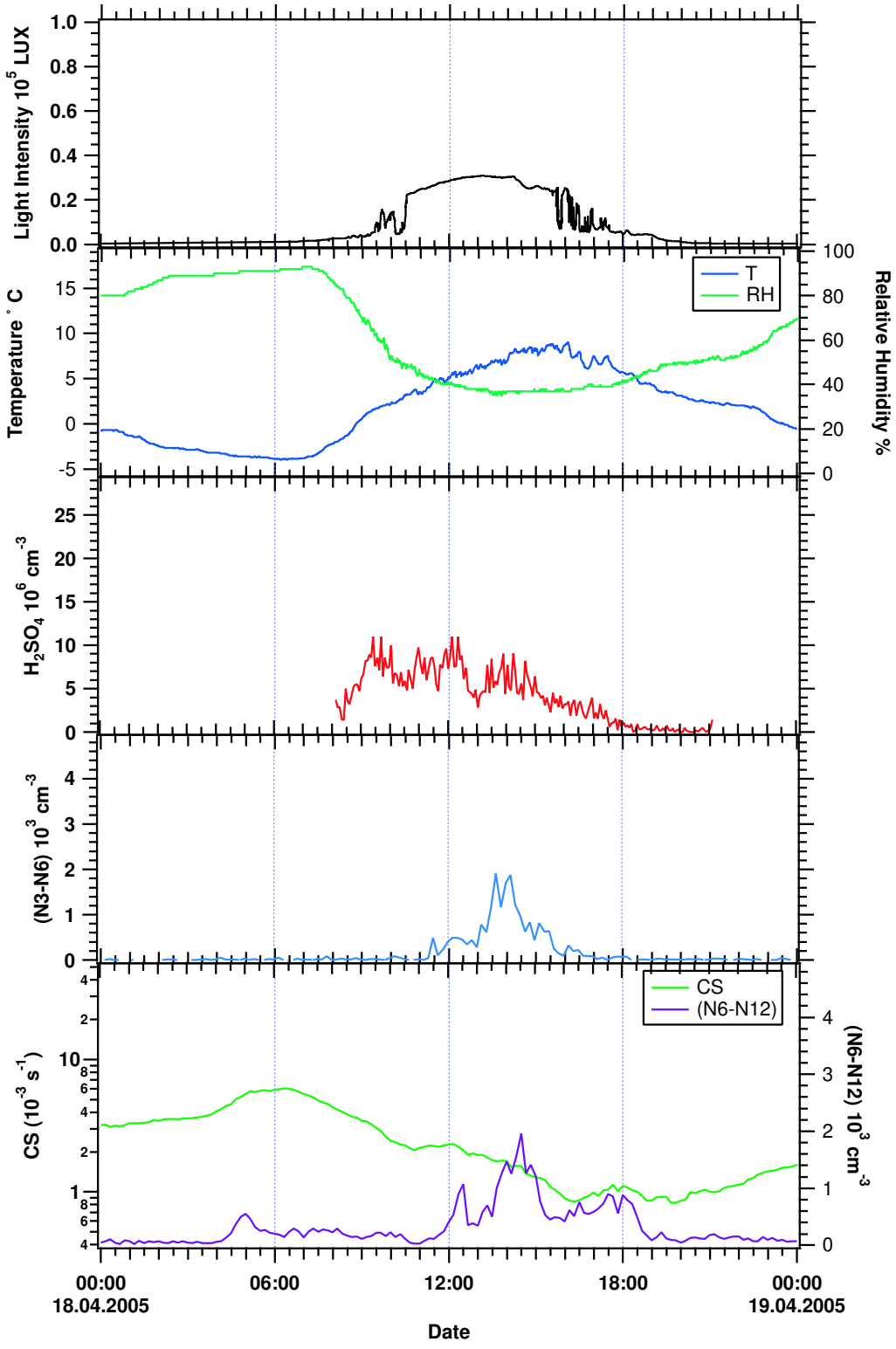

Figure A.10: Sulfuric acid number concentrations compared to particle and meteorological parameters measured on the 18th of April (Event day).

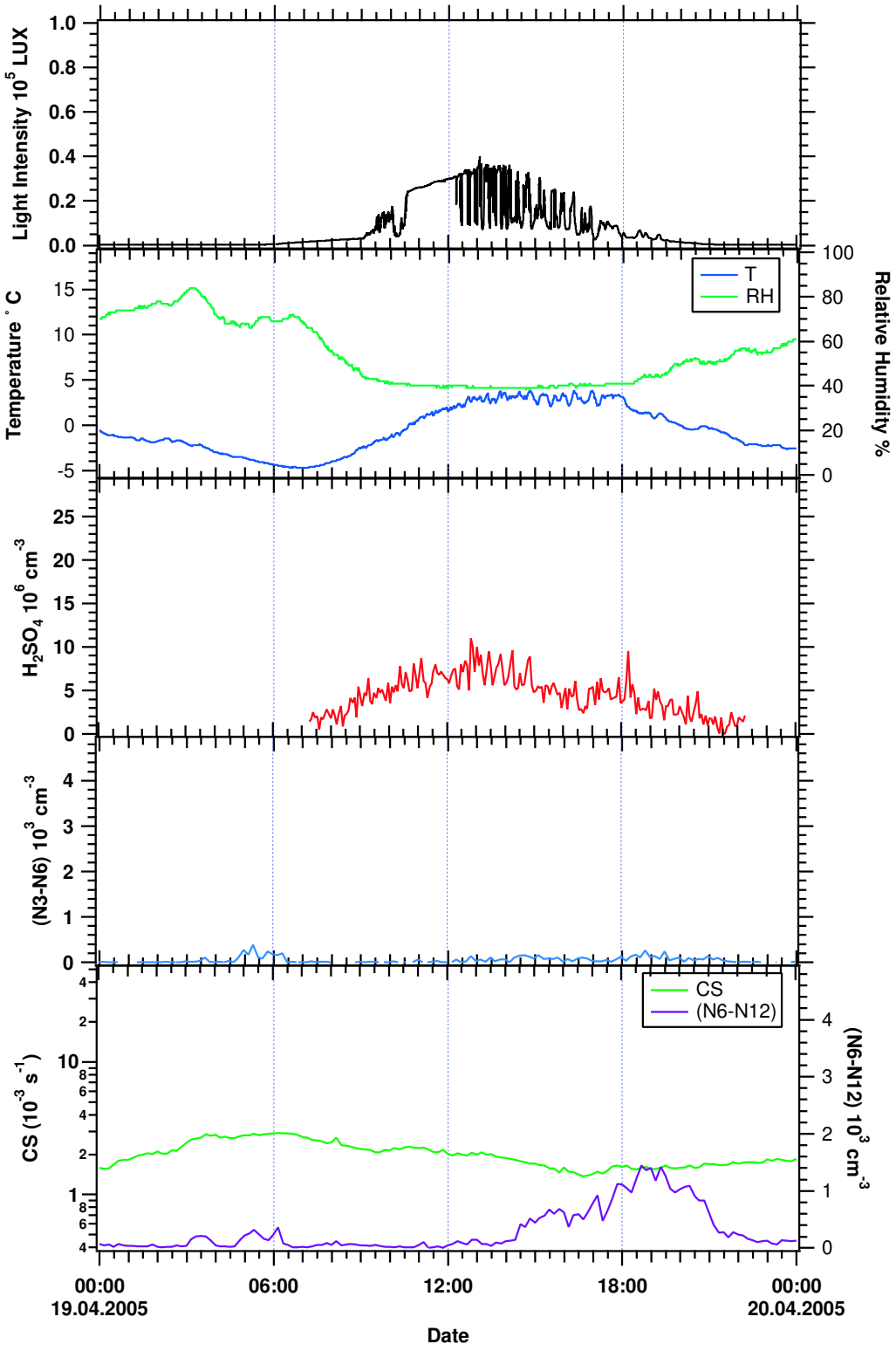

Figure A.11: Sulfuric acid number concentrations compared to particle and meteorological parameters measured on the 19th of April (Non-event day).

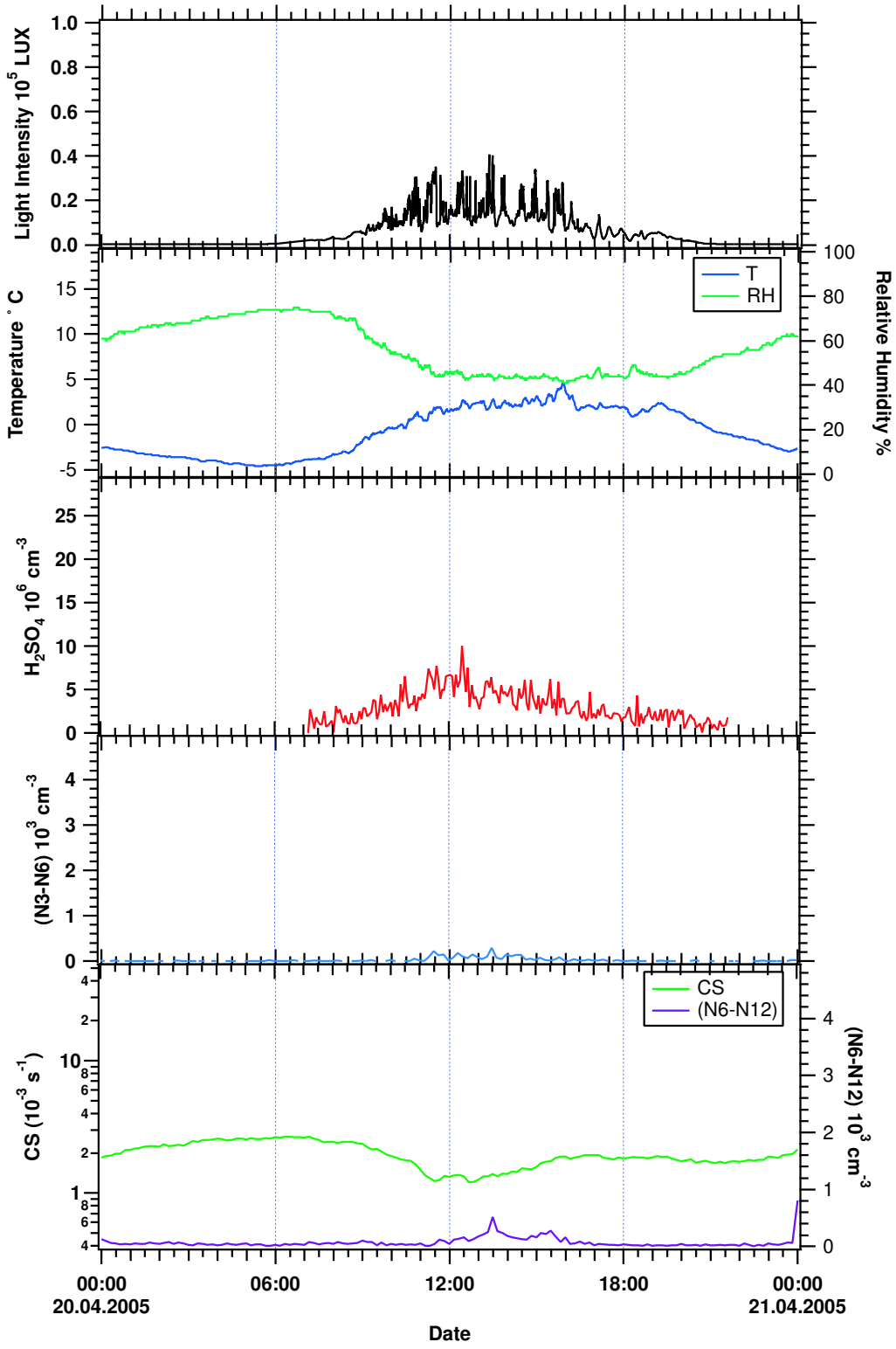

Figure A.12: Sulfuric acid number concentrations compared to particle and meteorological parameters measured on the 20th of April (Non-event day).

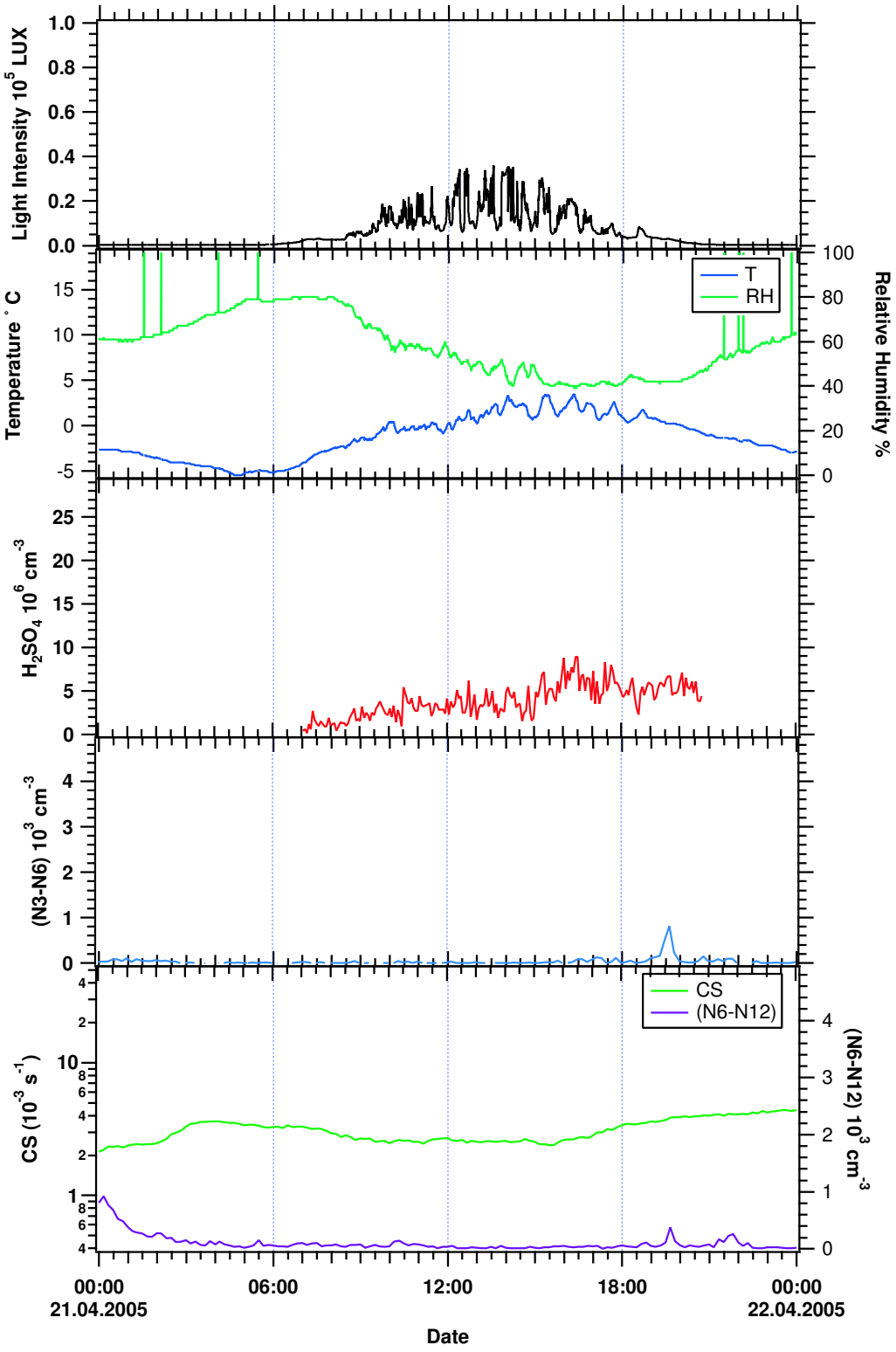

Figure A.13: Sulfuric acid number concentrations compared to particle and meteorological parameters measured on the 21th of April (Non-event day).

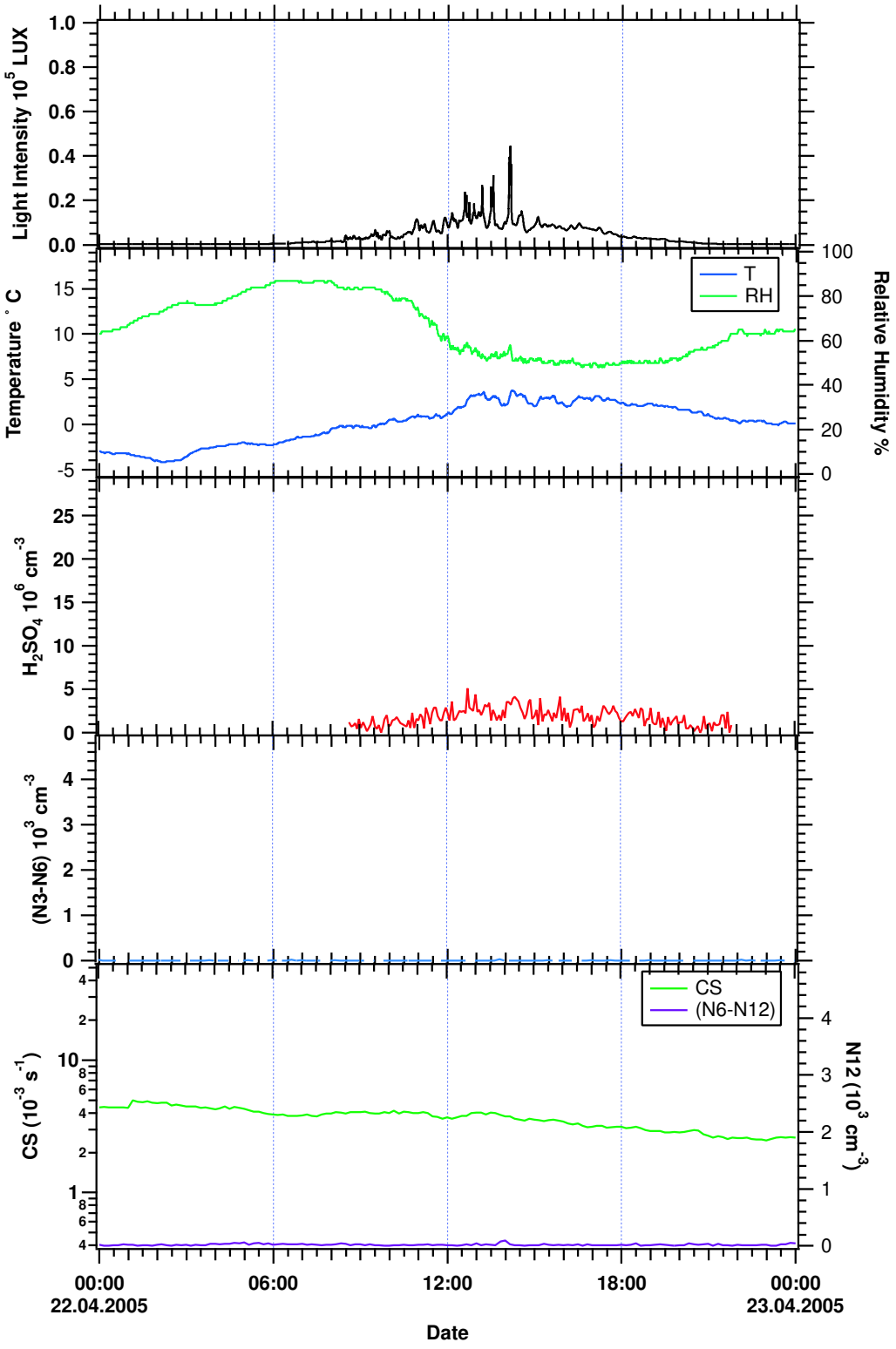

Figure A.14: Sulfuric acid number concentrations compared to particle and meteorological parameters measured on the 22th of April (Non-event day).

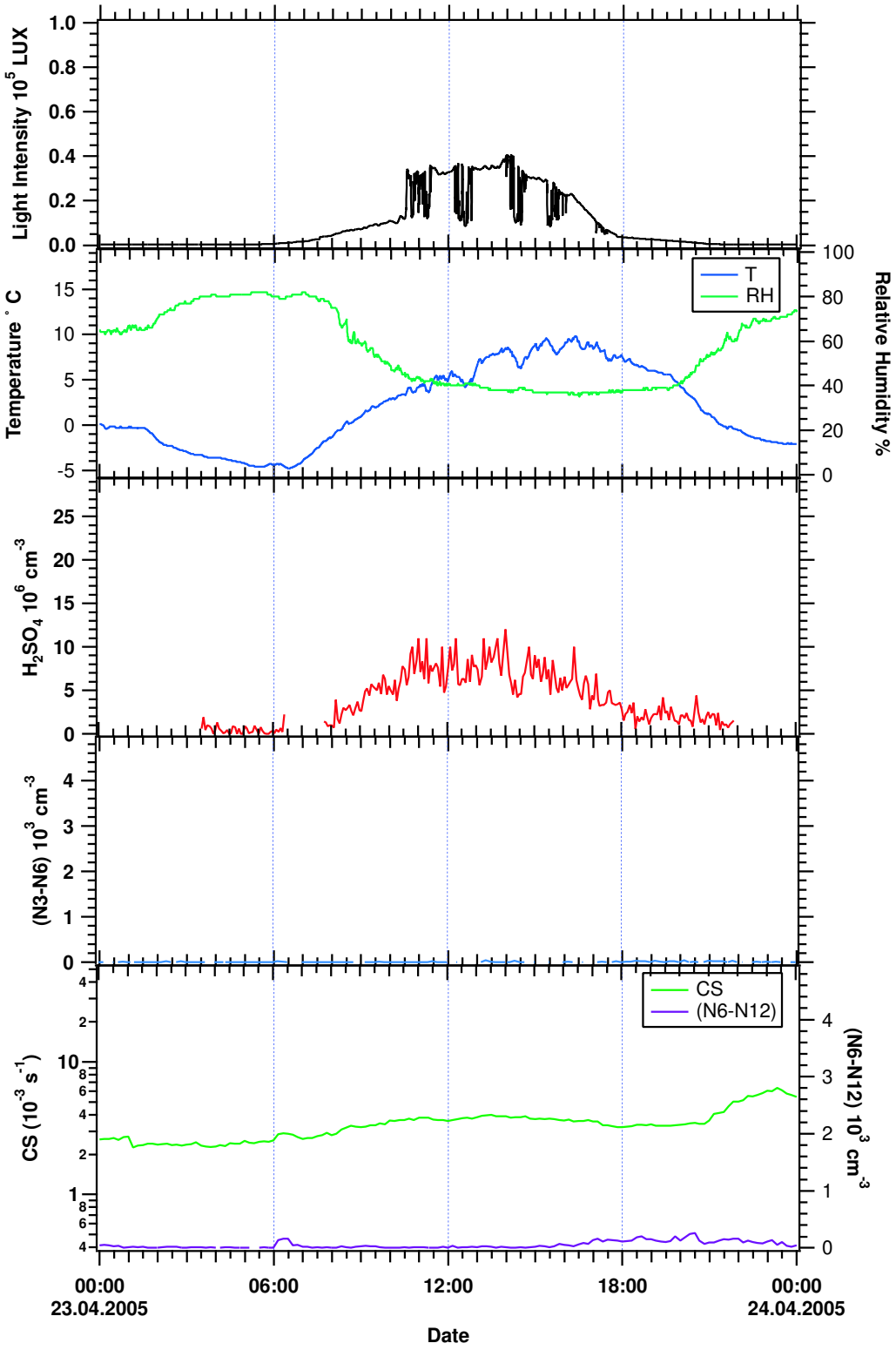

Figure A.15: Sulfuric acid number concentrations compared to particle and meteorological parameters measured on the 23th of April (Non-event day).

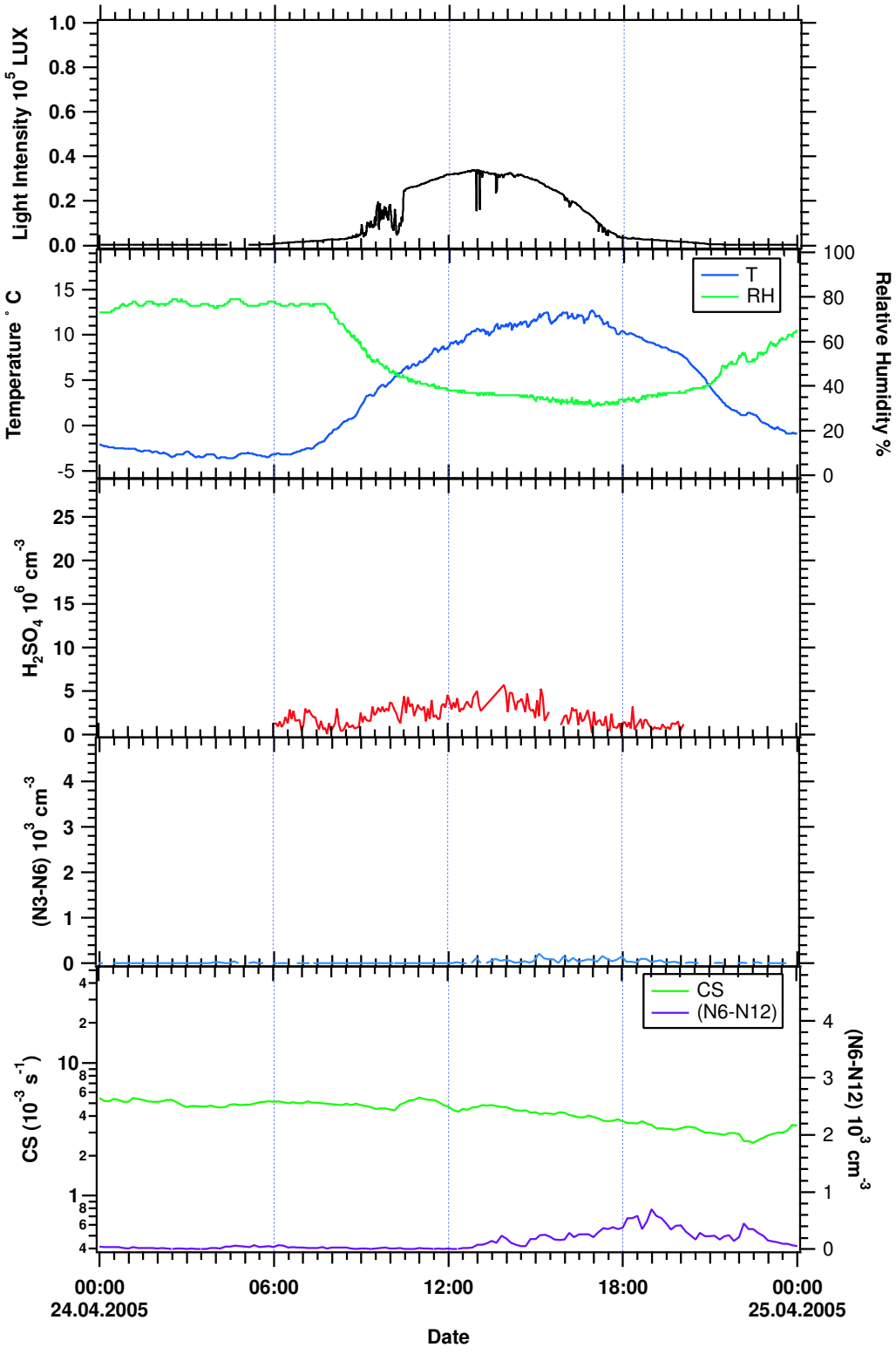

Figure A.16: Sulfuric acid number concentrations compared to particle and meteorological parameters measured on the 24th of April (Non-event day).

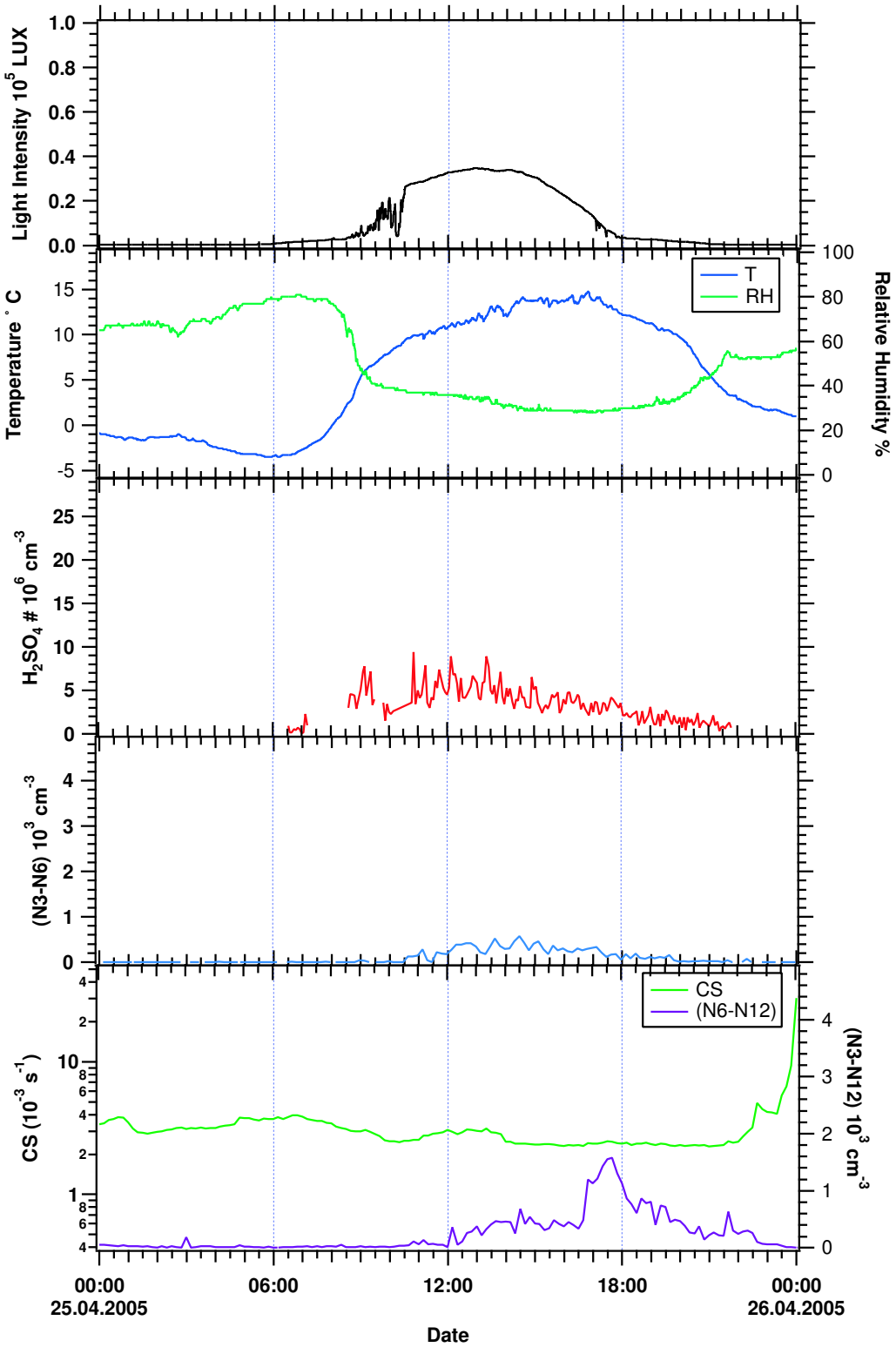

Figure A.17: Sulfuric acid number concentrations compared to particle and meteorological parameters measured on the 25th of April (Event day).

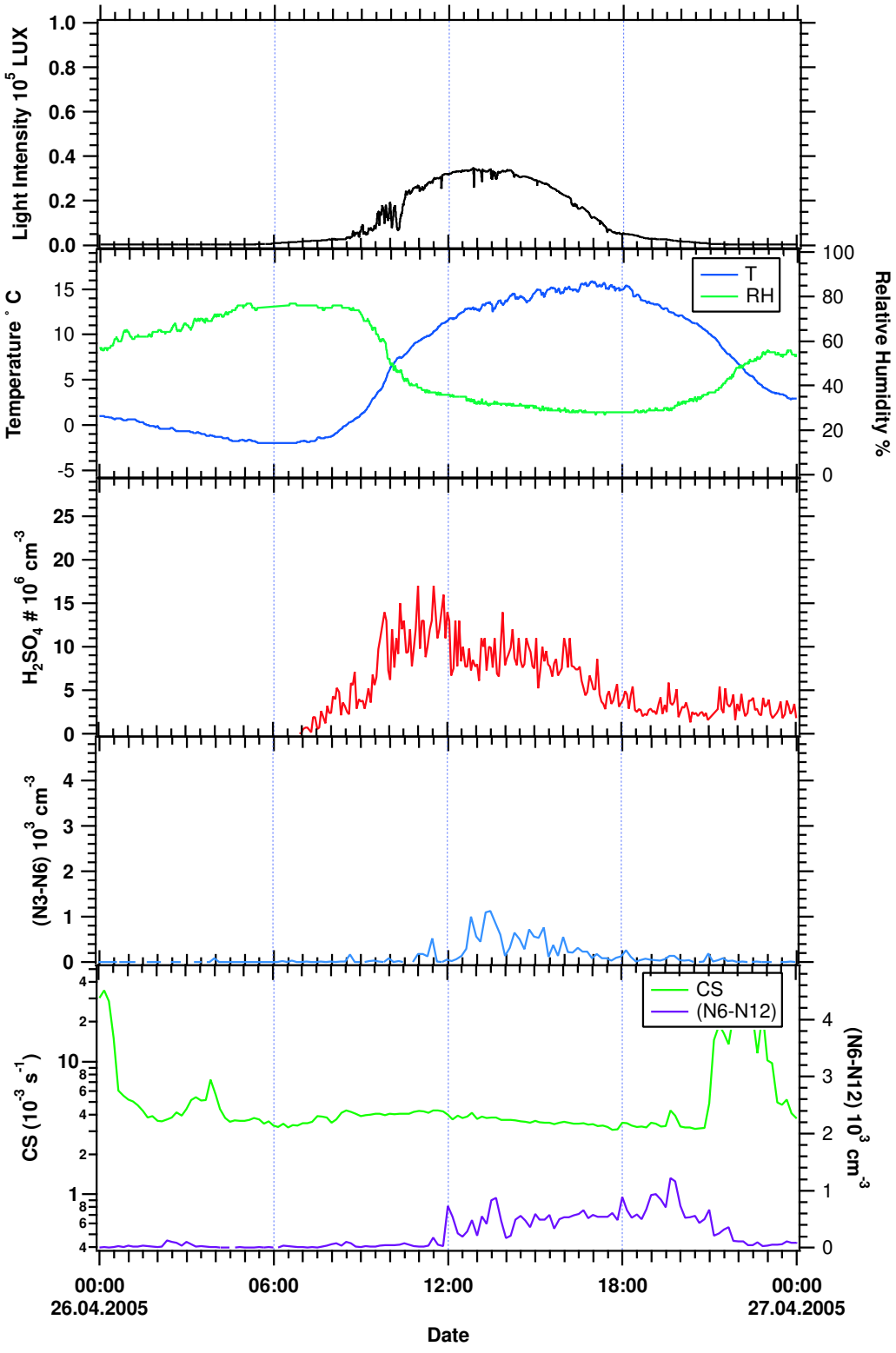

Figure A.18: Sulfuric acid number concentrations compared to particle and meteorological parameters measured on the 26th of April (Event day).

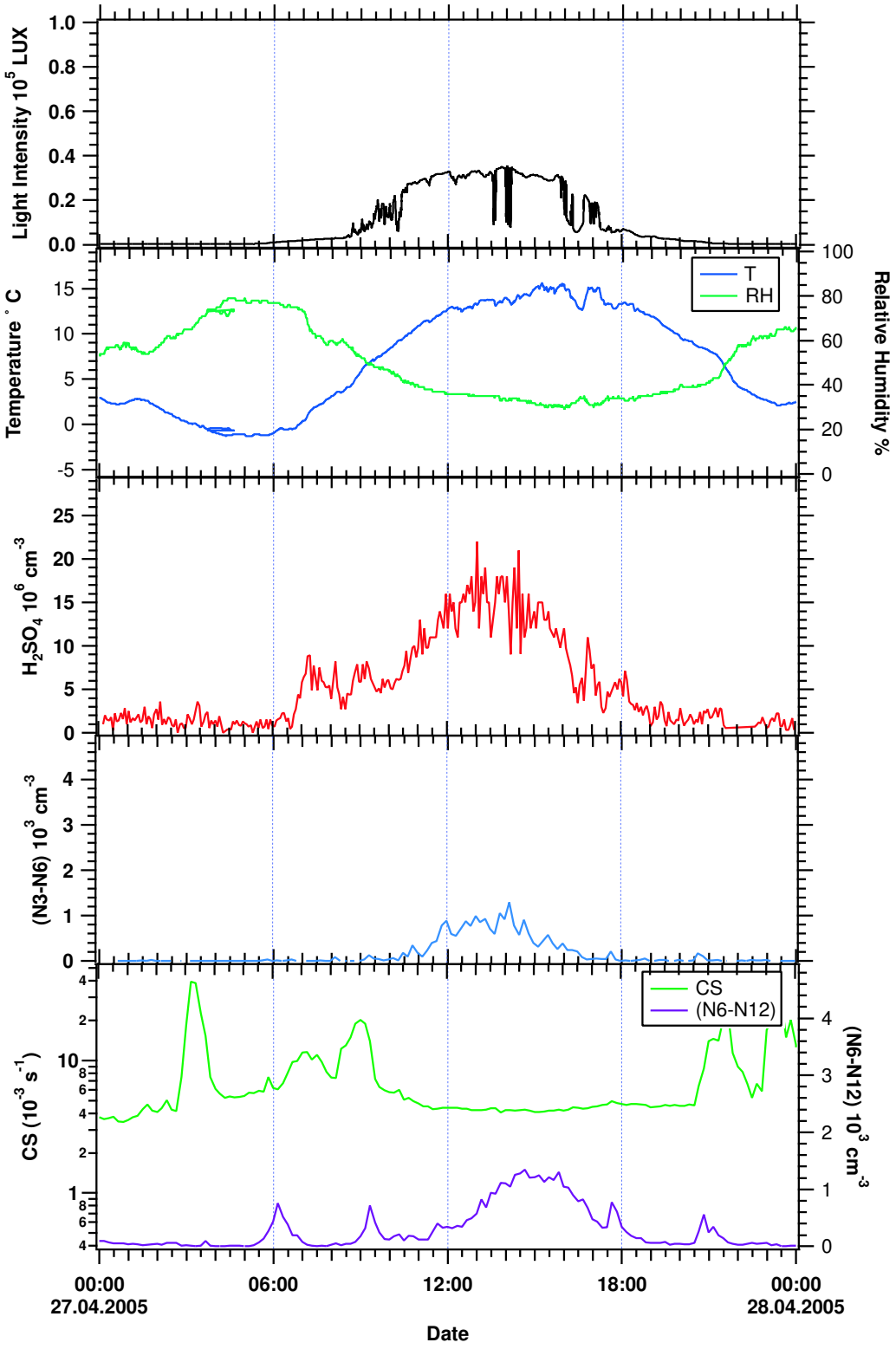

Figure A.19: Sulfuric acid number concentrations compared to particle and meteorological parameters measured on the 27th of April (Event day).

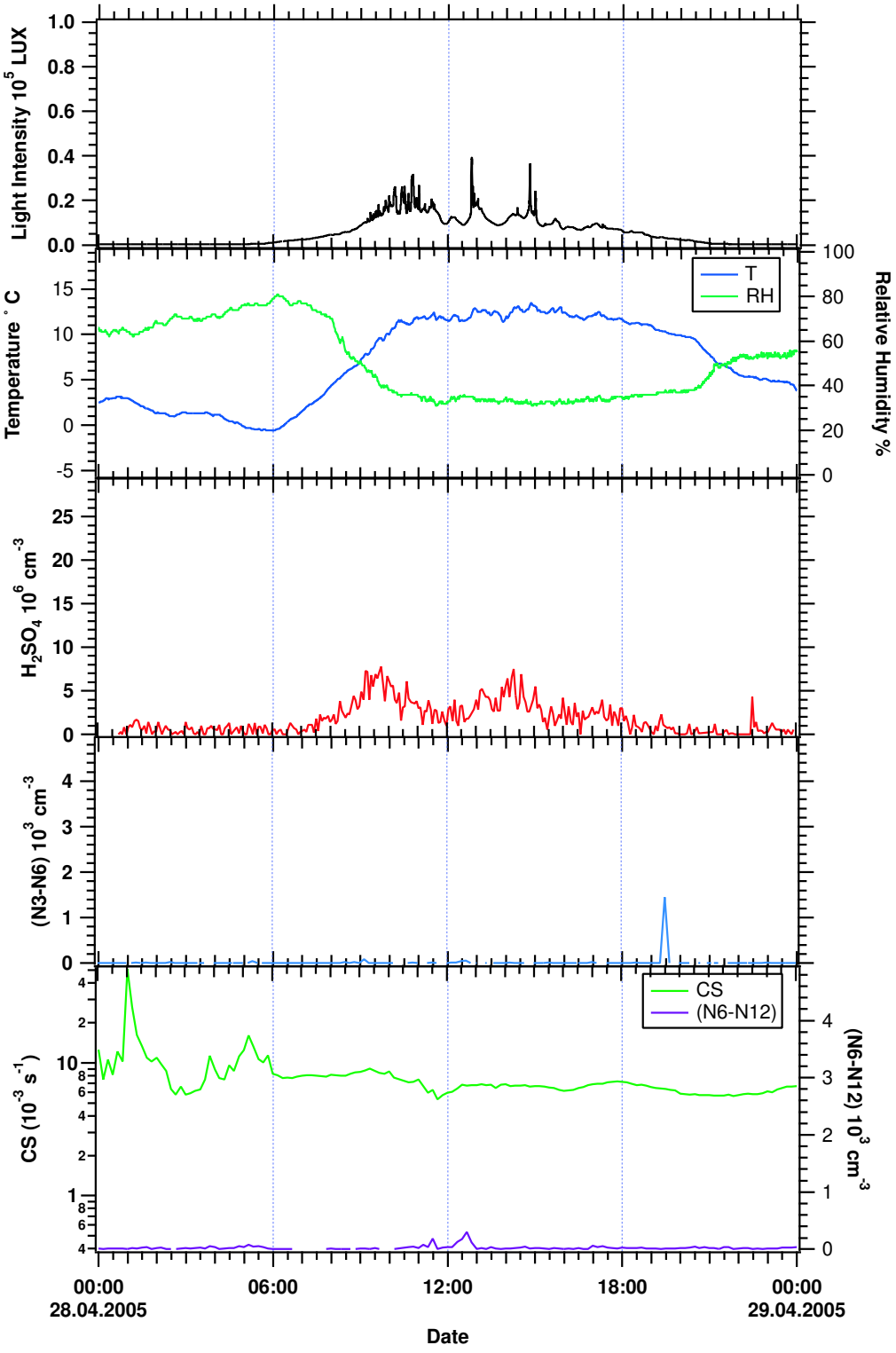

Figure A.20: Sulfuric acid number concentrations compared to particle and meteorological parameters measured on the 28th of April (Non-event day).

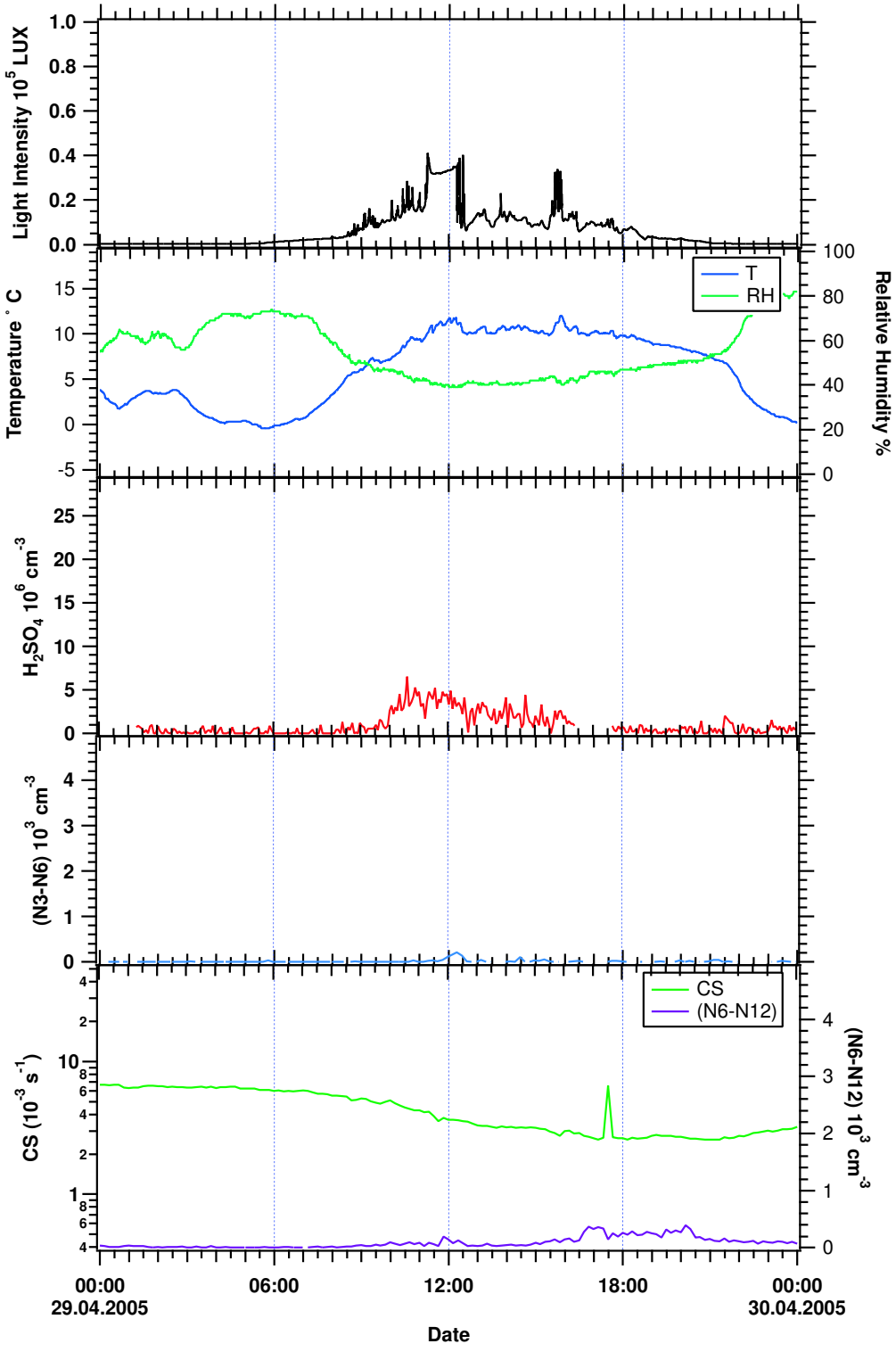

Figure A.21: Sulfuric acid number concentrations compared to particle and meteorological parameters measured on the 29th of April (Non-event day).

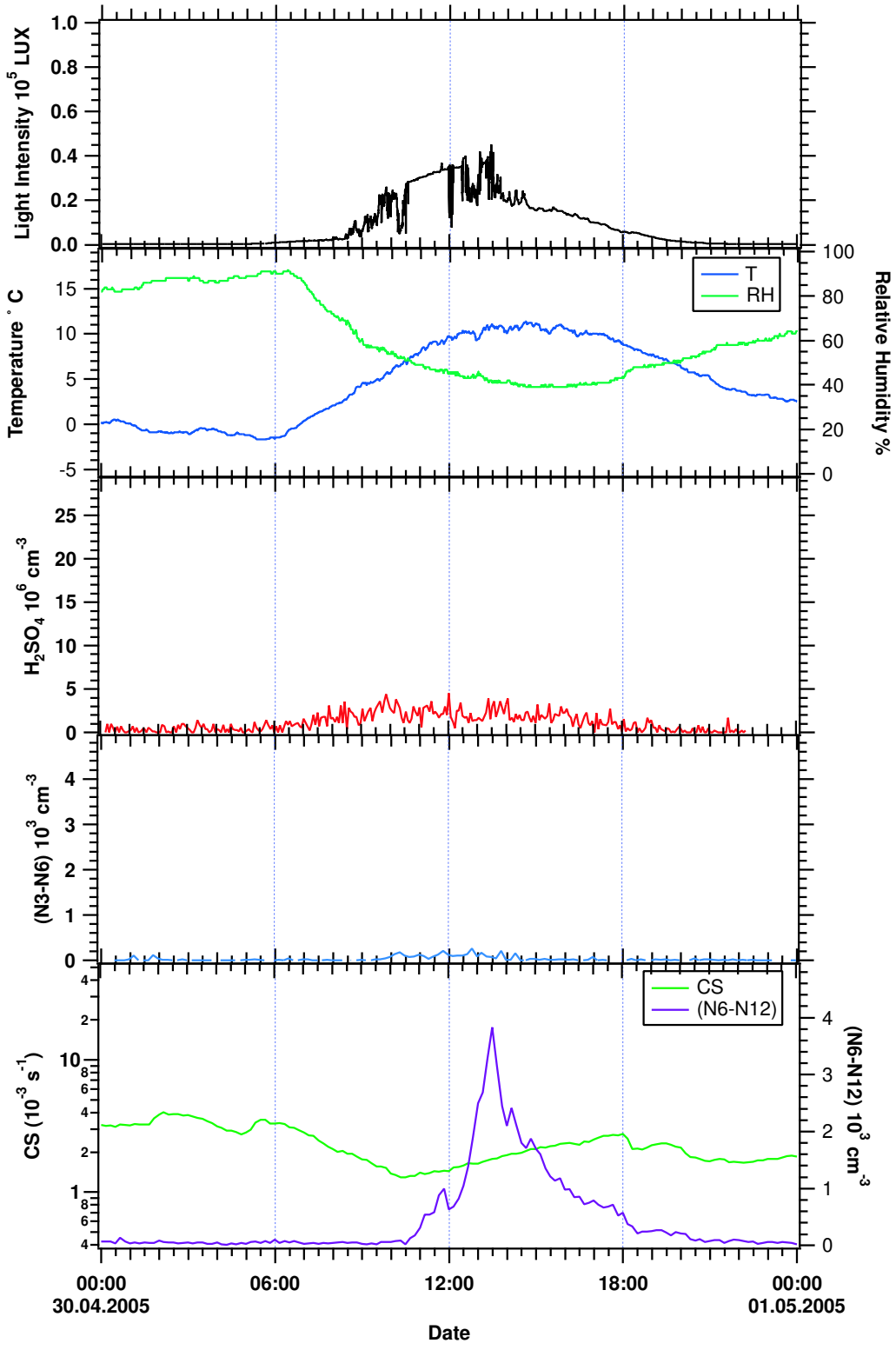

Figure A.22: Sulfuric acid number concentrations compared to particle and meteorological parameters measured on the 30th of April (Event day).

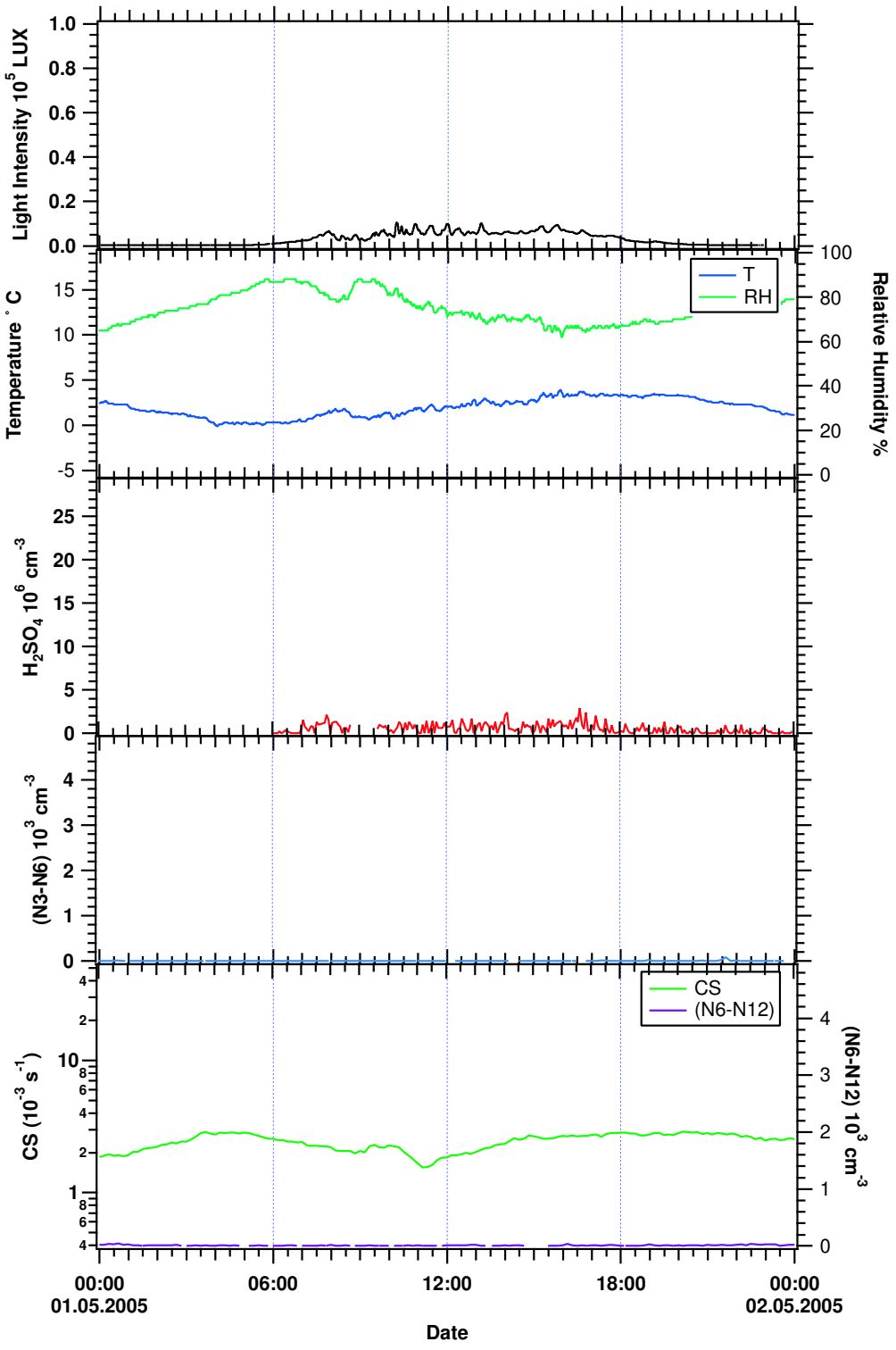

Figure A.23: Sulfuric acid number concentrations compared to particle and meteorological parameters measured on the 1st of May (Non-event day).

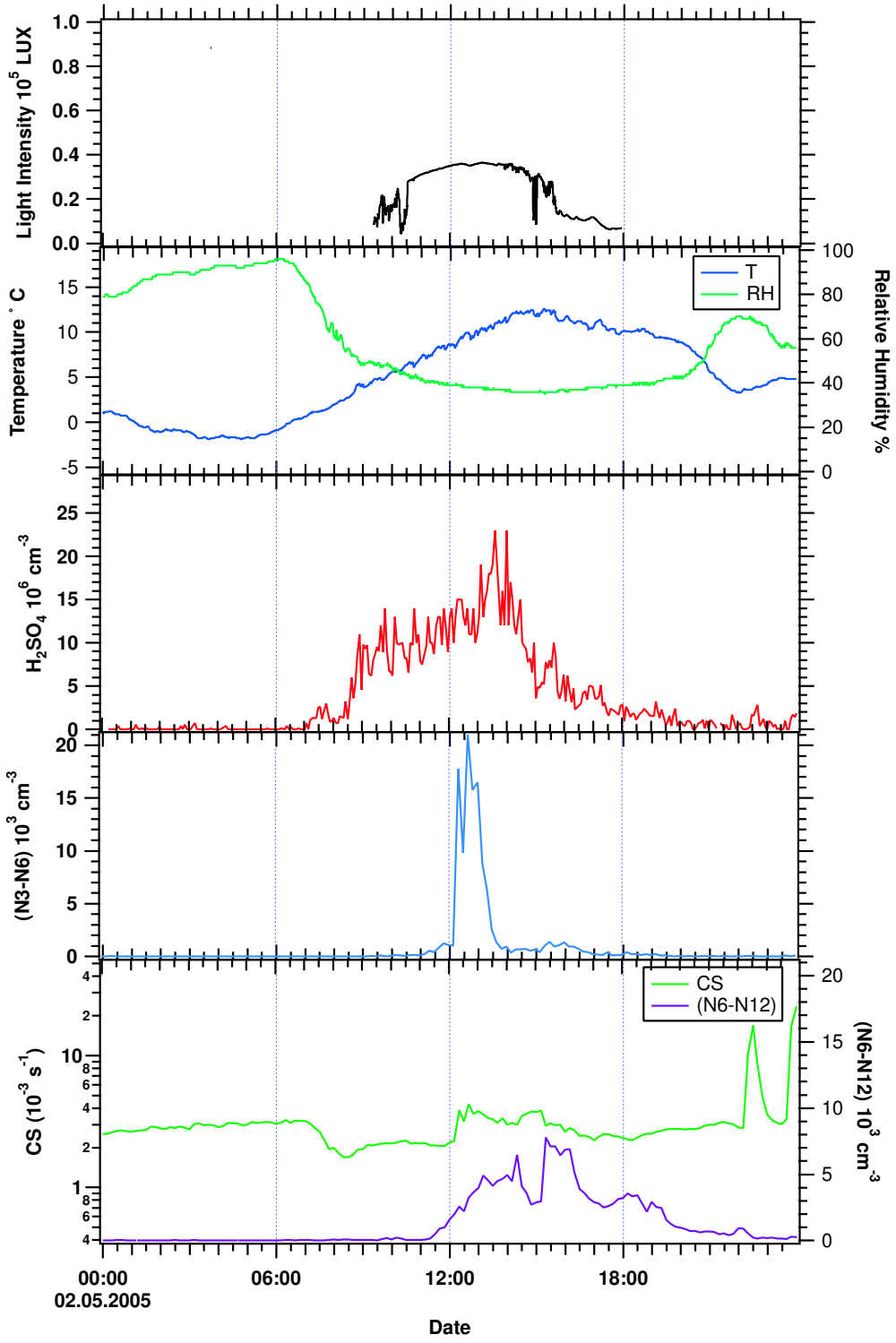

Figure A.24: Sulfuric acid number concentrations compared to particle and meteorological parameters measured on the 2nd of May (Event day).

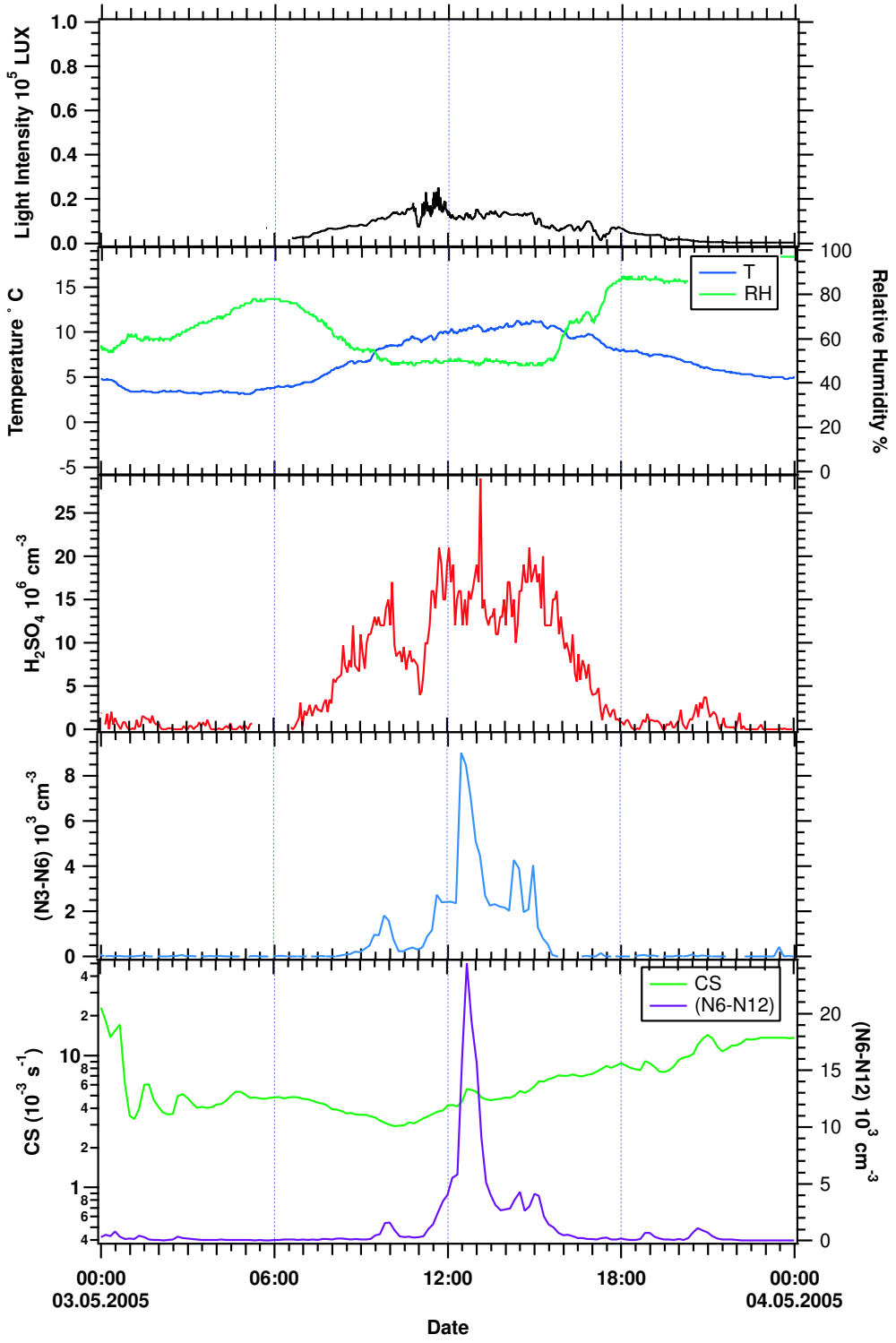

Figure A.25: Sulfuric acid number concentrations compared to particle and meteorological parameters measured on the 3rd of May (Event day).

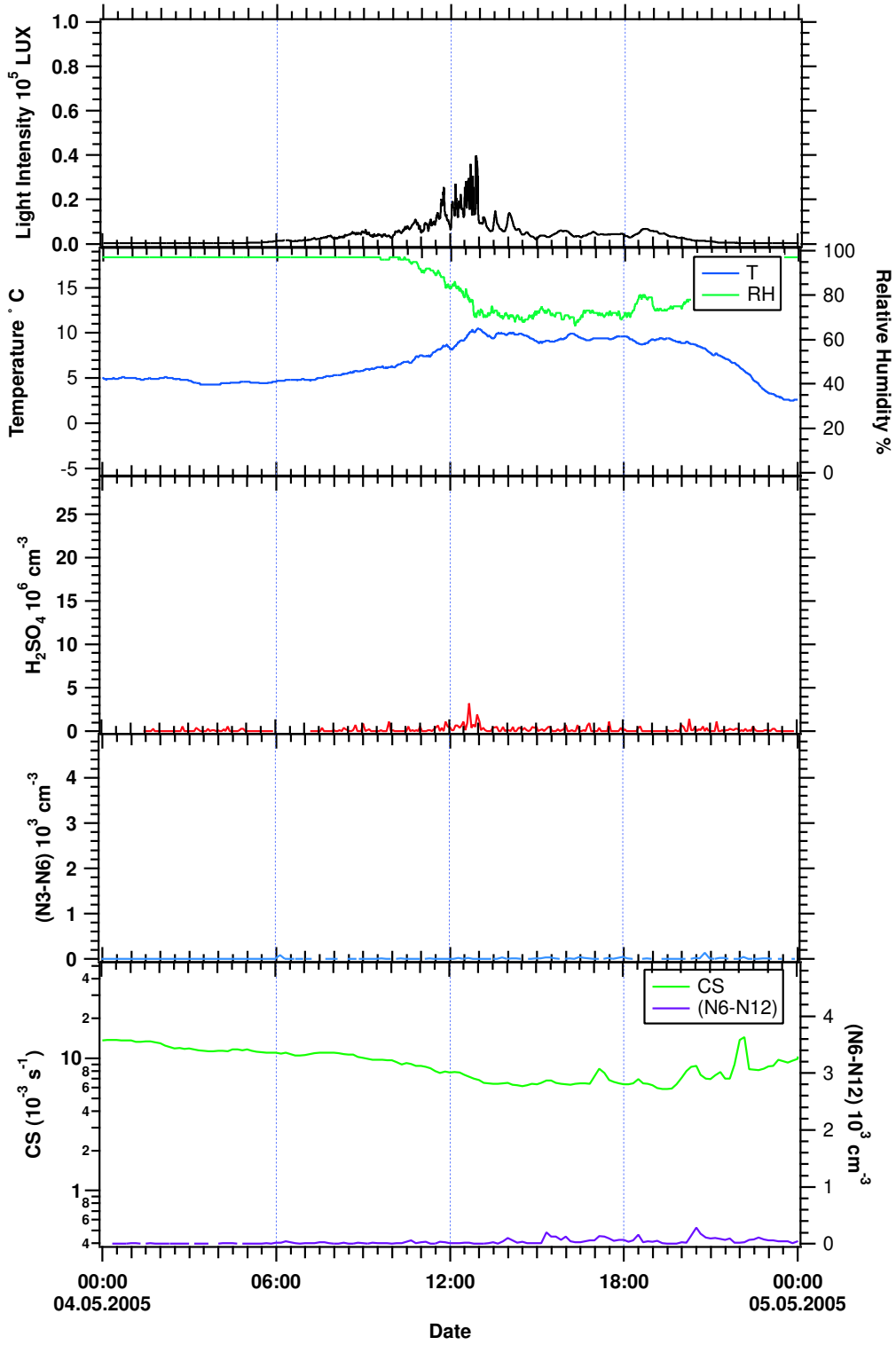

Figure A.26: Sulfuric acid number concentrations compared to particle and meteorological parameters measured on the 4th of May (Non-event day).

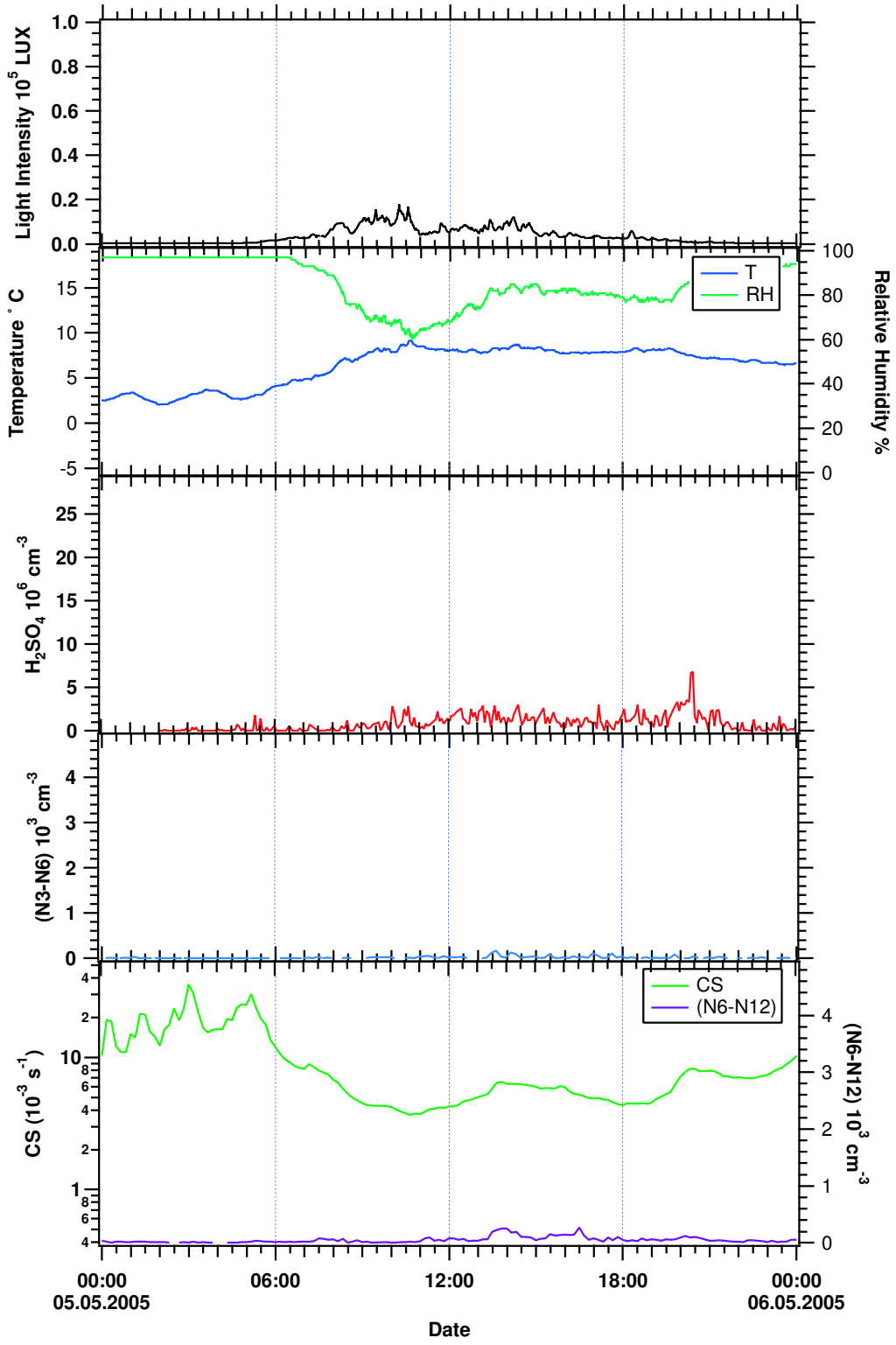

Figure A.27: Sulfuric acid number concentrations compared to particle and meteorological parameters measured on the 5th of May (Non-event day).

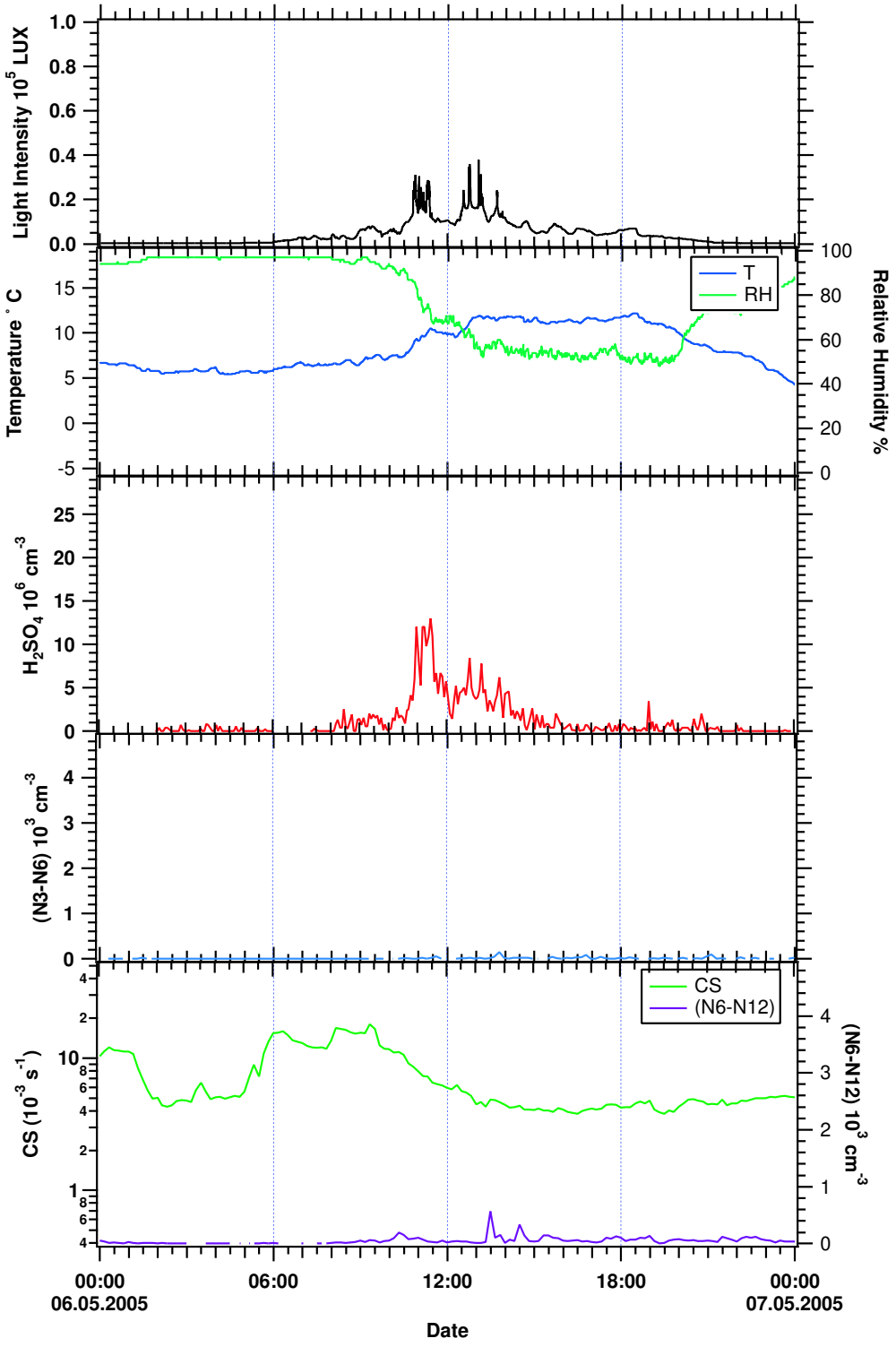

Figure A.28: Sulfuric acid number concentrations compared to particle and meteorological parameters measured on the 6th of May (Non-event day).

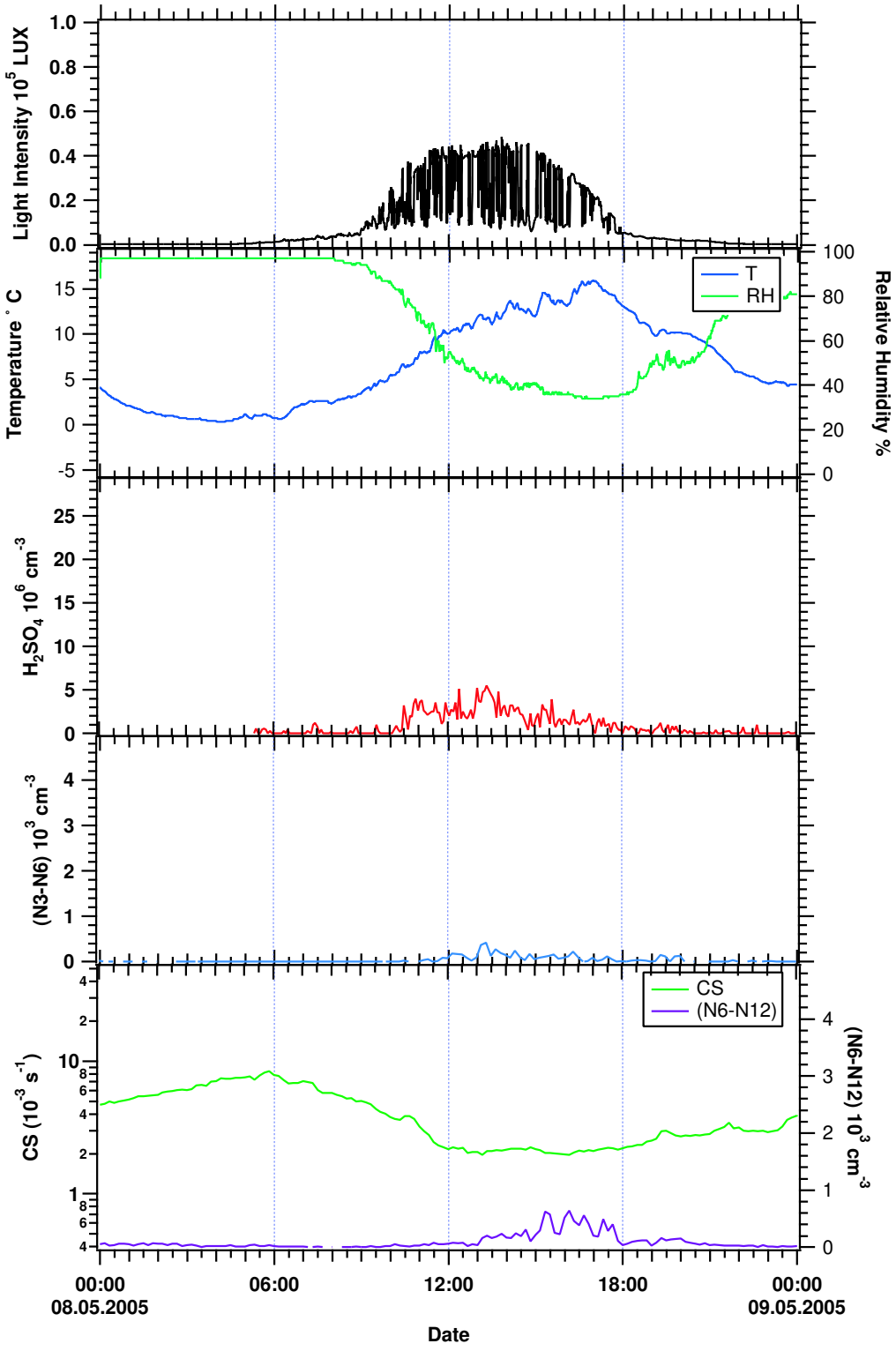

Figure A.29: Sulfuric acid number concentrations compared to particle and meteorological parameters measured on the 8th of May (Non-event day).

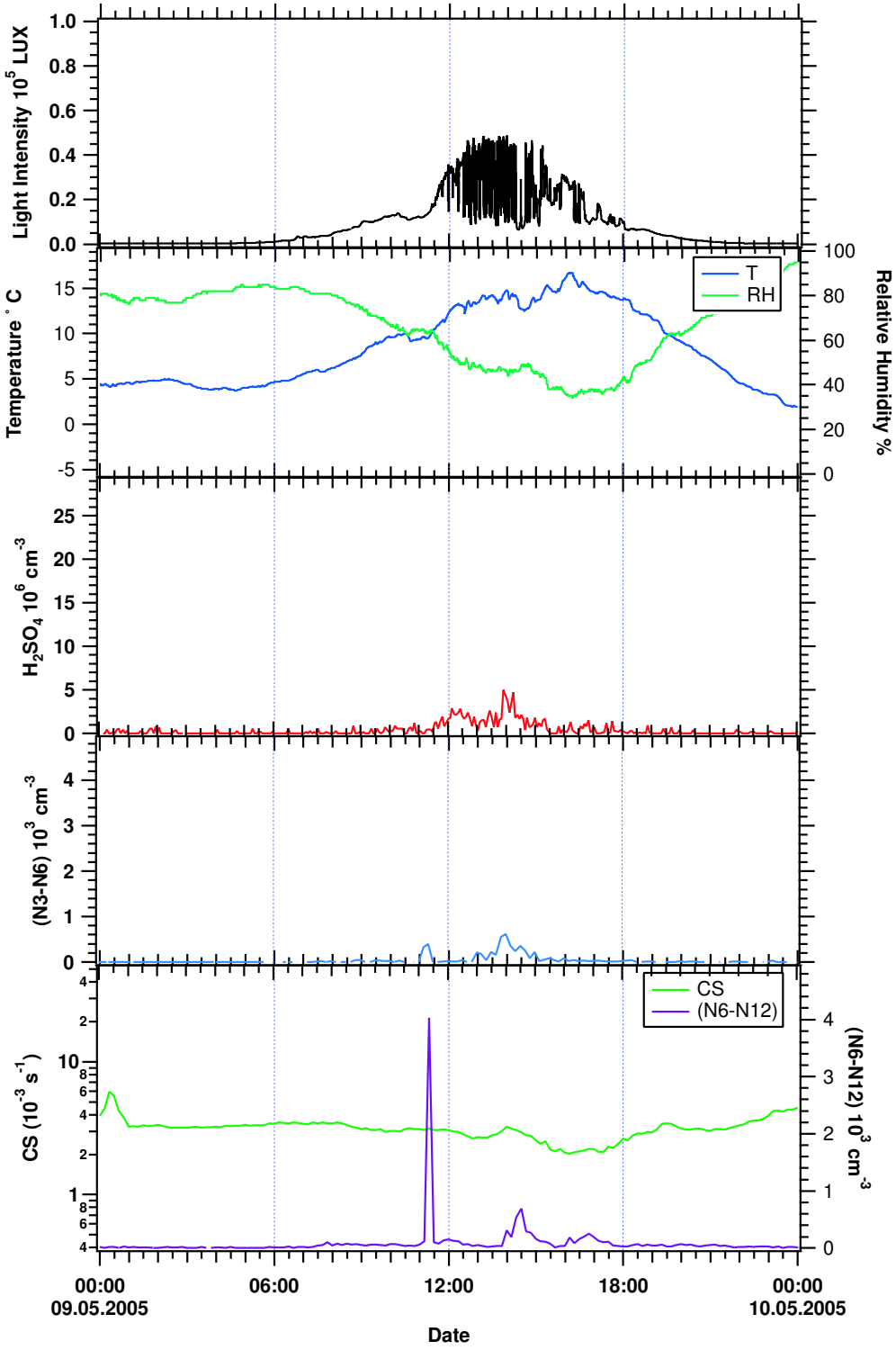

Figure A.30: Sulfuric acid number concentrations compared to particle and meteorological parameters measured on the 9th of May (Non-event day).

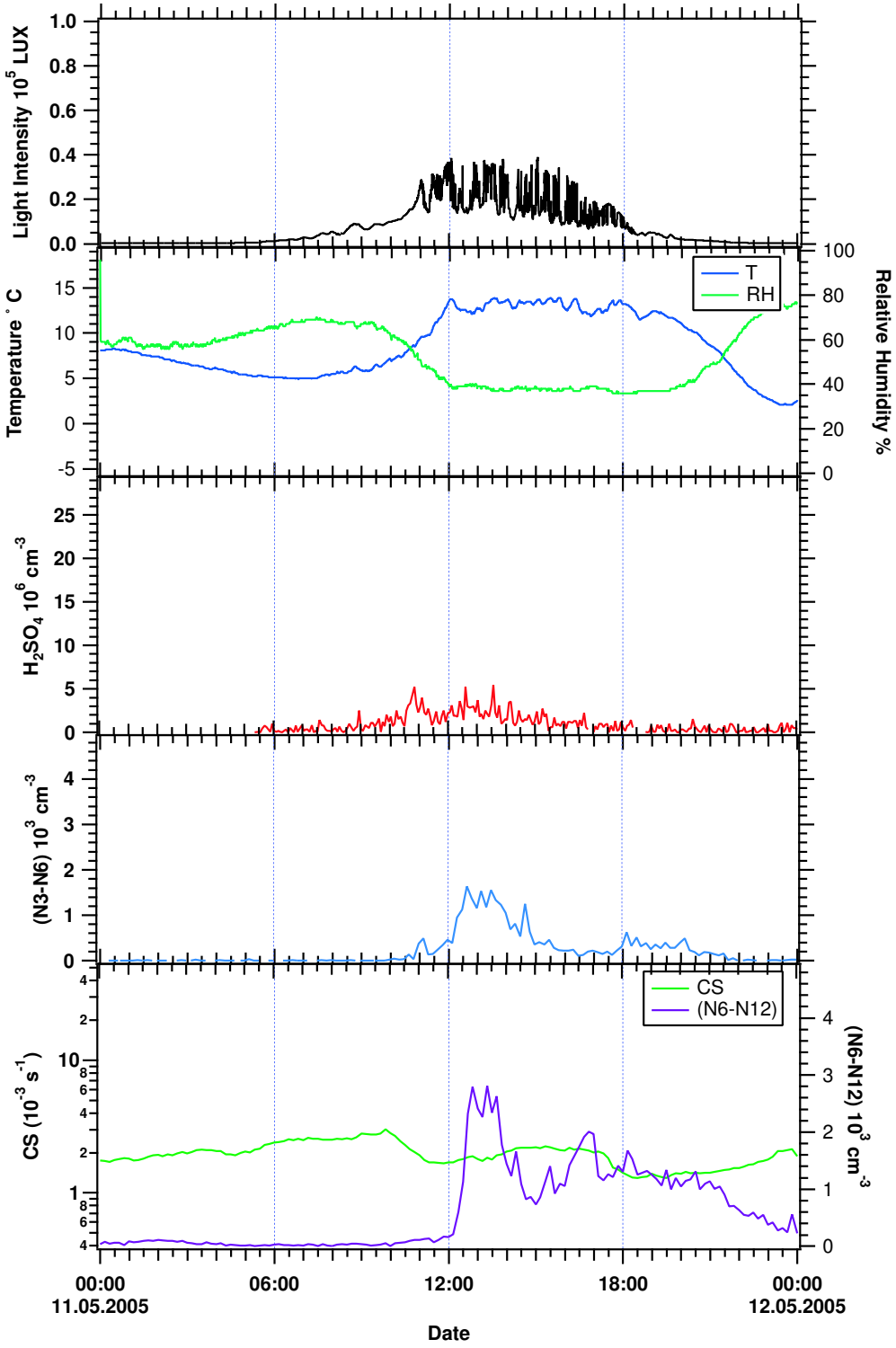

Figure A.31: Sulfuric acid number concentrations compared to particle and meteorological parameters measured on the 11th of May (Event day).

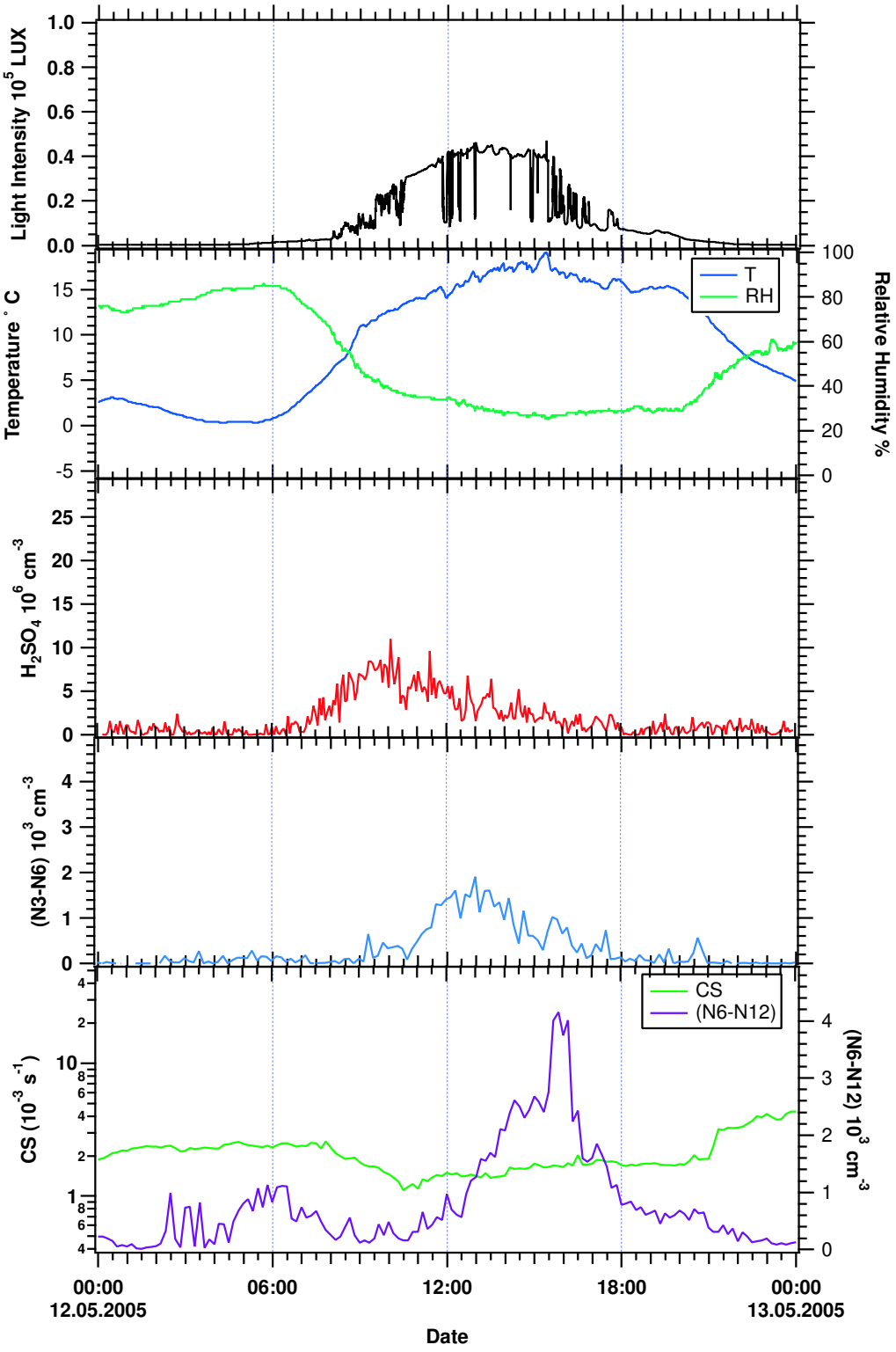

Figure A.32: Sulfuric acid number concentrations compared to particle and meteorological parameters measured on the 12th of May (Event day).

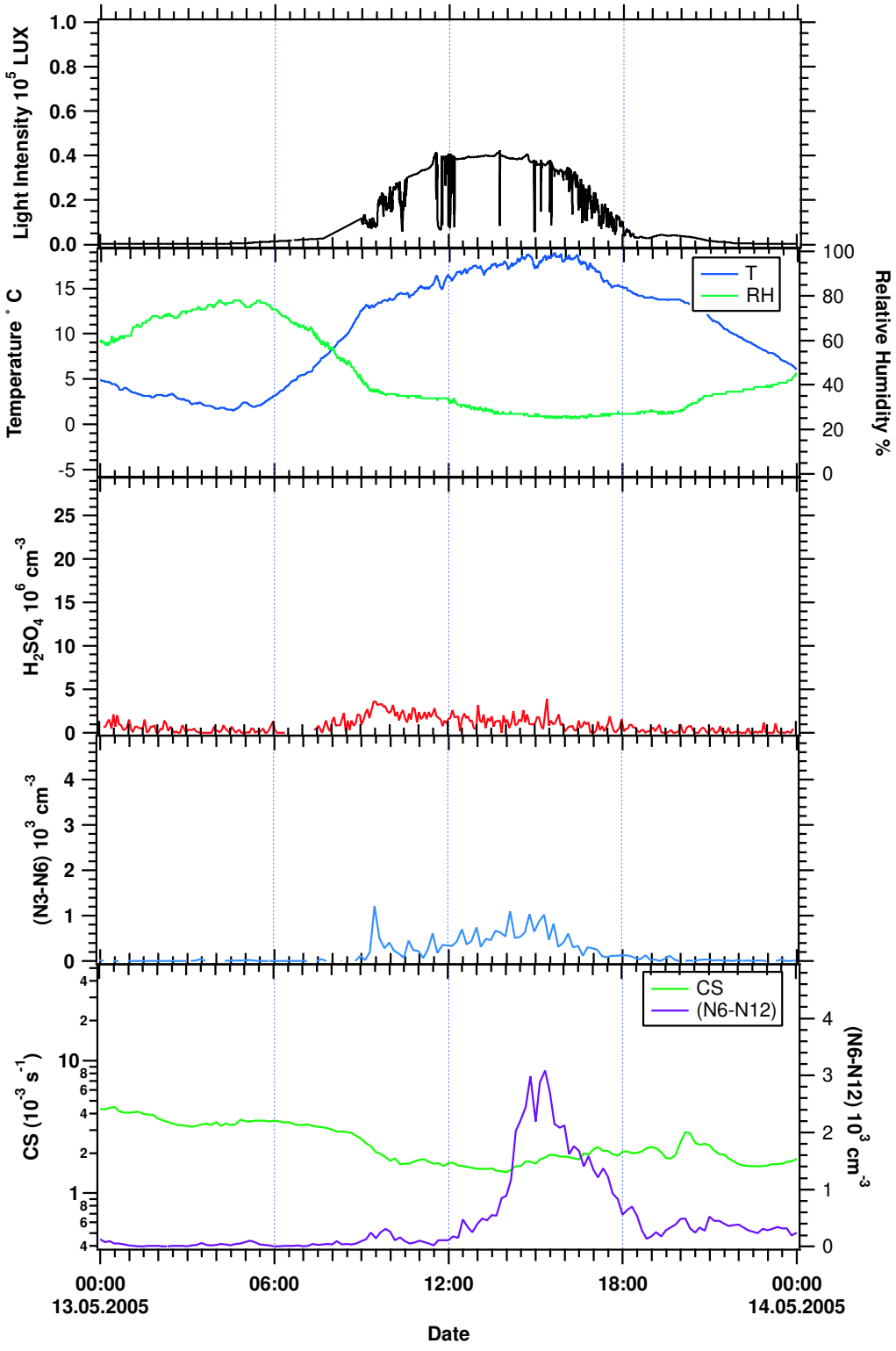

Figure A.33: Sulfuric acid number concentrations compared to particle and meteorological parameters measured on the 13th of May (Event day).

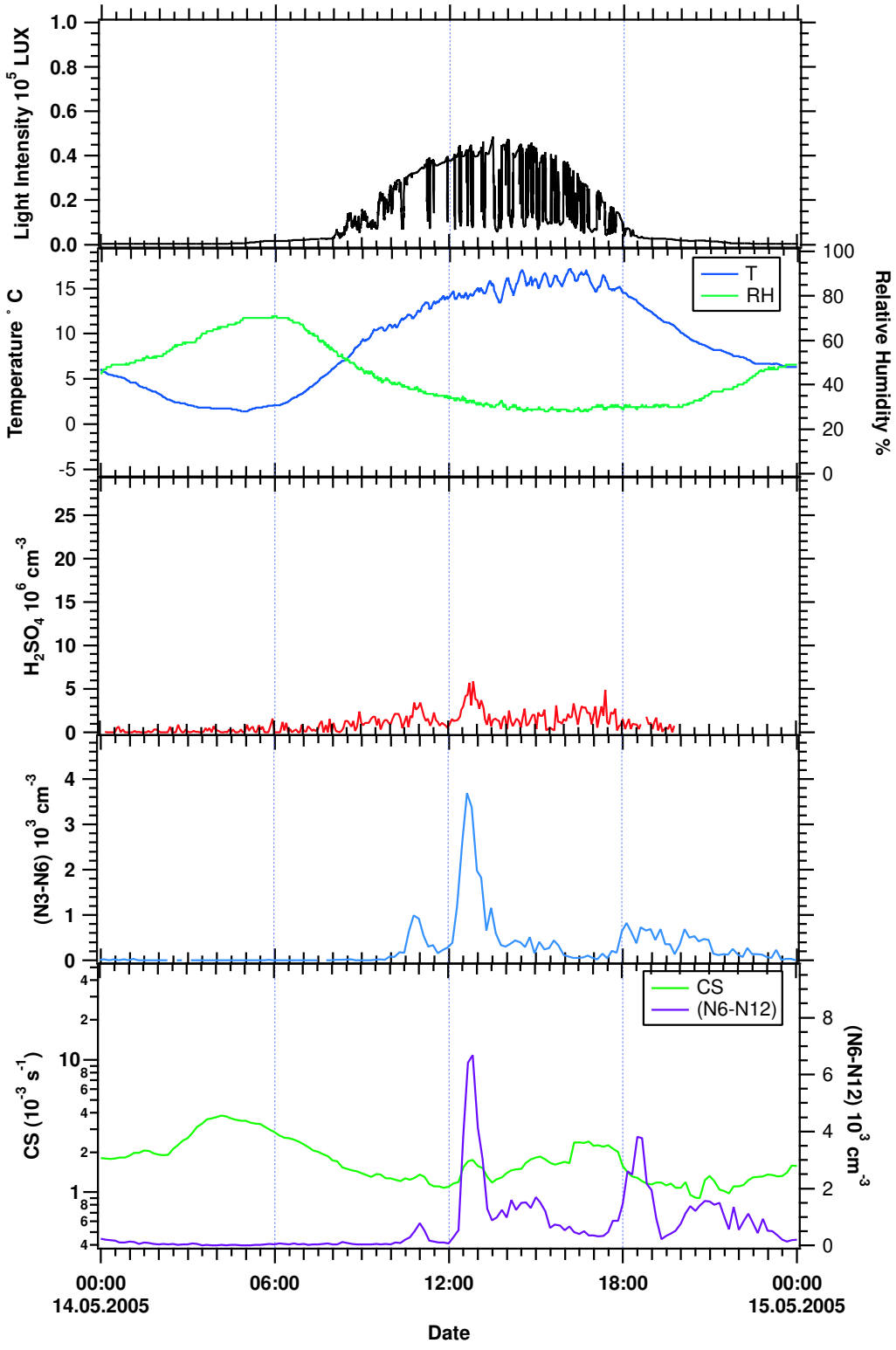

Figure A.34: Sulfuric acid number concentrations compared to particle and meteorological parameters measured on the 14th of May (Event day).

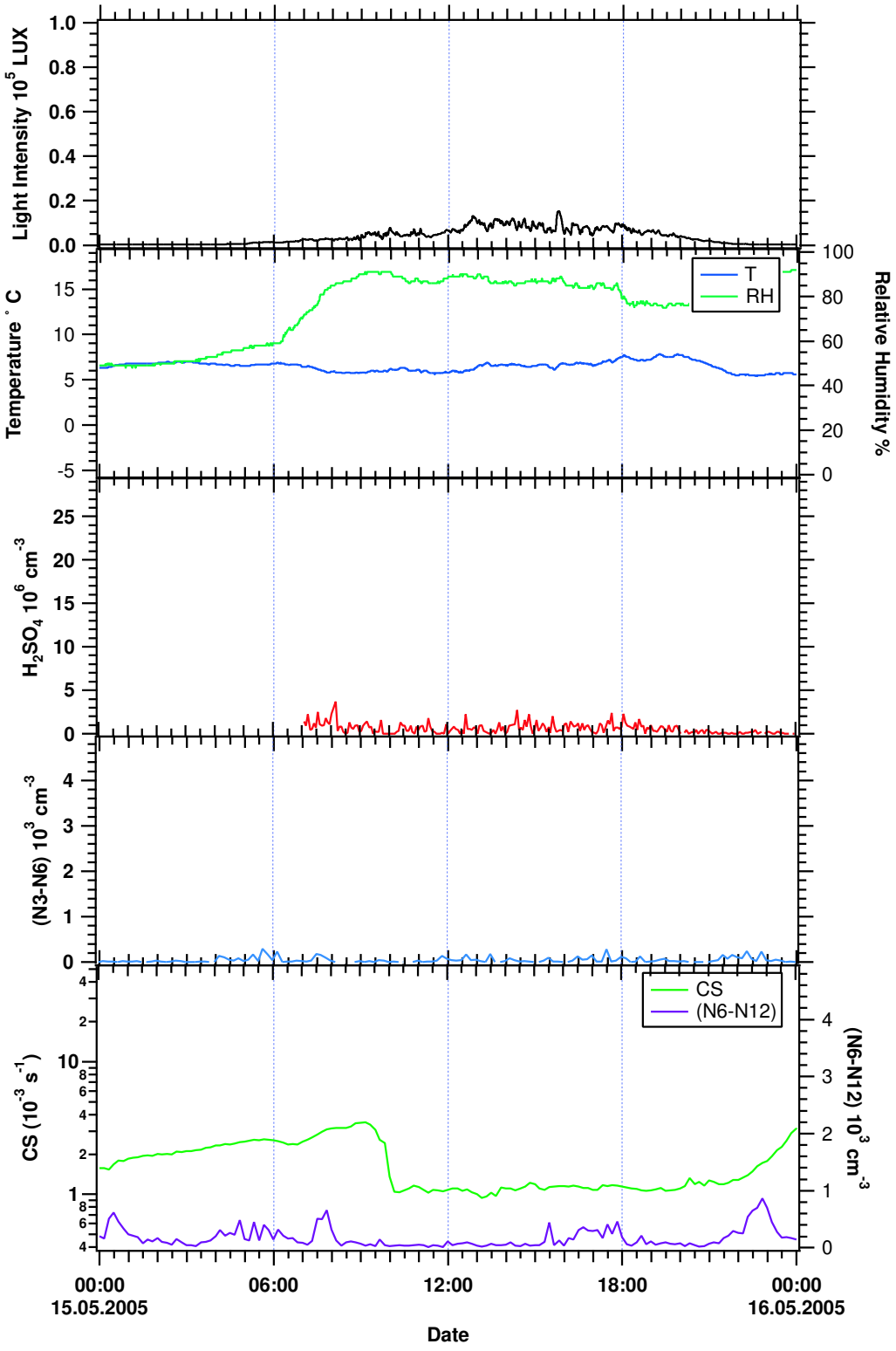

Figure A.35: Sulfuric acid number concentrations compared to particle and meteorological parameters measured on the 15th of May (Non-event day).

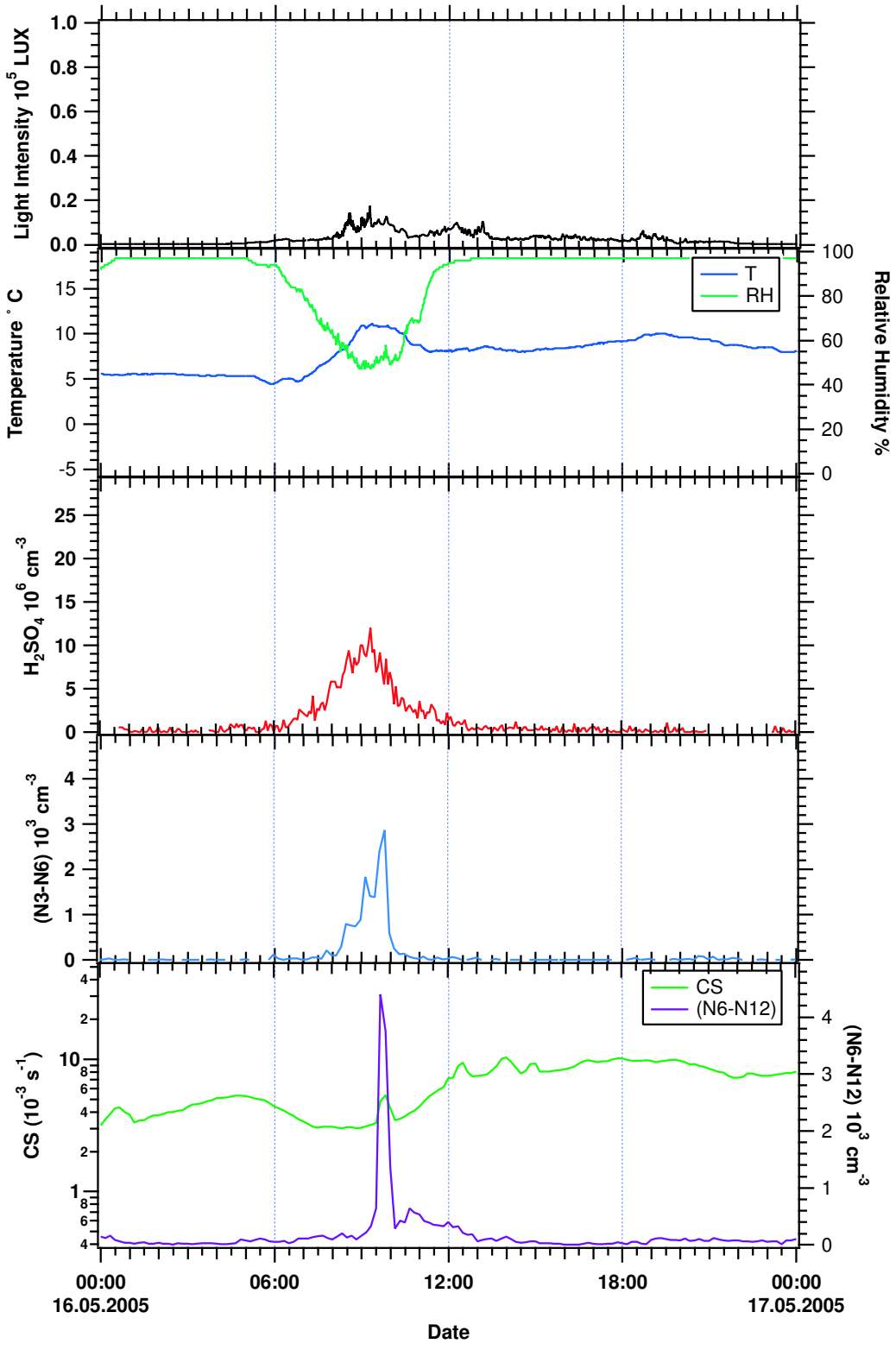

Figure A.36: Sulfuric acid number concentrations compared to particle and meteorological parameters measured on the 16th of May (Non-event day).

Appendix B

Correlation Plots

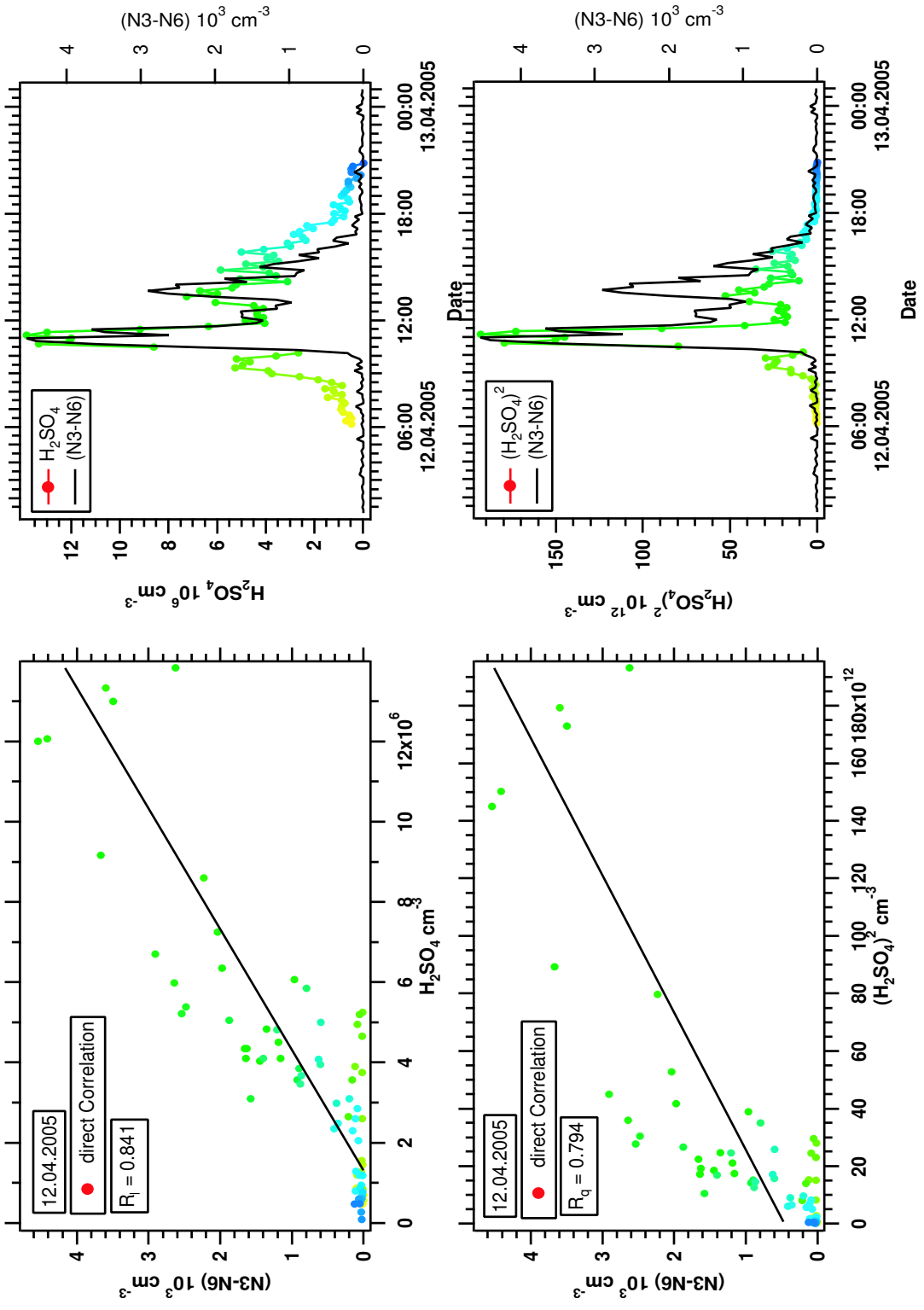

Figure B.1: Direct correlation plots for the 12th of April. (Timeshift analysis was not applied). On the left side time series of (N3-N6) and of H_2SO_4 concentration (linear and squared) are compared. On the left side the corresponding scatter plots are shown.

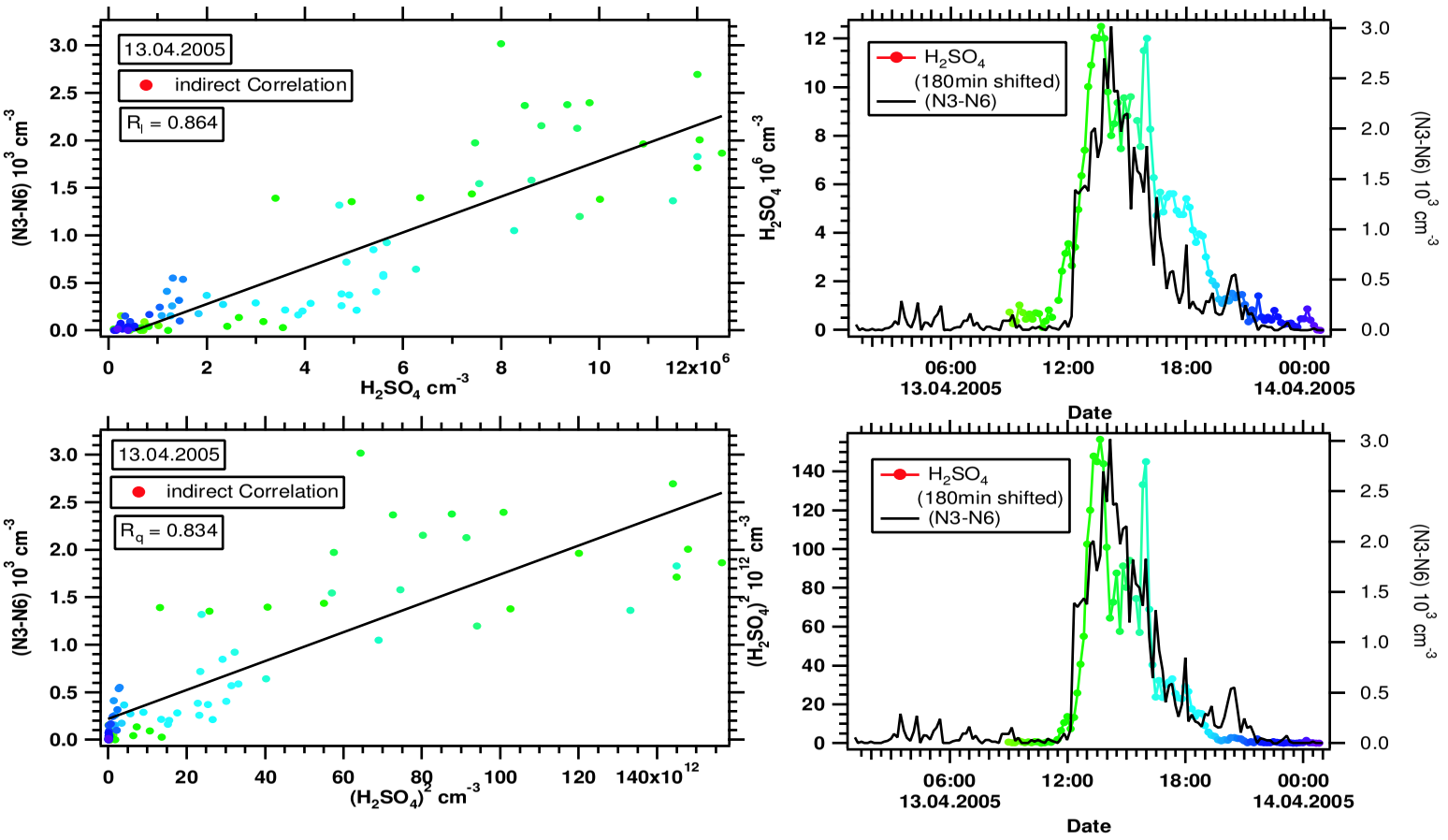

Figure B.2: Indirect correlation plots for the 13th of April. (Timeshift analysis was applied). On the left side time series of (N3-N6) and of H_2SO_4 concentration (linear and squared) are compared. On the left side the corresponding scatter plots are shown.

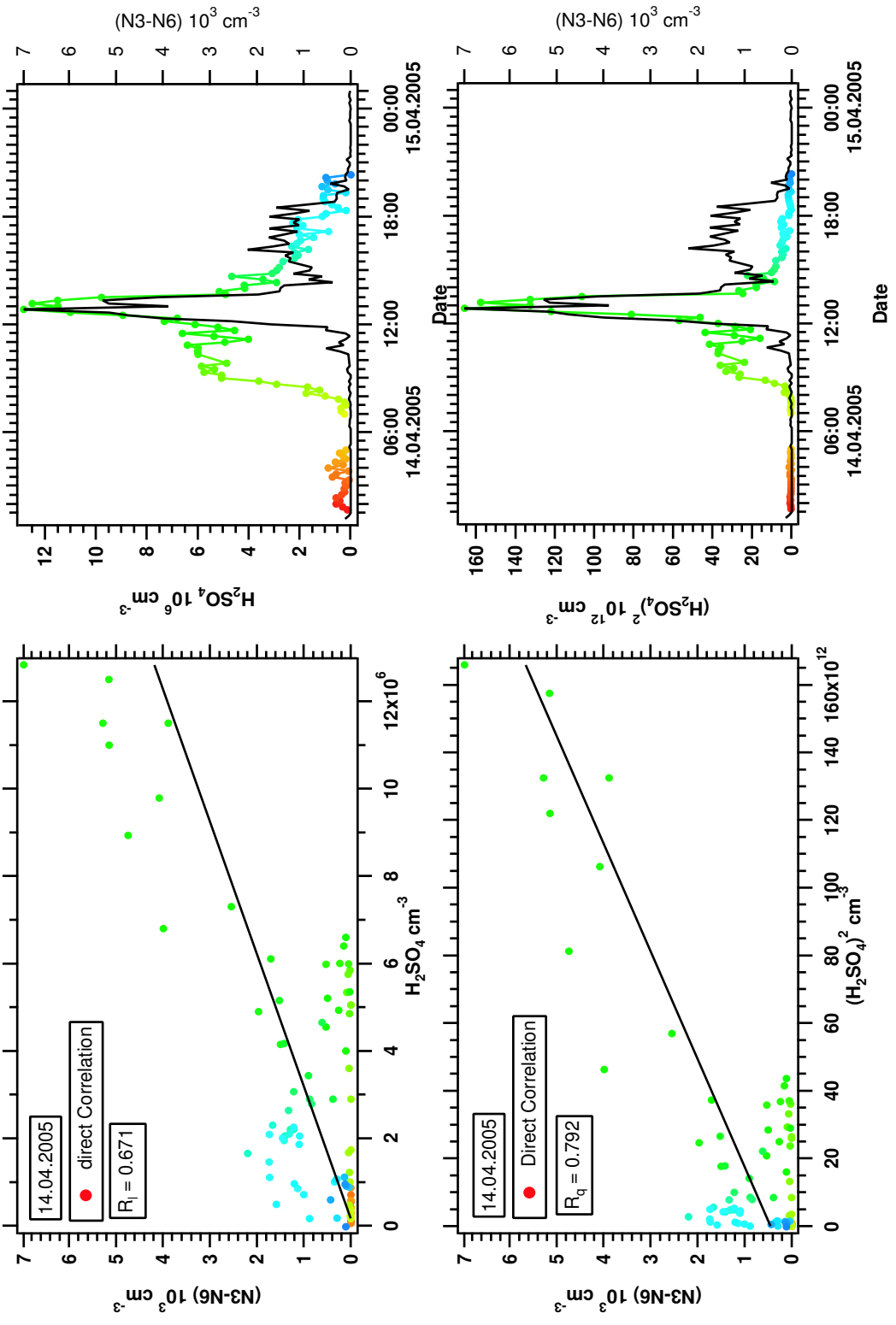

Figure B.3: Direct correlation plots for the 14th of April. (Timeshift analysis was not applied). On the left side time series of (N3-N6) and of H_2SO_4 concentration (linear and squared) are compared. On the left side the corresponding scatter plots are shown.

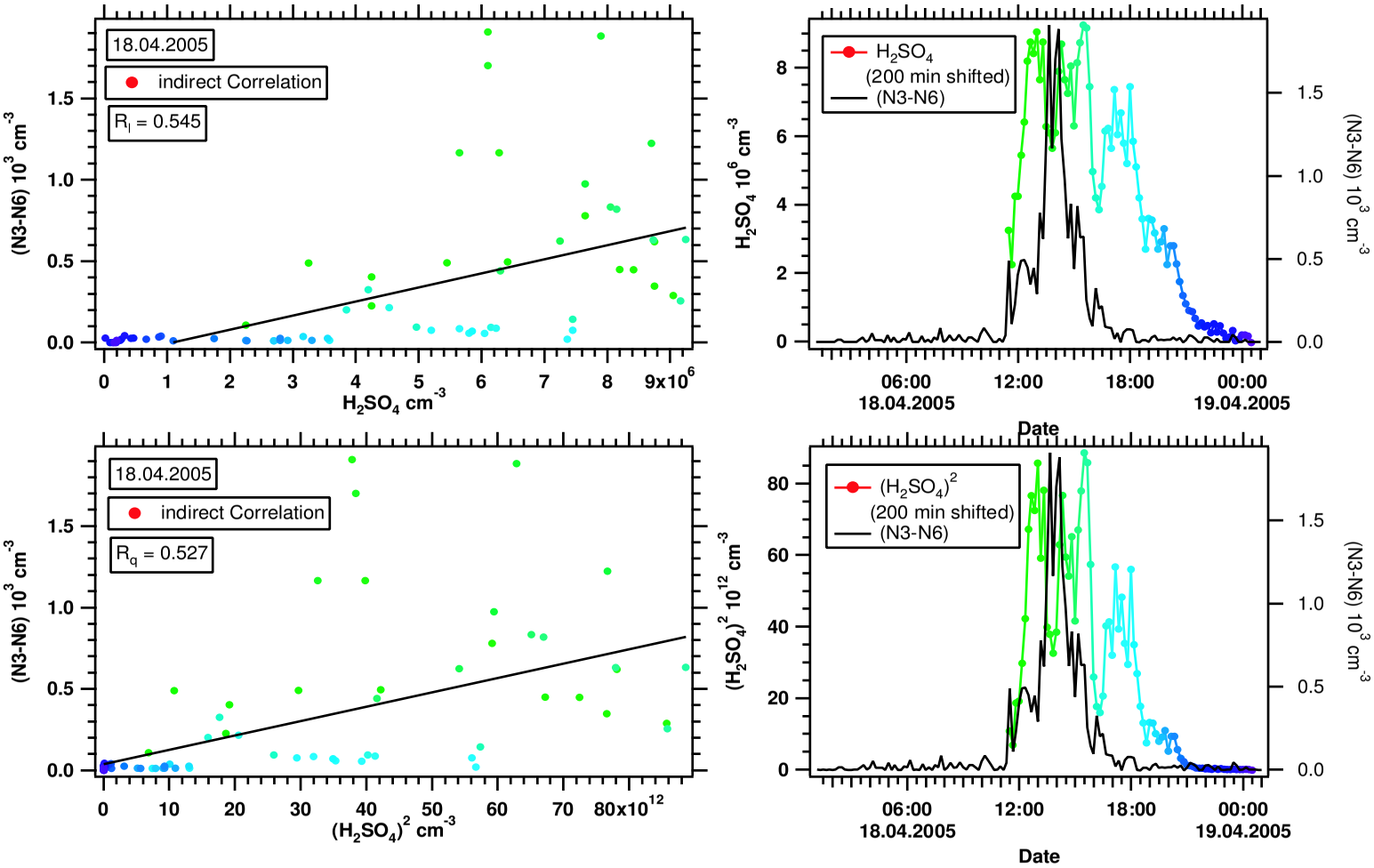

Figure B.4: Indirect correlation plots for the 18th of April. (Timeshift analysis was applied). On the left side time series of (N3-N6) and of H_2SO_4 concentration (linear and squared) are compared. On the left side the corresponding scatter plots are shown.

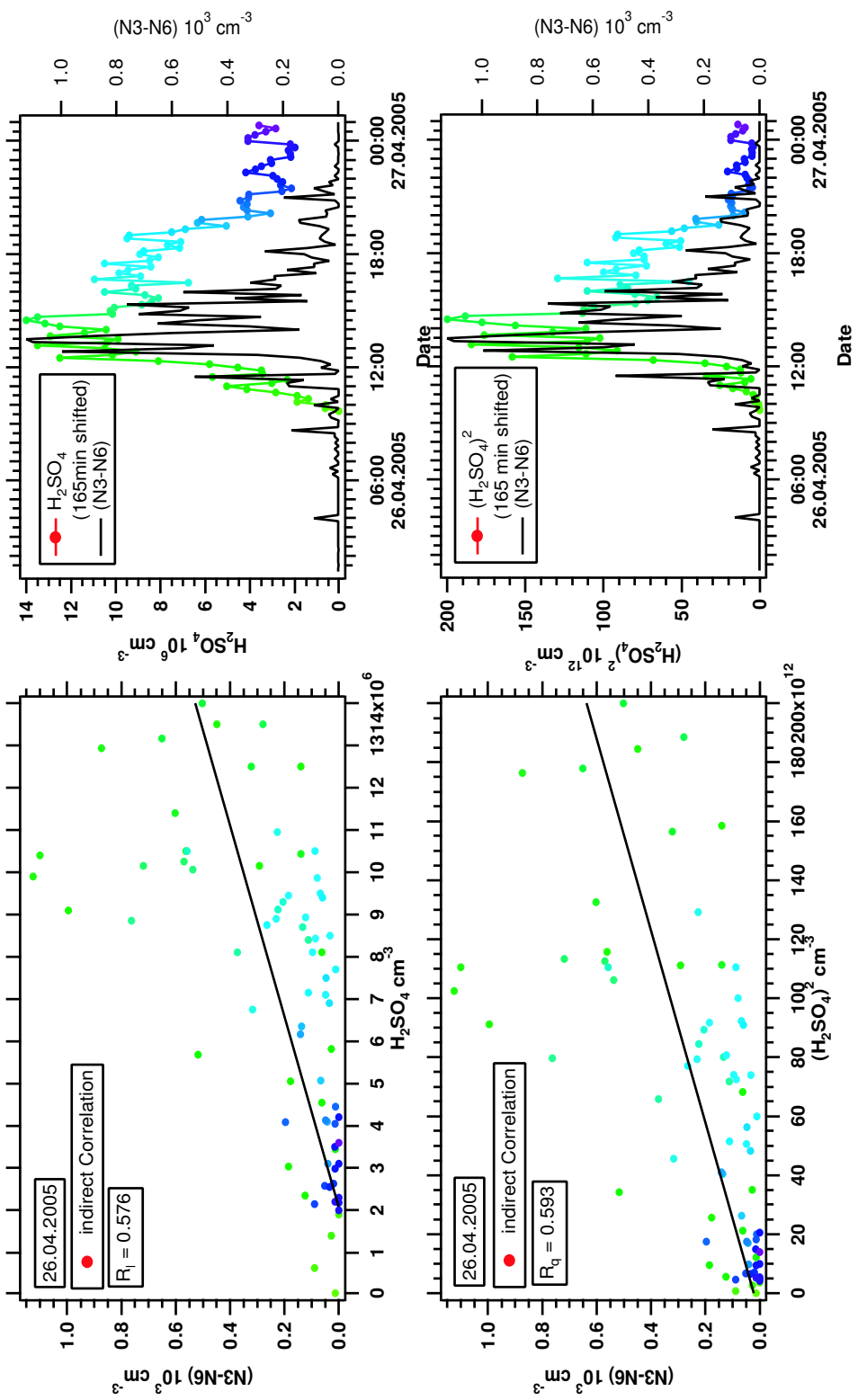

Figure B.5: Indirect correlation plots for the 26th of April. (Timeshift analysis was applied). On the left side time series of (N3-N6) and of H_2SO_4 concentration (linear and squared) are compared. On the left side the corresponding scatter plots are shown.

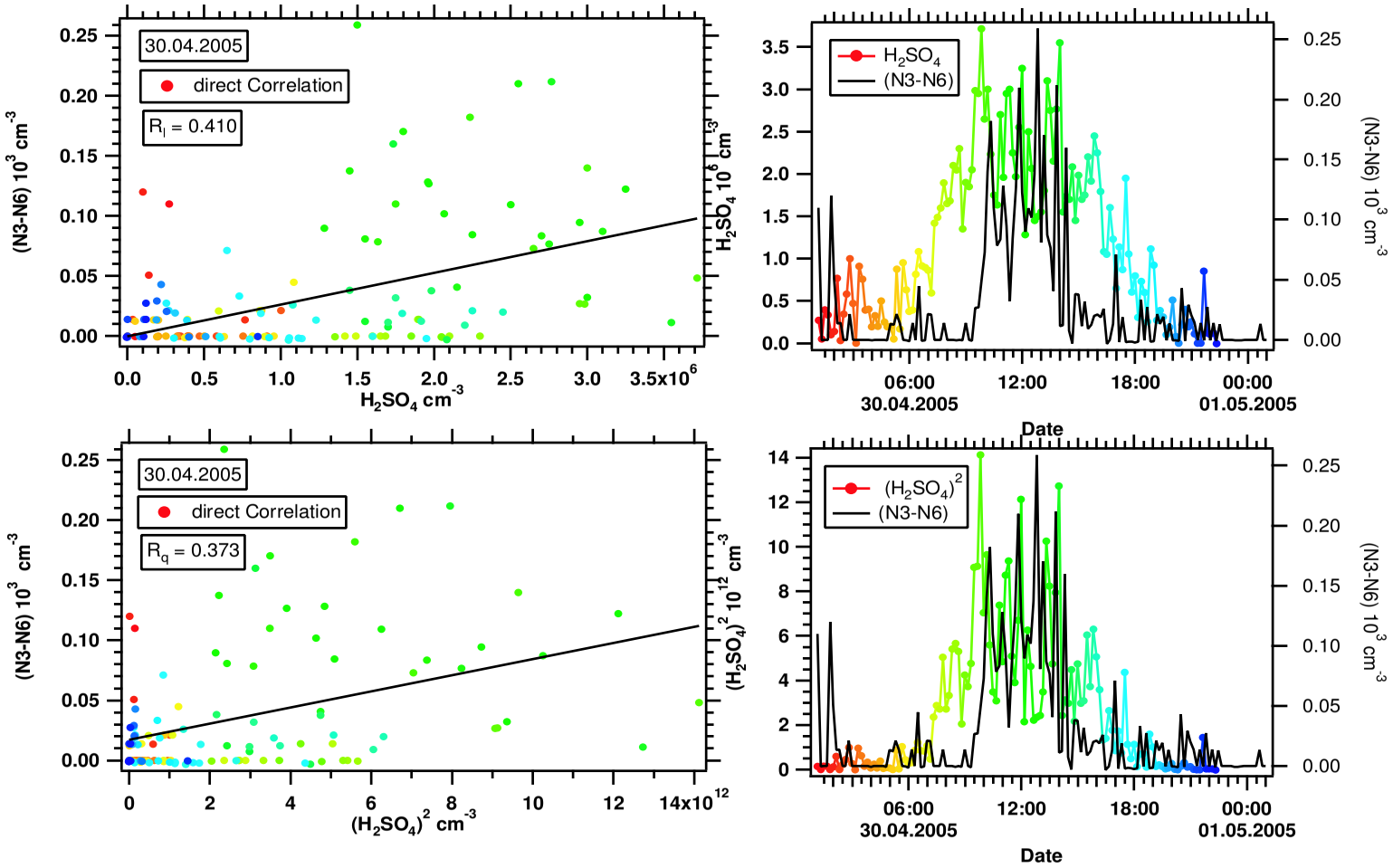

Figure B.6: Direct correlation plots for the 30th of April. (Timeshift analysis was not applied). On the left side time series of (N3-N6) and of H_2SO_4 concentration (linear and squared) are compared. On the left side the corresponding scatter plots are shown.

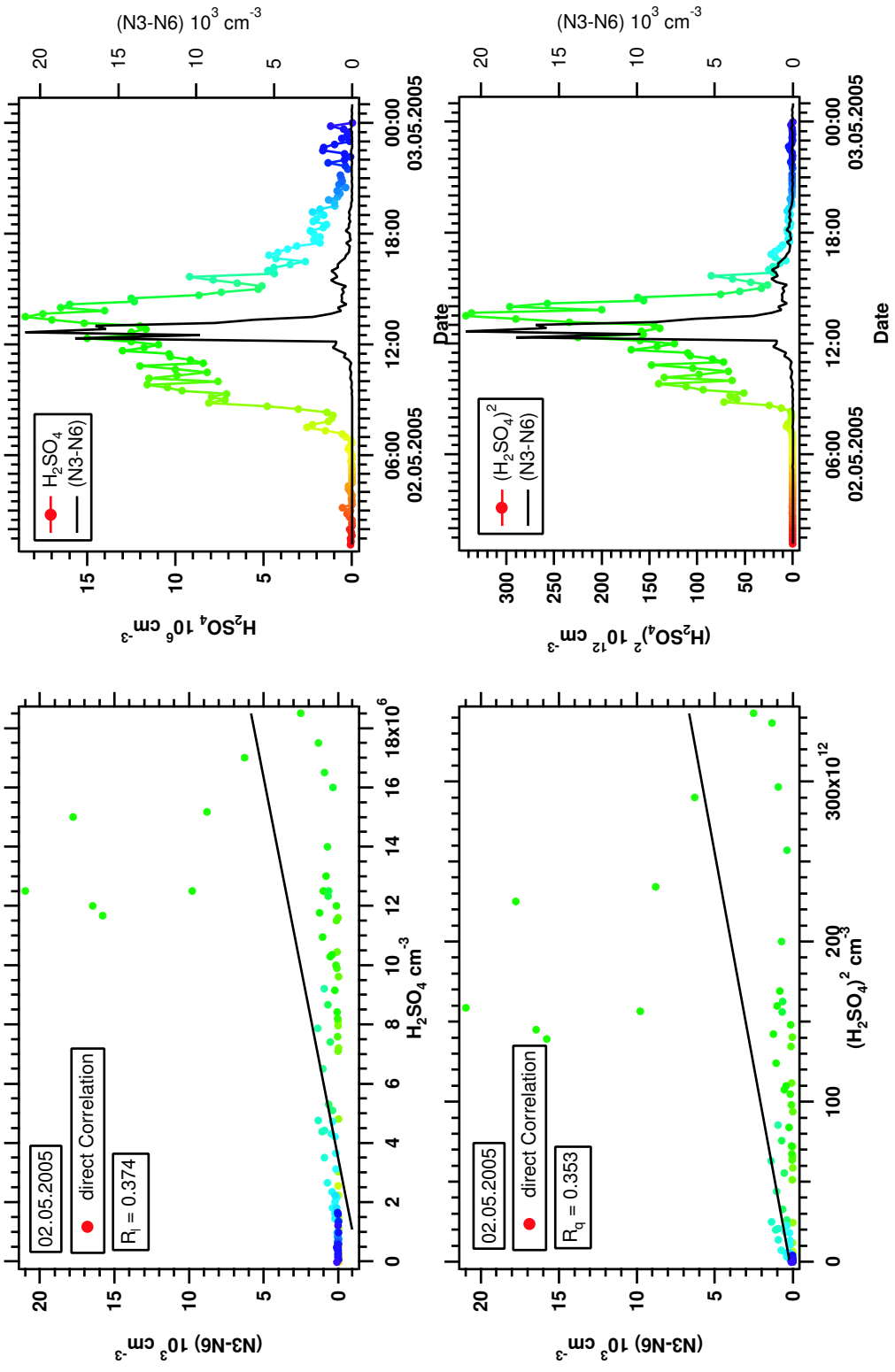

Figure B.7: Direct correlation plots for the 02nd of May. (Timeshift analysis was not applied). On the left side time series of (N3-N6) and of H_2SO_4 concentration (linear and squared) are compared. On the left side the corresponding scatter plots are shown.

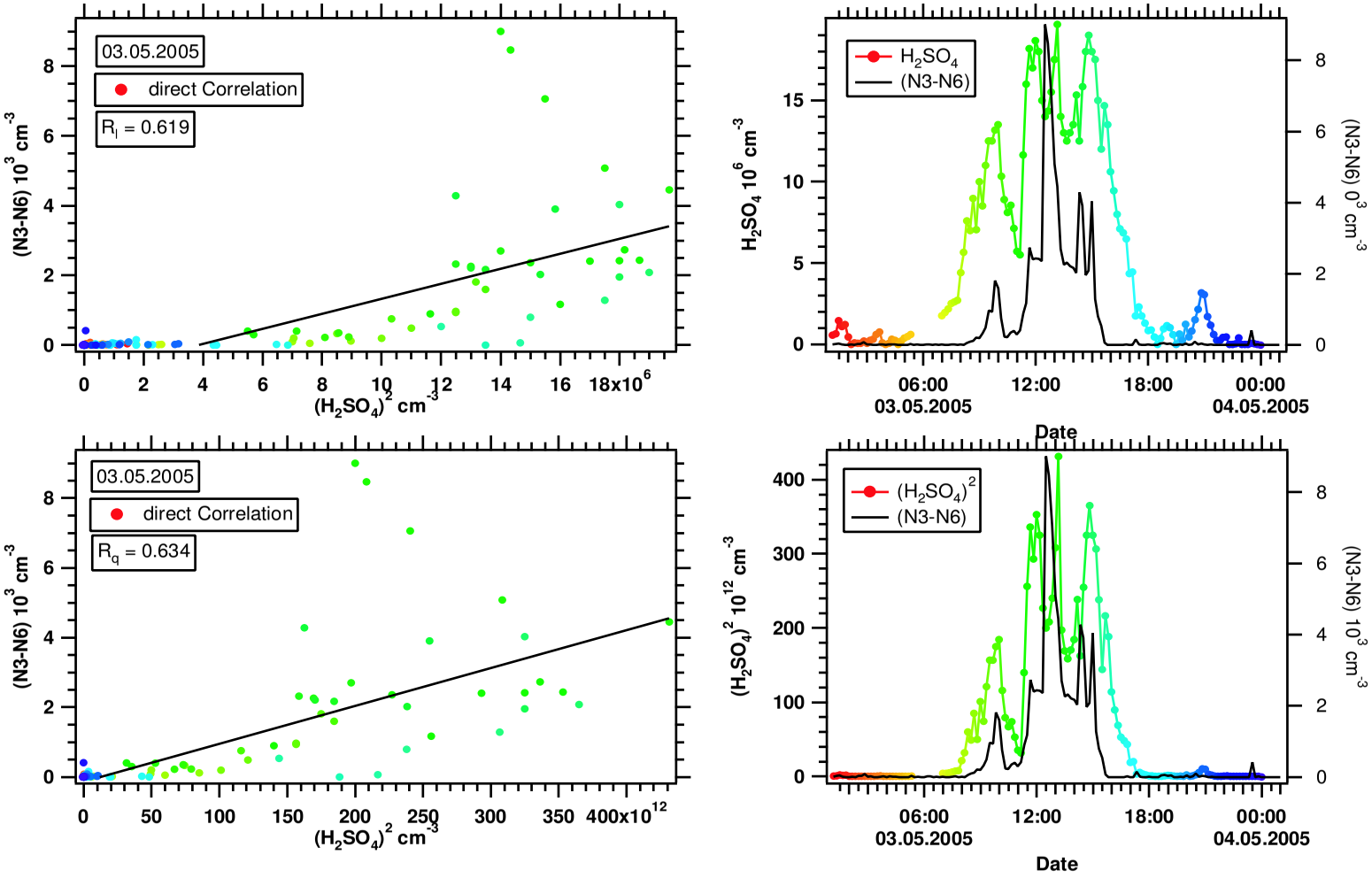

Figure B.8: Direct correlation plots for the 03rd of May. (Timeshift analysis was not applied). On the left side time series of (N3-N6) and of H_2SO_4 concentration (linear and squared) are compared. On the left side the corresponding scatter plots are shown.

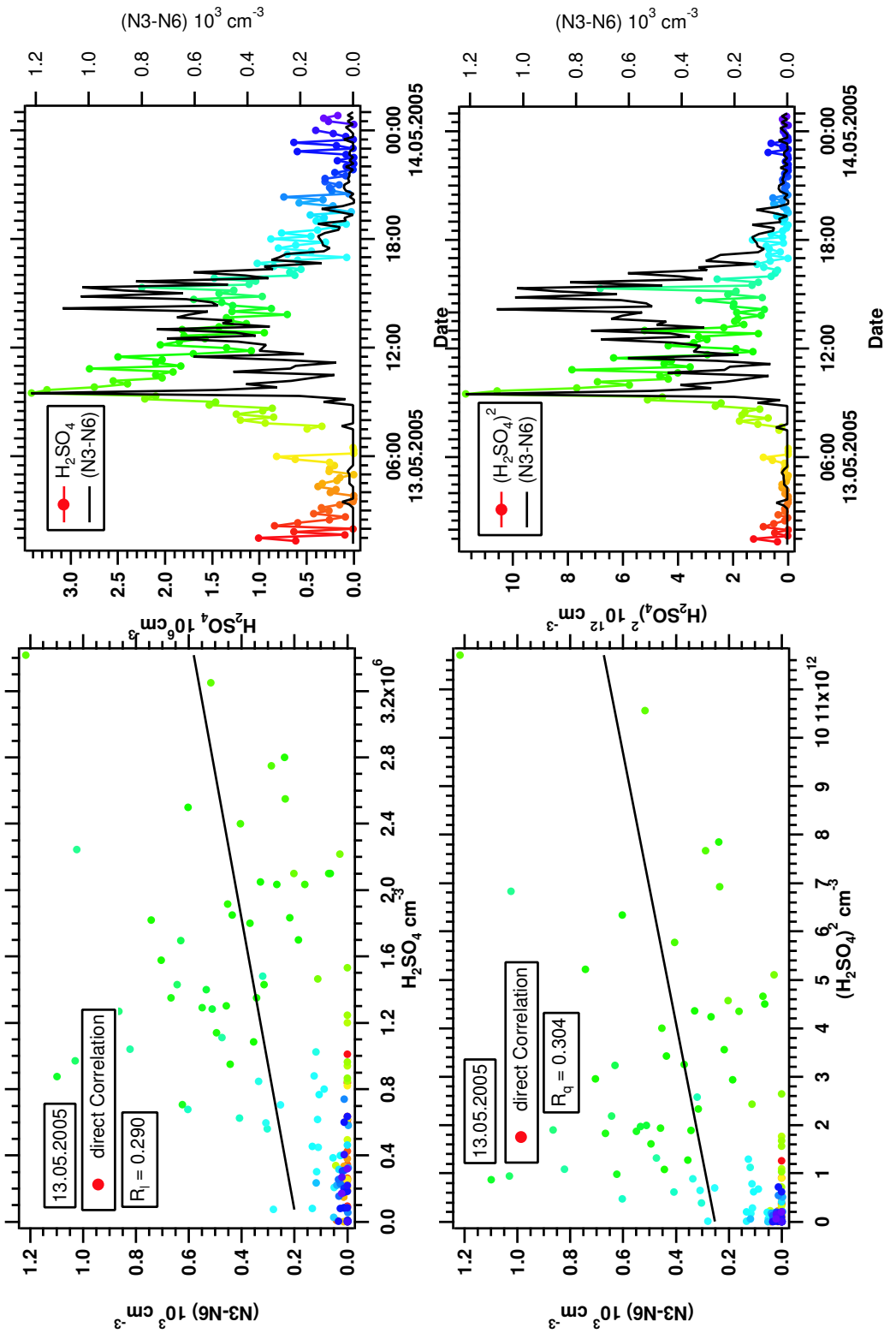

Figure B.9: Direct correlation plots for the 13th of May. (Timeshift analysis was not applied). On the left side time series of (N3-N6) and of H_2SO_4 concentration (linear and squared) are compared. On the left side the corresponding scatter plots are shown.

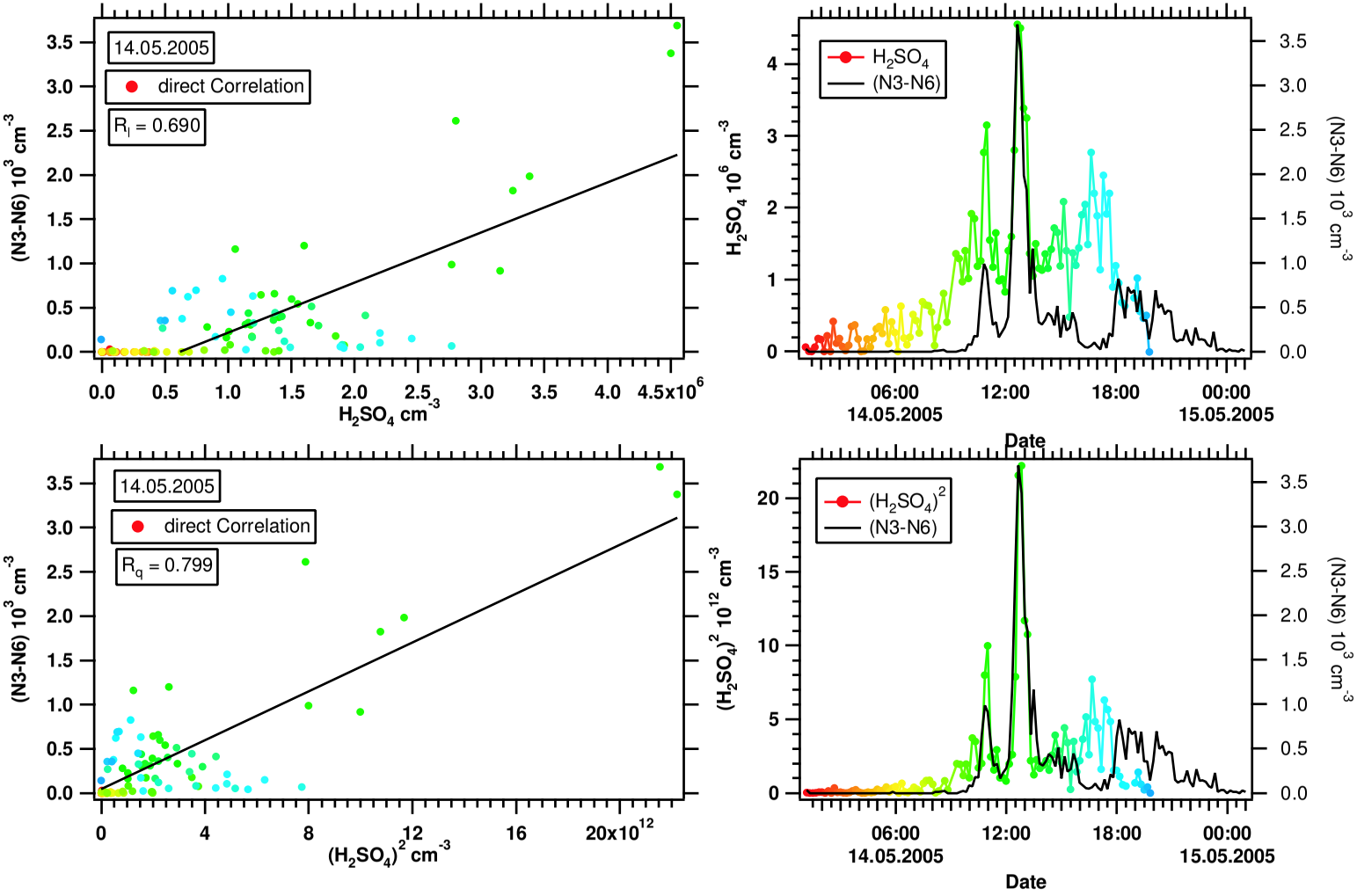

Figure B.10: Direct correlation plots for the 14th of May. (Timeshift analysis was not applied). On the left side time series of (N3-N6) and of H_2SO_4 concentration (linear and squared) are compared. On the left side the corresponding scatter plots are shown.

Appendix C

Scout - Measurements of Sulfur Dioxide

Sulfur dioxide was introduced in Chapter 2 as the precursor gas of sulphuric acid. Last year SO_2 concentrations were obtained during an aircraft campaign in Darwin, Australia as part of the Scout-project. The data of one flight will be presented and a derivation of the production rate of H_2SO_4 from these SO_2 measurements will be shown.

In November-December 2005 the SCOUT-O3 tropical Aircraft Campaign took place in the northern, tropical part of Australia, around Darwin. The campaign included survey flights between Europe and Australia and local flights from Darwin. Data was continuously acquired from Europe to Australia and back. Several stopovers to refuel were made (in Larnaca (Cyprus), Dubayy (United Arab Emirates), Hyderabad (India), U-Tapao (Thailand) and Brunei). The central objective of the SCOUT-campaign was to gain a more detailed understanding of the fundamental processes of convective injection and transport in the upper troposphere and lower stratosphere (UTLS). The tropics are of particular importance, since the tropopause level is higher and if convective systems overshoot into the lower stratosphere an exchange of air masses occurs. These air masses can be transported over large distances. A large thunderstorm called "Hector" forms over the Tiwi-Islands north of Darwin at altitudes of up to 20 kilometers almost daily in the pre-monsoon period. This convective system was investigated during the local flights, which were performed by the German Falcon (DLR) and the Russian Geophysica. [MacKenzie et al., 2006]. As part of the in-situ instruments on the Falcon, our group measured SO_2 concentrations during the entire campaign (survey flights and local flights).

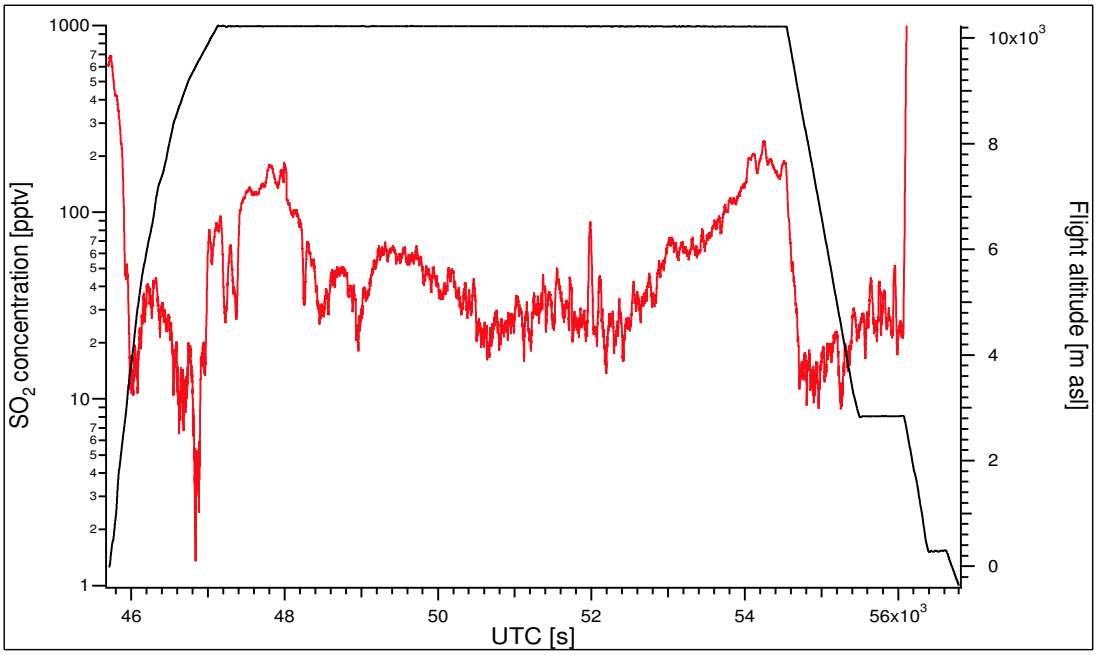

Figure C.1: Sulfur dioxide concentration and flight altitude versus time during the second transfer flight from Larnaca to Dubai. Interesting patterns in the SO_2 concentration are recognizable. The flight altitude was mostly at 10.2 km.

C.1 Measurements

A modified measurement procedure and aircraft adapted experimental setup was used to measure sulfur dioxide. The measurement principle is based on the ITCIMS-method. A detailed description of measurement principle and experimental setup during SO_2 measurements on aircrafts can be found in [Speidel, 2005], [Aufmhoff, 2004].

Out of the transfer flights and the local flights, the second transfer flight, from Larnaca to Dubayy, is presented in this section. The Falcon flew mainly over the Arabian Peninsula which consists mostly of semi-desert and desert. Thus most parts are uninhabited apart from the interior oases and coastal areas.

The measured SO_2 concentration during this flight are shown in **Figure C.1**. Some interesting patterns can be recognized in the plot. In the beginning and the end of the flight, during ascent and decent at altitudes below 3km, high concentrations of SO_2up to 600 pptv were

measured, which results from a high degree of pollution in the cities of Larnaca and Dubai. At an altitude of 10.2 km the SO_2 concentrations varied strongly throughout the flight. To be able to understand the patterns in the measured SO_2 concentration, the additional data obtained on the Falcon by other groups had to be analyzed. From NO_x and NO_y concentrations information about the age of passed air masses can be gathered. H_2O data provides a measure of cloud frequency. In clouds SO_2 may dissolve in water droplets in the presence of H_2O_2 and is thereby washed out. Thus clouds are usually recognizable in the spectra as regions of very low concentrations. For instance, the low SO_2 concentration at $47 \cdot 10^3$ s in **Figure C.1** might result from a cloud passed during flight.

C.2 H_2SO_4 production rate

Via the reaction of SO_2 and OH, which results from photochemical dissociation, H_2SO_4 can be produced. In Chapter 2 it was explained that mainly the Stockwell-Calvert-Mechanism leads to H_2SO_4 production.

$$SO_2 + OH + M \longrightarrow HSO_3 + M, \tag{C.1}$$

$$HSO_3 + O_2 \longrightarrow SO_3 + HO_2, \tag{C.2}$$

$$SO_3 + H_2O + M \longrightarrow H_2SO_4 + M. \tag{C.3}$$

Therefore it is possible to derive the H_2SO_4 production rate if the OH-concentration is known. It is proportional to the loss rate of SO_2 and decreases with time. The production rate of H_2SO_4 can be calculated using the following equation

$$P_{GSA} = [SO_2] \cdot k \cdot [OH], \tag{C.4}$$

with $k = 1.5 \cdot 10^{-12} cm^{-3} s^{-1}$ being the rate coefficient of the reaction.

The OH - concentration in the atmosphere can be described by a model. It is a function of the local time, the flight altitude, the latitude and the season. The time series follows the light intensity, thus during noon the highest amount is created. A constant value of OH-concentration can be assumed if measurements obtained during noon are investigated. Another possibility is to take a mean value into account. A reasonable value for European latitudes is 10^6 cm^{-3}.

The H_2SO_4 concentrations can be calculated from the production rate of H_2SO_4. The time series of H_2SO_4 increases exponentially if a constant amount of OH-radicals is assumed. To calculate the actual H_2SO_4 concentrations in the atmosphere, the measured particle data

had to be taken into account. H_2SO_4 molecules condense onto particles. This process is determined by interactions of particle and carrier gas, in particular by aerosol surface. The Condensation Sink which provides information on how rapidly H_2SO_4 molecules condense onto aerosol is derived from the particle number concentrations.

By applying models the aerosol production may be estimated from H_2SO_4 concentrations. That means the influence of combustion and industry on aerosol formation might be determined more precisely. As aerosols scatter sunlight and act as cloud condensation nuclei, which affects the climate, such investigations contribute to climate models. Further investigations will include analyzing trajectories to be able to observe the long-distant transport and assess the origin of pollution.

List of Figures

List of Tables

Bibliography

[Arnold, 1982] Arnold, F. (1982). Ion nucleation - a potential source for stratospheric aerosols. *Nature*, 299:134–137.

[Arnold and Fabian, 1980] Arnold, F. and Fabian, R. (1980). First measurements of gas phase sulfuric acid in the stratosphere. *Nature*, 283:55–57.

[Arnold and Viggiano, 1980] Arnold, F. and Viggiano, A. A. (1980). *Pl. Space Sci.*, 30:1295.

[Arnold, 1978] Arnold, F. und Henschen, G. (1978). First mass analysis of stratospheric negative ions. *Nature*, 275:521–522.

[Aufmhoff, 2004] Aufmhoff, H. (2004). *Atmosphärische gasförmige Vorläufer von Aerosol und Ozon: Messungen mit CIMS-Methoden auf einem Flugzeug und am Boden.* PhD thesis, Universität Heidelberg.

[Bernd et al., 2005] Bernd, T., Böge, O., Stratmann, F., Heintzenberg, J., and Kulmala, M. (2005). Rapid formation of new sulfuric acid particles at near-atmospheric conditions. *Science*, 307(5710):698–700.

[Bonn et al., 2005] Bonn, B., Korhonen, H., Hakola, H., and Kulmala, M. (2005). Competing Mechanisms for Atmospheric Nucleation in Boreal Forest Environments.

[Boy et al., 2004] Boy, M., Kulmala, M., Ruuskanen, T., Pihlatie, M., Reissell, A., Aalto, P., Keronen, P., Hellen, H., Hakola, H., Jansson, R., Hanke, M., and Arnold, F. (2004). Sulphuric acid closure and contribution to nucleation mode particle growth. Submitted. *J. of Atmospheric Chemistry and Physics.*

[Bransford, 2002] Bransford, J. K. (2002). Global climate change and air pollution: Common origins with common solutions. *MD American Medical Association, JAMA*, 287,17.

[Eichkorn et al., 2002] Eichkorn, S., Wilhelm, S., Aufmhoff, H., Wohlfrom, K. H., and F., A. (2002). Cosmic ray-induced aerosol-formation: First observational evidence from aircraft-based ion mass spectrometer measurements in the upper troposphere. *Geophys. Res. Lett.*, 29.

[Eisele and Tanner, 1993] Eisele, F. and Tanner, D. (1993). Measurements of the gas phase concentrations of H_2SO_4 and methane sulfonic acid and estimates of H_2SO_4 production and loss in the atmosphere. *Journal of Geophysical Research*, 98:9001–9010.

[Fiedler, 2004] Fiedler, V. (2004). The Atmospheric Aerosol Precursor Gas Sulphuric Acid: Mass Spectrometric Measurements in the Atmospheric Boundary Layer in Finnland and Germany. Diplomarbeit, Universität Heidelberg.

[Fiedler et al., 2005] Fiedler, V., Dal Maso, M., Boy, M., Aufmhoff, H., Hoffmann, J., Schuck, T., Birmili, W., Arnold, F., and Kulmala, M. (2005). The contribution of sulphuric acid to atmospheric particle formation and growth: a comparison between boundary layers in northern and central europe. *Atmos. Chem. Phys. Discuss.*, 5:1–33.

[Finlayson-Pitts and Pitts, 2000] Finlayson-Pitts, B. J. and Pitts, J. N. J. (2000). *Chemistry of the upper and lower atmosphere.* Academic Press, San Diego, London, 1 edition.

[Flood, 1934] Flood, H. (1934). *Z. Phys. Chemie A*, 170:280.

[Gosh, 1995] Gosh, P. (1995). *Ion Traps.* Clarendon Press, Oxford.

[Hanke, 1999] Hanke, M. (1999). *Development of a Novel Method for Measuring Atmospheric Peroxy Radicals : Calibration, Aircraft-Borne Measurements and Speciated Measurements of HO_2 and RO_2.* PhD thesis, Universität Heidelberg.

[Hardin and Kahn, 2005] Hardin, M. and Kahn, R. (2005). Aerosols and climate change. *http://geography.berkeley.edu:16080/ProgramCourses/CoursePagesFA2005/Geog142.*

[Hoffmann, 2004] Hoffmann, J. (2004). Atmosphärische Aerosolbildung: Messungen des Aerosolvorläufergases Schwefelsäure und neu gebildeter Aerosolteilchen. Diplomarbeit, Universität Heidelberg.

[Kashchiev, 1982] Kashchiev, D. (1982). On the relation between nucleation work, nucleus size, and nucleation rate. *J. Chem. Phys.*, 76(10):5098–5102.

[Knop and Arnold, 1985] Knop, G. and Arnold, F. (1985). Nitric acid vapour measurements in the troposphere and lower stratosphere by chemical ionisation mass spectrometry. *Planetary Space Science*, 33/II:983–986.

[Kolb et al., 1994] Kolb, C., Jayne, J., Worsnop, D., Molina, M., Meads, R., and Viggiano, A. (1994). Gas phase reaction of sulphur trioxide with water vapor. *J. Am. Chem. Soc.*, 116:10314–10315.

[Korhonen et al., 2004] Korhonen, H., Lehtinen, K. E. J., and Kulmala, M. (2004). Multicomponent aerosol dynamics model UHMA: model development and validation. *J. Atmos. Chem. Phys.*, 4:757–771.

[Korhonen et al., 1999] Korhonen, P., Kulmala, M., Laaksonen, A., Viisanen, Y., McGraw, R., and Seinfeld, J. (1999). Ternary nucleation of H_2SO_4, NH_3 and H_2O in the atmosphere. *J. Geophys. Res.*, 104:26349–26353.

[Kreyling et al., 2006] Kreyling, W., Semmler-Behnke, M., and Möller, W. (2006). Review: Ultrafine Particle-Lung Interactions: Does Size Matter? *Journal of Aerosol Medicine*, 19:74–83.

[Kulmala, 2003] Kulmala, M. (2003). How Particles Nucleate and Grow. *Science*, 302:1000–1001.

[Kulmala, 2004] Kulmala, M. (2004). Research unit on biosphere-cloud-climate-interactions. *www.fysik.lu.se/eriksw/bacci-lund/presentations/kulmala-bacci.ppt.*

[Kulmala et al., 2001] Kulmala, M., Dal Maso, M., Mäkelä, J., Pirjola, L., Väkevä, M., Aalto, P., Miikulainen, P., Hämeri, K., and O'Dowd, C. (2001). On the formation, growth and composition of nucleation mode particles. *Tellus B*, 53:479–490.

[Kulmala et al., 2004a] Kulmala, M., Kerminen, V.-M., Anttila, T., Laaksonen, A., and O'Dowd, C. D. (2004a). Organic aerosol formation via sulphate cluster activation. *J. Geophys. Research*, 109:D04205.

[Kulmala et al., 2004b] Kulmala, M., Laakso, L., Lehtinen, K., Riipinen, I., Dal Maso, M., Anttila, T., Kerminen, V., Hõrrak, U., Vana, M., and Tammet, H. (2004b). Initial Steps of Aerosol Growth. *Atmos. Phys. Discuss.*, 4:5433–5454.

[Kulmala et al., 2005] Kulmala, M., Lehtinen, K. E. J., and Laaksonen, A. (2005). Why formation rate of 3nm particles depends linearly on sulphuric acid concentration? *Atmospheric Chemistry and Physics Discussions*, 5:11277–11293.

[Kulmala et al., 2000] Kulmala, M., Pirjola, L., and Mäkelä, J. (2000). Stable sulphate clusters as a source of new atmospheric particles. *Nature*, 404:66–69.

[Laakso et al., 2004] Laakso, L., Anttila, T., Lehtinen, K. E. J., Aalto, P. P., Kulmala, M., Horrak, U., Paatero, J., Hanke, M., and Arnold, F. (2004). Kinetic nucleation and ions in boreal particle formation events. *Atmos. Chem. Phys. Discuss.*, 4:39113945.

[Lee et al., 2003] Lee, S.-H., Reeves, J., Wilson, J., Hunton, D., Viggiano, A., Miller, T., Ballenthin, J., and Lait, L. (2003). Particle formation by ion nucleation in the upper troposphere and lower stratosphere. *Science.*, 301:1886–1889.

[Lovejoy et al., 1996] Lovejoy, E., Hanson, D., and Huey, L. (1996). Kinetics and products of the gas phase reaction of so_2 with water. *J. Phys. Chem.*, 100:19911–19916.

[MacKenzie et al., 2006] MacKenzie, A. R., Schiller, C., Th., P., and the SCOUT-O3 tropical aircraft team (2006). The SCOUT-O3 Tropical Aircraft Campaign Darwin 2005 - an Overview. *Geophysical Research Abstracts*, 8:08967.

[March and Hughes, 1989] March, R. and Hughes, R. (1989). *Quadrupole Storage Mass Spectrometry.* John Wiley & Sons, New York.

[Mathieu, 1868] Mathieu, E. (1868). Memoire sur le mouvement vibratoire d´une membrane de forme elliptique. *J. Math. Pures Appl.*, 13:137.

[McLachlan, 1947] McLachlan, N. (1947). *Theory and Applications of Mathieu Functions.* Clarendon, Oxford.

[Mirabel et al., 2001] Mirabel, P., Guyon, P., Rausch, A., and de Coninck, H. (2001). Aerosol formation in the atmosphere. *Notes from the 3rd COACh International school*, pages 272–286.

[Neumann and Döring, 1940] Neumann, K. and Döring, W. (1940). *Z. Phys. Chemie A*, 186:203.

[Paul and Raether, 1955] Paul, W. and Raether, M. (1955). Das elektrische Massenfilter. *Zeitschrift für Physik*, 140:161–273.

[Paul et al., 1958] Paul, W., Reinhard, H., and von Zahn, U. (1958). Das elektrische Massenfilter als Massenspektrometer und Isotopentrenner. *Zeitschrift für Physik*, 152:143–182.

[Paul and Steinwedel, 1953] Paul, W. and Steinwedel, H. (1953). Ein neues Massenspektrometer ohne Magnetfeld. *Zeitschrift für Naturforschung*, pages 448–450.

[Pope et al., 2002] Pope, C., Arden, and et. al (2002). Cancer, cardiopulmonary mortality, and long-term exposure to fine particulate air pollution. *Journal of the American Medical Association*, 287:1132–1141.

[Reimann, 2000] Reimann, J. (2000). Entwicklung und Aufbau einer Kalibrationsquelle für OH-, HO_2- und RO_2-Radikale. Diplomarbeit, Universität Heidelberg.

[Reiner and Arnold, 1993] Reiner, T. and Arnold, F. (1993). Laboratory flow reactor measurements of the reaction $SO_3 + H_2O + M \rightarrow H_2SO_4 + M$: Implications for gaseous H_2SO_4 and aerosol formation in the plume of jet aircraft. *Geophysical Research Letters*, 20:2659–2662.

[Reiner and Arnold, 1994] Reiner, T. and Arnold, F. (1994). Laboratory investigations of gaseous sulfuric acid formation via $SO_3 + H_2O + M \rightarrow H_2SO_4 + M$: Measurements of the rate constant and products identification. *J. Chem. Phys.*, 101:7399–7407.

[Reiss, 1950] Reiss, H. (1950). *J. Chem. Phys.*, 18:840.

[Roedel, 2000] Roedel, W. (2000). *Physik unserer Umwelt: Die Atmosphäre*. Springer Verlag.

[Scholz, 2004] Scholz, S. (2004). Messung der atmosphärischen Spurengase Schwefelsäure und Methansulfonsäure mittels Ionen-Molekül-Reaktions-Massenspektrometrie. Diplomarbeit, Universität Heidelberg.

[Seinfeld and Pandis, 1998] Seinfeld, J. and Pandis, S. N. (1998). *Atmospheric Chemistry and Physics*. John Wiley & Sons, Inc.

[Speidel, 2005] Speidel, M. (2005). *Atmospheric Aerosol Particle Formation: Aircraft-Based Mass Spectrometric Measurements of Gaseous and Ionic Aerosol Precursors.* PhD thesis, University of Heidelberg.

[Stauffer, 1976] Stauffer, D. (1976). *Journal of Aerosol Science*, 7:319.

[Uecker, 2002] Uecker, J. (2002). *Messung der atmosphärischen Radikale OH, HO_2, RO_2 sowie des Ultraspurengases H_2SO_4 - Weiterentwicklung, Kalibration und Einsatz einer hochempfindlichen massenspektrometrischen Analysemethode.* PhD thesis, Universität Heidelberg.

[Viggiano et al., 1997] Viggiano, A., Seeley, J., Mundis, P., Williamson, J., and Morrison, R. (1997). Rate constants for the reaction of $XHO_3^-(H_2O)$(X=C, HC and N) and $NO_3^-(HNO_3)_n$ with H_2SO_4: Implications for atmospheric detection of H_2SO_4. *Journal of Physical Chemistry A*, 101:8275–8278.

[Volmer, 1939] Volmer, M. (1939). Kinetik der Phasenbildung. *Verlag Von Theodor Steinkopff, Dresden und Leipzig.*

[Wayne, 2000] Wayne, R. P. (2000). *Chemistry of Atmospheres.* Oxford University Press.

[Weber et al., 1996] Weber, R., Marti, J., McMurry, P., Eisele, F., Tanner, D., and Jefferson, A. (1996). Measured atmospheric new particle formation rates: Implications for nucleation mechanisms. *Chemical Engineering Communications*, 151:53–64.

[Weber et al., 1997] Weber, R., Marti, J., McMurry, P., Eisele, F., Tanner, D., and Jefferson, A. (1997). Measurements of new particle formation and ultrafine particle growth at a clear continental site. *Journal of Geophysical Research*, 102:4375–4385.

[Wilhelm et al., 2004] Wilhelm, S., Eichkorn, S., Wiedner, D., Pirjola, L., and Arnold, F. (2004). Ion-induced aerosol formation: new insights from laboratory measurements of mixed cluster ions HSO4-(H2SO4)a(H2O)w and H+ (H2SO4)a(H2O)w. *Atmospheric Environment*, 38:1735–1744.

[Wollny, 1998] Wollny, A. (1998). Flugzeugmessungen atmosphärischer Spurengase mittels Ionen-Molekül-Reaktions-Massenspektrometrie: Methodische Untersuchungen zur Reaktionskinetik. Master's thesis, Universität Heidelberg.

[Yue and Chan, 1979] Yue, G. and Chan, L. (1979). Theory of formation of aerosols of volatile binary solutions through the ion-induced nucleation process. *J. Colloid Interface Sci.*, 68:501.

[Zylka-Menhorn, 2005] Zylka-Menhorn, V. (2005). Luftschadstoffe: Feinstäube - Winzlinge mit grosser Wirkung. *Deutsches Ärzteblatt 102*, 14:A–954,B–808,C–755.

Erklärung :

Ich versichere, dass ich diese Arbeit selbständig verfasst und keine anderen als die angegebenen Quellen und Hilfsmittel benutzt habe.

Heidelberg, den 18.04.2006